Autonomous Closed-loop Photochemical Reaction Optimization for the Synthesis of Various Angiotensin II Receptor Blocker Molecules

Dnyaneshwar Aand,[a,b] Abhilash Rana,[a,b] Amirreza Mottafegh,[c] Dong Pyo Kim,[c] and Ajay K. Singh[*a,b]

[a] Department of Organic Synthesis and Process Chemistry, CSIR-Indian Institute of Chemical Technology, Hyderabad-500007, India.

[b] Academy of Scientific and Innovative Research (AcSIR), Ghaziabad 201002, India.

[c] Center for Intelligent Microprocess of Pharmaceutical Synthesis, Department of Chemical Engineering, Pohang University of Science and Technology (POSTECH), Pohang 37673, Republic of Korea

[*]Corresponding author. E-mail addresses: ajaysingh015@iict.res.in, ajaysingh015@gmail.com.

Table of contents:

	S3.2 Pilot scale synthesis of **4a.**	
	S3.3 Long-term experiment of K_2CO_3.	
	S3.4 General procedures for the continuous flow nucleophilic substitution for the synthesis of various sartan intermediates **4**.	
S4	S4.1 Fully integrated continuous flow platform for the synthesis of losartan intermediates **4a.**	S49
	S4.2 General procedure of fully integrated continuous flow platform the synthesis of various sartan intermediate **4**.	
S5	Spectra	S64
S6	References	S126

S1. General

S1.1. Materials

Most reagents and chemicals procured from Sigma-Aldrich were employed without further purification. Common organic chemicals and salts were acquired from Avra Chemicals, India. Deionized water with a conductivity of 18.2 mS was utilized in all experiments. All work-up and purification procedures were conducted using reagent-grade solvents under ambient conditions. Analytical thin-layer chromatography (TLC) was executed using analytical chromatography silica gel 60 F254 pre-coated plates with a thickness of 0.25 mm. Subsequently, the developed chromatogram was analyzed under a UV lamp with a wavelength of 254 nm. PTFE tubing with an inner diameter of 500 μm, T-junction, and high-purity PFA tubing was sourced from Upchurch IDEX HEALTH & SCIENCE. The RGB and Blue LED reactor was purchased from SmartChemSynth, India, and underwent slight modifications to facilitate continuous flow reactions.

S1.2. Analysis

High-resolution mass spectra (HRMS) were acquired using a JMS-T100TD instrument (DART) and Thermo Fisher Scientific Exactive (APCI). Nuclear magnetic resonance (NMR) spectra were recorded on a Bruker, 500, 400, or 600 MHz in CDCl$_3$, DMSO-d_6, solvent. Chemical shifts for ^{1}H NMR were expressed in parts per million (ppm) relative to tetramethylsilane (δ 0.00 ppm). Chemical shifts for ^{13}C NMR were expressed in ppm relative to CDCl$_3$ (δ 77.0 ppm) or DMSO-d_6 (39.5 ppm) and tetramethylsilane (δ 0.00 ppm) data were reported as follows: chemical shift, multiplicity (s = singlet, d = doublet, dd = doublet of doublets, t = triplet, q = quartet, quin = quintet, sext = sextet, m = multiplet), coupling constants (Hz), and integration. ATR analysis was conducted on a portable FTIR spectrometer Bruker ALPHA, and a programable power supply system was used to supply current and voltage to the LED rector. The melting point was conducted on POLMAN MP-96. Han's Yueming laser

series (model CMA0604-B-A, Carbon dioxide based, laser power 60W) and Inline IR study were conducted with React IR^{TM} 15, Mettler Toledo 7.1 Instrument, and iC IR 7.1.84.0 software.

S2. Photo-flow bromination.

S2.1 Preliminary setup for photo flow reactor & manual optimization of photo-flow bromination.

2.1.1 Fabrication of homemade photo-flow reactor:
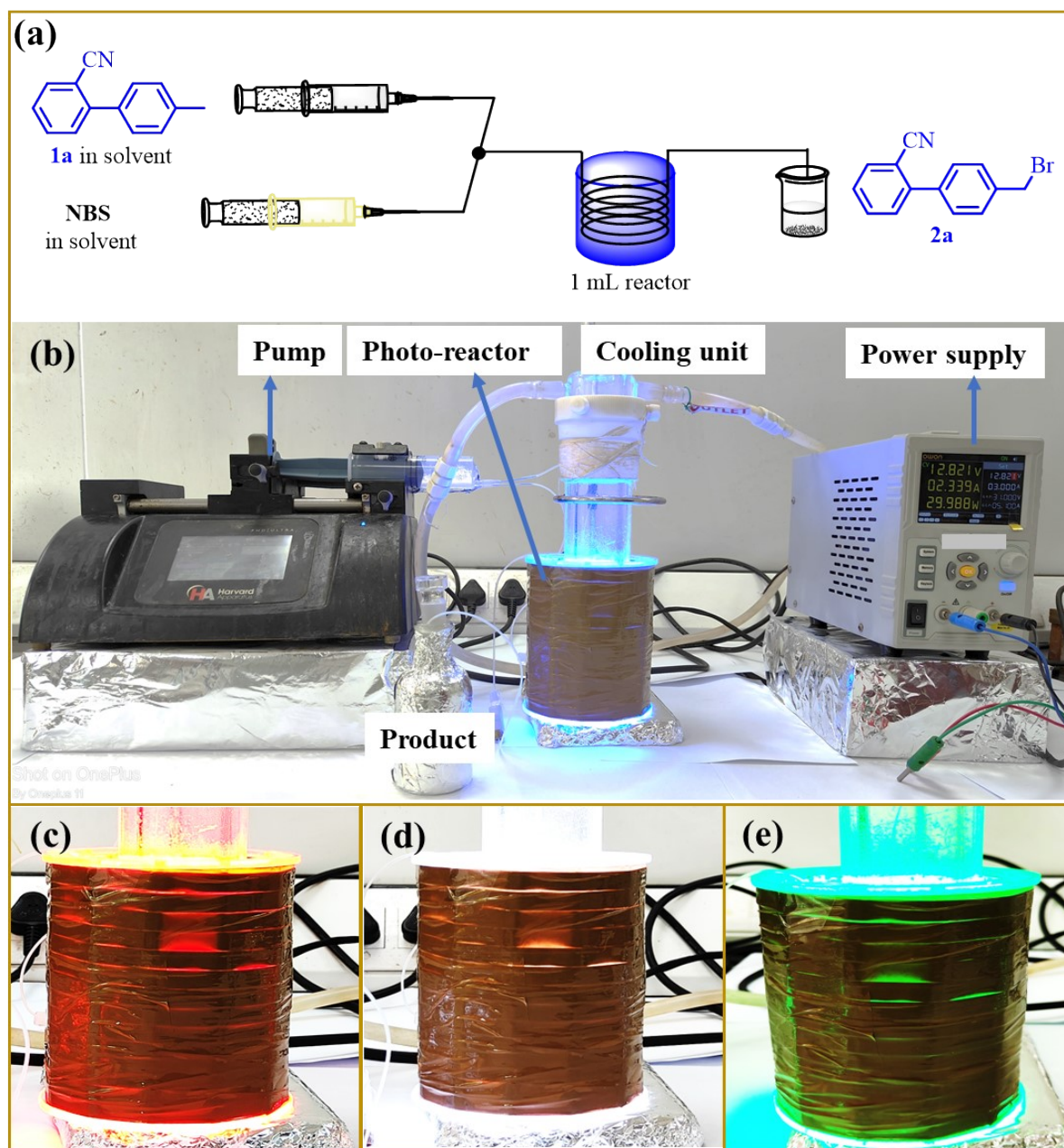
Fig. S1 Schematic graphic presentation of the photo-flow reactor for bromination; (a) blueprint of basic set-up; (b) original photograph basic set-up; (c) red light; (d) white light; (e) green light.

As shown in Fig. S1, a syringe pump was used to deliver the 2-cyano-4-methyl biphenyl (**1a**) (0.25M in ACN) in one syringe and *N*-bromosuccinimide (NBS) (0.253M in ACN) was in another syringe which was connected to the PFA (perfluoroalkoxy) tubing. Both solutions were introduced through a T-mixer at the same flow rate to maintain a stoichiometric ratio. Then they passed through a PFA (perfluoroalkoxy) tubing {outer diameter (od) = 1.58, inner diameter (id)=1mm, length (l) = 1.3 m, volume (v) = 1.0 mL}. The tubing reactor was wrapped within the helical grooves around a cylindrical-shaped frame. The reactor was cooled by circulating cooling water. The cylindrical reactor was placed for irradiation by a blue light. After reaction completion, the crude product was collected into a flask. As mentioned in Table S1, various reaction parameters, such as residence time, various light sources, light intensity (W), and solvent, were regulated to optimize reaction performance. Eventually, at a flow rate of 0.3 mL min^{-1} for each solution, using a blue light (30W) with a residence time of 1.67 min at room temperature generated the best yield of 91% of 4'-bromomethyl-2-cyanobiphenyl (**2a**) and 29 g/day productivity (Table S1, entry 4).

Table S1: Manual optimization of photo-flow bromination.
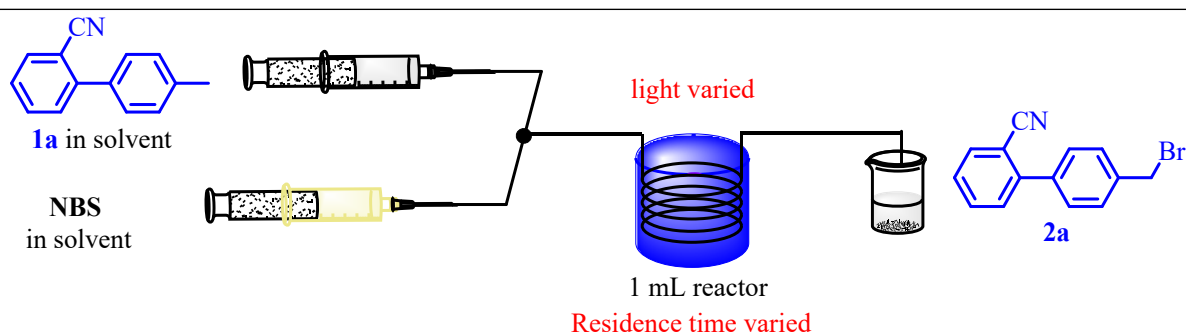
Entry	Flow rate (mL min^{-1})		Residence time (min)	Light source (W)	Yields (%)
	A	**B**			
1	0.2	0.2	2.5	10	85
2	0.3	0.3	1.67	10	82
3	0.3	0.3	1.67	20	84
4	**0.3**	**0.3**	**1.67**	**30**	**91**
5	0.4	0.4	1.25	30	87
6[a]	0.3	0.3	1.67	30	60
7[b]	0.3	0.3	1.67	30	35
8[c]	0.3	0.3	1.67	30	10
9[d]	0.3	0.3	1.67	30	15
10[e]	**0.3**	**0.3**	**0.3**	**30**	**90**
11[f]	0.3	0.3	1.67	30	25
12[g]	0.3	0.3	1.67	30	18
13[h]	0.3	0.3	1.67	30	56

Reaction condition: 1a (0.25M in ACN), NBS (0.253M in ACN); 1 mL PFA reactor (id = 1mm, v = 1.3 mL); blue light (W); instead of ACN solvents (a) THF; (b) DCM; (c) DMF; (d) DMSO, (e) **1a** in EA and NBS in ethyl acetate (EA): ACN (4:1) *due to partial solubility of NBS in EA; instead of blue light (f) red light (g) green light (h) white light; yields are based on LC-MS.

S2.2 Basic experimental setups for the photochemical auto-optimization platform.

2.2.1 Microreactor system:

A homemade PFA tubular reactor (volume 1 mL; od 1.58 mm, id 1 mm, l = 1.3 meter) was fabricated for the bromination reaction. The cylindrical reactor was placed for irradiation by a blue light lamp. The entire reactor was covered with aluminum foil to enhance light absorption.

2.2.2 Blue LED reactor

We obtained a commercially available cylindrical-shaped 60W blue LED for the photochemical reaction. We utilized a programmable power supply to control the lamp's power (in watts) by controlling the current and voltage (**Fig. S2**). The power supply was connected to the central system through RS 232 to control the current and voltage.
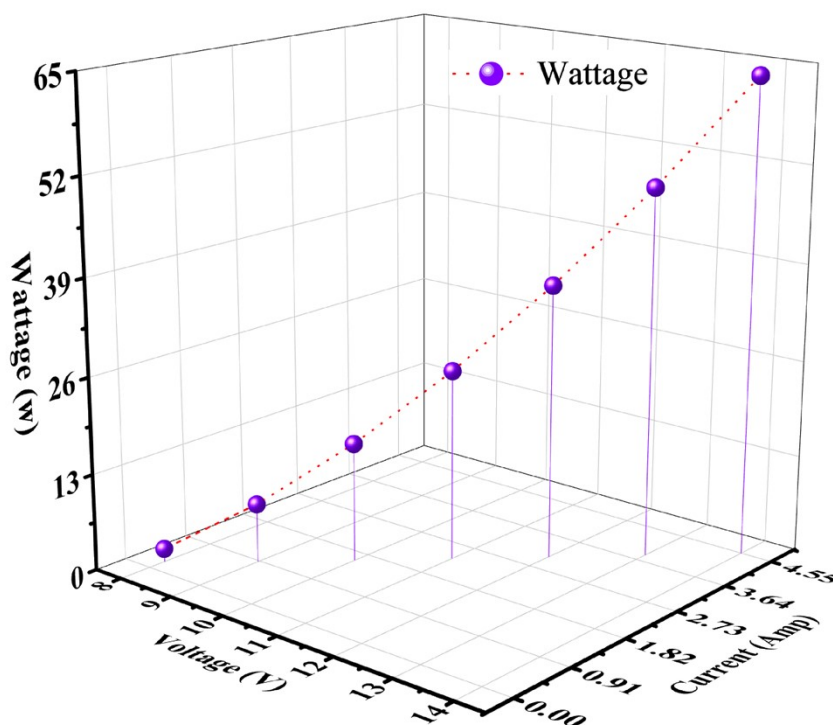
Fig. S2 3D graph of the relation between voltage (V), current (Amp) and blue light intensity (W).

2.2.3 Pumps:

The HPLC pumps were directly connected to the main computer via an RS-232 interface. These

pumps introduced reactants and reagent solutions into the microreactor at the central computer's prescribed flow rate (fr). To convey information regarding the flow rate, operational status, and duration, serial communication utilizing ASCII code was employed between the central computer and the HPLC pump. This allowed the main computer to transmit the necessary details to the pumps, enabling them to initiate their operations accordingly.

2.2.4 In-line FT-IR Analysis:

The success of the automated optimization platform depended on the accuracy of a predictive analytics model, which was achieved by employing the Mettler-Toledo ReactIR 15 equipped with an Ag-halide Di-comp Flow Cell. This platform continuously recorded IR spectra at 15-second intervals in real time for reaction analysis. During the development of the predictive model, careful consideration was given to the scan rate to strike a balance between reliable predictions and rapid reaction analysis. A 15-second scan time proved sufficient for the specific chemistry application, ensuring the accuracy of the predictive model.

The analysis and interpretation of spectral data unfolded within the Mettler Toledo iC IR software environment (version 7.1). Ahead of each experiment, a background spectrum was meticulously recorded and cross-referenced with previously obtained spectra to guarantee consistency across experiments. Our initial steps involved subjecting specific 0.25M molar solutions of the reactant **(1a)**, NBS, the reaction mixture before and after light exposure under pre-optimized conditions, and the pure product (**2a**) to IR background analysis. To streamline the calibration of our model, we generated IR trend spectra using a uniform absorption spectrum of **1a** and **2a**. Our primary focus during the investigation rested on the spectral region between 1100–1300 cm^{-1}, which emerged as the optimal range for examination due to its distinct C–Br (wag) IR peak at 1230 cm^{-1} for product **2a** (**Fig. S3**).

2.2.5 Inline ReactIR for real-time acquisition of IR spectra:

The Python-based program supported various functions, including mouse and keyboard control. One of the essential mouse control functions was 'clicking.' The In-line ReactIR15 function utilized the image processing command within the Spectra IR15 software. It measured FT-IR spectroscopy in the background and then initiated the analysis function. This function measured the FT-IR spectra of the sample and waited until the process was completed. The spectral information was saved in a 'csv' format that the spyder program could decode.

The spyder function opened the spectra analysis program by simulating a click on its logo. The system exported the 'csv' file to a designated directory within the spectra analysis program. Subsequently, the system imported the 'csv' file, and React IR 7.1 reopened the spectra measurement program. This capability was necessary because React IR and spyder operated independently. Therefore, In-line React IR managed the FT-IR spectroscopy measurements and saving process while Spyder read the IR file, processed the data, and provided feedback to the pumps.

2.2.6 The interpretation of FT-IR spectra data:

The characteristic peak was shifted from 1245 cm^{-1} of NBS disappeared, and a new peak formed from 1230 cm^{-1} in product **2a**, corresponding to the CH_2-Br.
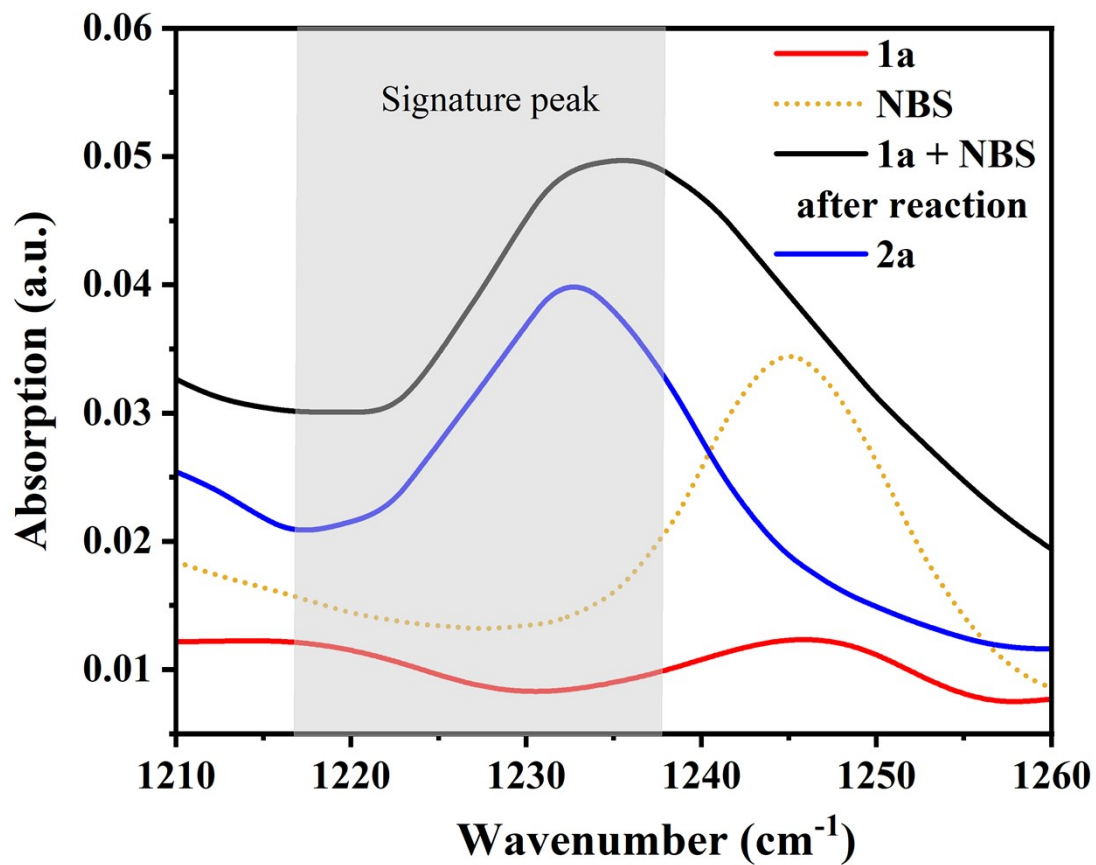
Fig. S3 In-line IR background analysis of **1a**, **NBS**, **1a + NBS** after reaction, and **2a** in ACN.

2.2.7 Auto-collector:

We acquired a commercially available 3D printer for the auto-sampler. The Python program on the central computer interfaced with the 3D printer. The Python program commanded the 3D printer to rotate, and this information was communicated to USB serial communication. This setup allowed us to control the 3D printer for tasks such as sample collection, reactor stabilization, and washing in various situations (**Fig. S4**).
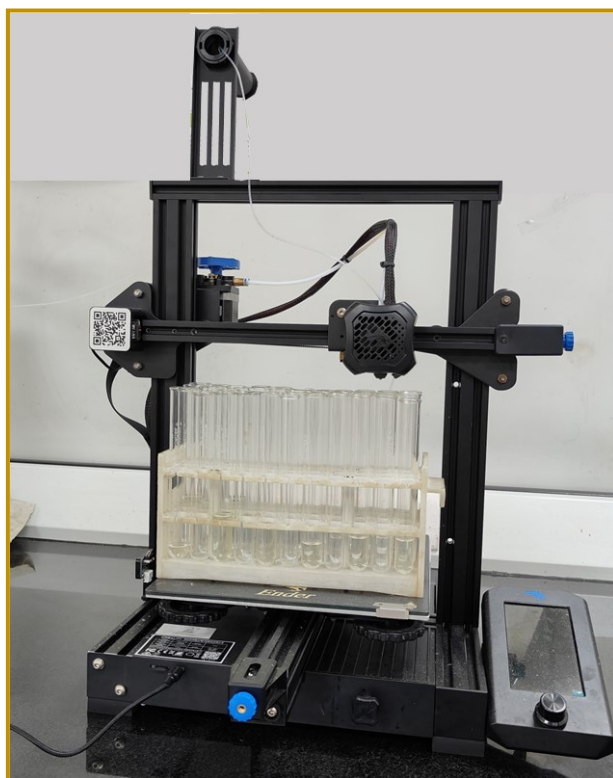
Fig S4 Original photograph of auto-collector.

2.2.8 Auto-optimized reactor system:

We have all accessories like pumps, LED light reactor, Owon power supply, and In-line IR connected to the central computer system with RS 232 and USB cable. We have made a combined program including Bayesian optimization for automatically changing the parameters such as flow rate and power of irradiation of blue light to maximize yield.

S2.3 Bayesian optimization algorithm.

The Bayesian optimization algorithm used in this platform was a modified version of a meta-optimizer (MO) algorithm[1, 2] consisting of multiple surrogate models and a single acquisition function. The surrogate models used in this algorithm were similar to the original reported one, and the surrogate model was selected as an expected improvement. To proceed with the optimization process, the Sobol algorithm was chosen to generate the initial point before the commencement of the main Bayesian optimization loop for 3 consecutive rounds. Then, the meta-optimizer loop was started to maximize the reaction build (**Fig. S5**).
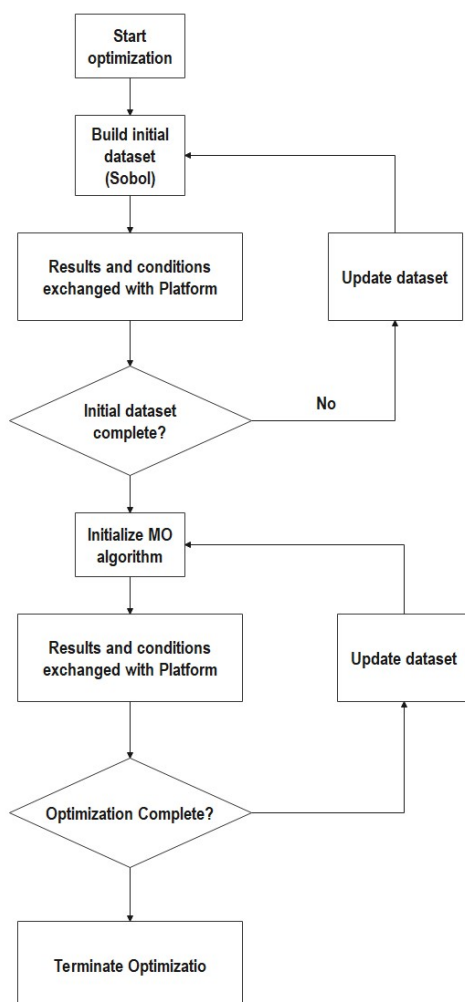
Fig. S5 Algorithm flow chart of user-planning mode with two variables in the auto-optimization**.**

S2.4 Experimental design via Bayesian optimization (EDBO) for the photo flow bromination.

The two HPLC pumps were manipulated as programmed in the central computer to inject and control the flow rates of the two respective solutions comprising **1a** and NBS in ACN solvent. Both solutions were introduced through a T-mixer at the same flow rate (Q) to maintain a stoichiometric ratio and then passed through a PFA tubing (od = 1/16, id = 1mm, l = 1.3 m, v = 1mL) under various blue light intensity (W) exposure. The reaction room temperature of the reactor was controlled by water circulation and a fan at the bottom of the photochemical reaction. The resulting solution was passed through a ReactIR for in-line FT-IR analysis and after stabilized spectral data obtained by in-line FT-IR. After the steady state of the EDBO was confirmed by the in-line analysis, the resulting solution was collected for 2 min (**Fig. 1**). Then, the user planning presented the following values for the variable flow rate and blue light (W). The collected mixture was extracted with EA and washed with brine. The organic phase was dried over sodium sulfate. The organic layer was concentrated on a rotary evaporator under reduced pressure. The crude was purified by column chromatography to give the desired product. In the user-planning mode of ultrafast chemistry, two starting reagents were injected by HPLC pumps at equal flow rates with a maintaining (1:1) ratio of reagents with various total flow rates (Q).

```python
from os import listdir
from os.path import isfile, join
import serial

import numpy as np
import pandas as pd
import time
from scipy.integrate import trapz

#step1: be sure to the address of the files that the ftir data is exported is matching to line 11 (mypath)
mypath = "C:\\Users\Admin\Desktop\Dnya\\Exp 20230714"
onlyfiles = [f for f in listdir(mypath) if isfile(join(mypath, f))]


#step2: make sure that pump and the potentiostat is correctly addressed in the line 16 and 17
pump_1 = serial.serial_for_url("socket://169.254.1.51:10001",9600) #HPLC Pump LAN
port = serial.Serial("COM1",115200)
pump_2 = serial.Serial("COM5",9600) #HPLC Pump
printer = serial.Serial("COM6", 115200, timeout=1)

#step 3: grab the lines from 22 to 90 and presss f9
def area_under(data,start,end):
    x = np.flip(data.iloc[start:end,0].to_numpy())
    y = np.flip(data.iloc[start:end,1].to_numpy())
    area = trapz(y,x)
    return np.abs(area)

def file_namer(num):
    str1 = str(num)
    length = int(len((str1)))
    empt = ''
    for i in range(5-length):
        empt = empt+'0'

    return empt+str1


def ftir_extract(filename,init,end):

    filename = filename

    temp_df = pd.read_csv(filename)
    # nump_df = temp_df.to_numpy()
    area = area_under(temp_df, init, end)
    # max_peak = np.max(nump_df[90:120,1])
    print(area)

    return area


def function(flowrate_1,flowrate_2,v,i):

     #set the pumps with the flowrate as the desired flowrate for the function

    fr_1 = flowrate_1*1000   #ml/min
    pump_1.write(('flow:'+ str(fr_1) + '\r').encode())
```

```python
59
60        time.sleep(0.1)
61        fr_2=flowrate_2*1000 #converting ml/min to ul/min as pump takes this as input val
62        pump_2.write(('flow:'+ str(fr_2) + '\r').encode())
63
64        #set the com port for potentiostat and set the voltage and current
65        vol = v
66        curr = i
67        port.write(('VOLT '+str(vol)+'\r\n').encode())      #to change the voltge we need to use "VOLT 1" command
68        port.write(('CURR '+str(curr)+'\r\n').encode())     #to change the current we need to use "CURR 1" command
69
70
71        #pumps run
72        pump_1.write(b'on\r')
73        time.sleep(0.1)
74        pump_2.write(b'on\r')
75
76        time.sleep(480)
77
78 def function2():
79        time.sleep(180) # Last 3 minutes
80        files = [f for f in listdir(mypath) if isfile(join(mypath, f))]
81
82        val = 0
83
84        #change wavelengths as per product here.
85        f_row=19 #first row of range for wavelength as per IR CSV
86        l_row=24 #last row of range for wavelength as per IR CSV
87
88        val += ftir_extract(files[-1],f_row,l_row)
89        val += ftir_extract(files[-2],f_row,l_row)
90        val += ftir_extract(files[-3],f_row,l_row)
91
92        avg_val = val/3
93
94        return avg_val
95
96
97 #step 4:grab the line 93 and f9
98 from skopt.optimizer import Optimizer
99
100
101 #step5:in line 96 we have to define the range that (flowrate,voltage,current) (from,to) and after (anytime) appllying changes you need to grab the l:
102 #flowrates are in ml/min, voltage in V, Current in Ampere
103 bounds = [(0.2,2.0),(10.0,15.0),(4.4,4.5)]
104 #step 6: grab the line 100 and f9
105 opter =Optimizer(bounds,base_estimator='gp',n_initial_points=3,acq_func="EI",random_state=np.random.randint(3326))
106
107
108 #step7: to selecte number of the cycles that you have to do the experiment and then grab the line 104 to 121 and f9: the closed loop experimentation
109 number_of_cycles =160
110 results = []
111 flowrates_1 = []
112 flowrates_2 = []
113 vs = []
114 currents = []
```

```
115
116    product_wavelength=True #set to true if product wavelengths being monitored
117
118    if product_wavelength == True:
119        val=1
120    else:
121        val=-1
122
123    # Step 8: Test Tubes on Printer
124    USE_PRINTER = True
125    REST_HEIGHT = 200
126    X_HOME = -5
127    Y_HOME = 20
128    Z_HOME = 175
129    DEFAULT_PUMP_TIME="1"
130    # Distance between test tubes
131    X_SPACING=20
132    Y_SPACING=20
133    # Number of test tubes
134    X_ROWS = 11
135    Y_COLUMNS = 4
136
137    def send_cmd(cmd):
138        print(cmd)
139        printer.write(f"{cmd}\n".encode("ASCII"))
140
141    def move(x=None, y=None, z=None):
142        s = "G0"
143        if x is not None:
144            s += f"X{x}"
145        if y is not None:
146            s += f"Y{y}"
147        if z is not None:
148            s += f"Z{z}"
149
150        s+= "F5000"
151        send_cmd(s)
152
153    def printer_positions():
154        for j in range(Y_COLUMNS):
155            for i in range(X_ROWS):
156                if j%2==1:
157                    yield (X_HOME + (X_ROWS - 1 - i) * X_SPACING, Y_HOME + j * Y_SPACING, Z_HOME)
158                else:
159                    yield (X_HOME + i * X_SPACING, Y_HOME + j * Y_SPACING, Z_HOME)
160
161    # Run this.
162    tube_location = list(printer_positions())
163
164    try:
165        for i in range(number_of_cycles):
166            move(*tube_location[2*i])
167            asked = opter.ask()
168            function(asked[0],asked[0],asked[1],asked[2])
169
170            move(*tube_location[2*i+1])
171            told= function2()
172
173            print(f"area under the curve in the round {i:.2f} = {told:.2f}")
174            opter.tell(asked,-told*val)
175            results.append(told)
176            flowrates_1.append(asked[0])
177            flowrates_2.append(asked[0])
178            vs.append(asked[1])
179            currents.append(asked[2])
180
181            dict1 = {"flowrate_1":flowrates_1,"flowrate_2":flowrates_2,"voltages":vs, "currents":currents,"area-results":results}
182            df2 = pd.DataFrame(dict1)
183            df2.to_csv("output round "+str(i)+".csv")
184    finally:
185        pump_1.write(b'off\r')
186        pump_2.write(b'off\r')
187
188
```

Fig. S6 Code for the 0.5M solution.

Table S2. Photo-flow auto-optimization reaction parameters boundary and optimized condition of 0.25 of **1a. Reaction condition: 1a** (0.25M in ACN), **NBS** (0.253M in ACN).

Parameter	Flow rates (mL/min^{-1})	Voltages (V)	Currents (I_{max})	Light power (W)	Res. time (min)	Cycles
Boundary	0.2–2.0	10.0–15.0	4.4–4.5	15–60	0.5–2.0	27

Optimized condition: 1a (0.25M in ACN), **NBS** (0.253M in ACN), residence time (1 min), under 60W blue light, gives 96%, corresponding to 102 equiv. of the photon, 0.98% quantum efficiency, and 1.98 gh^{-1} productivity.

Table S3 Photo-flow auto-optimization reaction parameters boundary and optimized condition of 0.5 of **1a**. **Reaction condition 2:** 0.5M of **1a** in ACN, 0.505M of **NBS** in ACN, photochemical auto-optimization.

Parameter	Flow rates (mL. min^{-1})	Voltages (V)	Currents (I_{max})	Light power (W)	Res. time (min)	Cycles
Boundary	0.2–2.0	10.0–5.0	4.4–4.5	15–60	0.5–4.0	160

Optimized condition: 1a (0.5M in ACN), **NBS** (0.505M in ACN), residence time (1 min), under 60W blue light, gives 84%, corresponding to 50.68 equiv. of the photons, 1.64% quantum efficiency, and 3.4 gh^{-1} productivity.

Supporting Video S1: The video represents the auto-optimization flow chart and online monitoring the product yield.

Scaleup of photoreactor:

After optimization, we scale up the photo-flow reactor from 1 mL to 5 mL (od = 1.58 mm, id = 1 mm, and l = 6.5 m) to enhance productivity and efficiency. Additionally, we changed the solvent from ACN to EA (Table 1, entry 10), which minimized waste during the workup stage to remove succinimide. Therefore, initially, we utilized **1a** (0.253 M in EA) and **NBS** (0.253 M in EA : ACN (4:1)) and conducted the reaction under optimized conditions from Table 2, with a flow rate of 2.5 mL for each solution, maintaining a 1.0 min residence time under 60W of blue light using the 5 mL PFA reactor, resulting in a 94% isolated yield. Similarly, we employed **1a** (0.5 M in EA) and **NBS** [0.505 M in EA : ACN (4:1)] under the same conditions, yielding a 78% isolated yield.

S2.5 Typical procedures for extraction and separation of the product in a photo flow bromination.
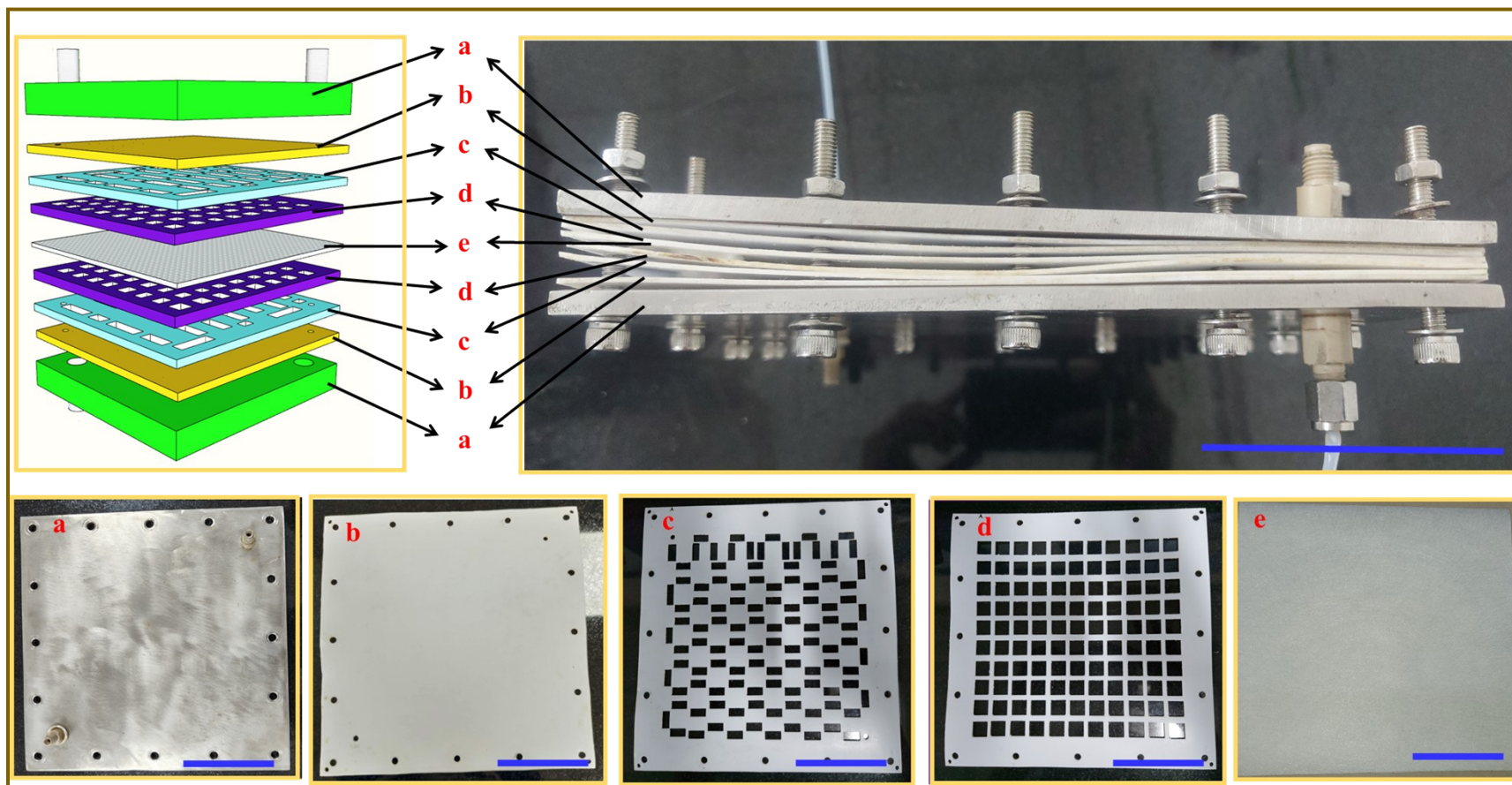
Fig. S7. Schematic diagram of liquid-liquid separator (A) 3D model (B) original photograph (a) SS metal holder (b) PTFE protection layer (c) direction channel (d) square well PTFE channel (e) polypropylene coated PTFE membrane, bar represents the 5 cm.

Fabrication of a pilot scale liquid-liquid separator: We employed a PTFE film laser ablation technique to make the proposed dual-channel device. The process started with 1 mm thick PTFE films subjected to UV laser ablation. This produced 110 square wells (12 mm width x 12 mm length) on one film and 109 rectangular wells (6 mm width x 15 mm length) on another, with 1 mm holes drilled at the corners for alignment. The ablated films were cleaned with acetone and dried. The device assembly involved placing a 0.45 μm pore, 47 mm diameter PTFE membrane (Whatman) between two PTFE film sheets matching the microchannel dimensions. This assembly was positioned in a nylon frame holder and aligned using metal bolts inserted through corner holes. Tightening the nylon frame holder with screws completed the device's sealing, resulting in the liquid-liquid separator's construction (**Fig. S6**).

Step 1: Photochemical reaction: A solution of **1a** (0.25 M in EA) and a solution of NBS [0.253 M in an EA: ACN (4:1)] were introduced into a microreactor equipped with a T-mixer (T_1) using syringe pumps. The flow rate of each solution was set at 2.5 mL min^{-1}, and they were allowed to flow into a 5.0 mL PFA reactor. The reaction mixture in the reactor was irradiated using a 60W blue LED.

Step 2: Formation of organic-aqueous droplets: Water was introduced into the reaction mixture after light exposure through a T-mixer (T_2).

Step 3: Extraction: The succinimide byproduct and ACN solvent in the reaction mixture were gradually moved to the aqueous droplet phase and real-time extraction through a PTFE capillary (od = 3.18 mm, id= 2.0 mm, l = 2.0 m, v = 6 mL).

Step 4: Complete separation: water was introduced into a T-mixer (T_2) to remove byproduct. The resulting mixture was then passed through a 6 mL PTFE coil reactor for extraction. The solution passed through a liquid-liquid separator (30 mL volume) developed and previously reported by our laboratory to facilitate extraction; for the aqueous waste removal of the crude organic solution

containing the brominated compound, a residence time of 2 min and a pressure of 1 bar were determined to be sufficient the crude organic solution analysis using LC-MS.

Table S4. Optimization of byproduct removal from aqueous-organic extraction work-up step.
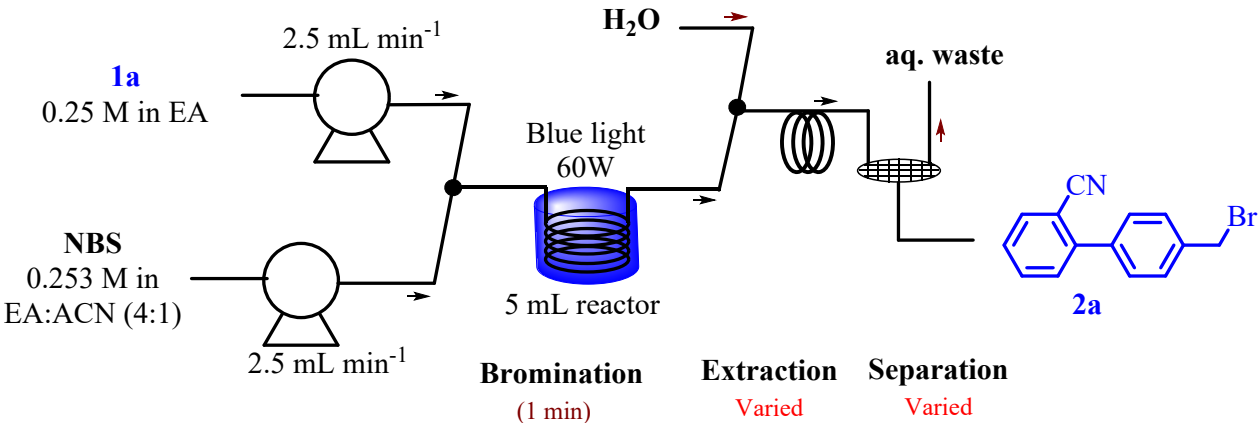
Entry	H$_2$O Flow rate (mL min^{-1})	Residence time (min)		Removal (%) of byproduct
		Extraction	**Separation**	
1	2	0.8	4.2	60
2	5	0.6	3	70
3	8	0.46	2.3	90
4	**10**	**0.4**	**2**	**99**
5	15	0.3	1.2	99

Reaction Condition: 1a (0.25 M in EA), NBS [0.25 M in EA: ACN (4:1)]; Extraction reactor (od = 3.18 mm, id = 2 mm, l= 2 m, v= 6mL); Separator volume 30 mL; byproduct removal from organic layer analysis by LC-MS and crude ^{1}H NMR.

S2.6 Procedure for the synthesis, extraction, and separation of the synthesis of 2.

A solution of **1** in (0.25 M in EA) and a solution of NBS [0.253 M in an EA: ACN (4:1)] are both solutions connected through the pump. Both reactants were introduced through a T-mixer (T_1) in a 2.5 mL min^{-1} flow rate to maintain the stoichiometry and then passed through a PFA tubing 5 mL to a homemade photo-flow reactor and used 60W blue light for the irradiation of light. As mentioned in auto-optimizing data, retention time 1.0 min., temperature 25±5 °C, power 60 W, and pressure 1 atm were the optimum reaction conditions. The light irradiation might generate heat; therefore, the reactor's temperature was maintained at room temperature by circulating chilled water. The out-flowing product mixture solution was further connected with the T-junction to remove the byproduct by introducing water (10 mL min^{-1}) to form organic-aqueous droplets. Complete extraction between organic-aqueous segments was accomplished for 0.4 min residence time by flowing through a 6 mL PTFE reactor. The complete separation was achieved by passing through the above-designed homemade liquid-liquid separator under 2.0 min. of residence time. The collected crude organic layer was dried over anhydrous Na$_2$SO$_4$, filtered, and concentrated under a vacuum. The compound was subsequently purified using silica gel column chromatography with a hexane/EA gradient (ranging from 100:0 to 100:10).

4'-(bromomethyl)-[1,1'-biphenyl]-2-carbonitrile (2a)

A solution of **1a** [0.25 M in EA (24.12 g in 500 mL)], and a solution of NBS [0.253 M in EA: ACN (4:1) (23.36 g in 500 mL)]. These stock solutions were introduced into a T-mixer at a flow rate of 2.5 mL min^{-1} for each solution and stoichiometry and then passed through a PFA 5 mL to a homemade photo-flow reactor and used 60W blue light for light irradiation. The out-flowing mixture for the

photo-flow reactor was further connected with the T-junction to remove the byproduct by introducing water (10 mL min^{-1}) to form organic-aqueous droplets. Complete extraction between organic-aqueous segments was accomplished for 0.4 min residence time by flowing through a 6 mL PTFE reactor. The complete separation was achieved by passing through the above-designed homemade liquid-liquid separator under 2.0 min. of residence time. The first 10 min reaction mixture was discarded, then collected for 2.5 h (675 mL), dried over anhydrous Na_2SO_4, filtered, and concentrated under a vacuum. The compound was purified using silica gel column chromatography with a hexane/EA gradient (100:10) to get 94% (23.97 g). The spectra data compared with those reported in the literature.[3] **Melting point:** 117 °C; **^{1}H NMR (400 MHz, CDCl$_3$):** δ 7.76 (dd, J = 7.8, 1.0 Hz, 1H), 7.64 (td, J = 7.7, 1.3 Hz, 1H), 7.56 – 7.48 (m, 5H), 7.45 (td, J = 7.6, 1.2 Hz, 1H), 4.54 (s, 2H); **^{13}C NMR (101 MHz, CDCl$_3$):** δ 144.70, 138.35, 138.20, 133.84, 132.96, 130.05, 129.46, 129.23, 127.86, 118.63, 111.22, 32.89; **IR (ν$_{max}$):** 3025, 2222, 1595, 1475, 1440, 1408, 1218, 881, 829, 756, 673 cm^{-1}; **HRMS(ESI):** m/z Calcd for **$C_{14}H_{10}NBrNa$** [M + Na] 293.9889, found 293.9880.

1-(bromomethyl)-4-iodobenzene (2b)
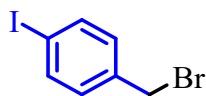
Compound **2b** was prepared according to the general procedure **S2.6**. The crude material was purified by silica gel column chromatography in hexane to provide a white solid (666 mg) with a 90% yield. The spectra data compared with those reported in the literature.[4, 5] **Melting Point:** 74 °C; **^{1}H NMR (400 MHz, CDCl$_3$):** δ 7.68 (d, J = 8.4 Hz, 2H), 7.13 (d, J = 8.3 Hz, 2H), 4.42 (s, 2H); **^{13}C NMR (101 MHz, CDCl$_3$):** δ 138.05, 137.51, 130.95, 94.29, 32.63; **IR (ν$_{max}$):** 3019, 2960, 2924, 1900, 1781, 1651, 1581, 1473, 1394, 1271, 1216, 1087, 1055, 1000, 949, 909, 812, 736 cm^{-1}.

1-bromo-4-(bromomethyl) benzene (2c)
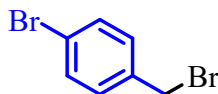
Compound **2c** was prepared according to the general procedure **S2.6**. The crude material was purified by silica gel column chromatography in hexane to provide a white solid (576 mg) with a 93% yield. The spectra data compared with those reported in the literature.[4, 5] **Melting Point:** 58 °C; **¹H NMR (400 MHz, CDCl₃):** δ 7.46 (d, J = 8.4 Hz, 2H), 7.25 (d, J = 8.4 Hz, 2H), 4.43 (s, 2H); **¹³C NMR (126 MHz, CDCl₃):** δ 136.91, 132.10, 131.96, 130.79, 128.27, 122.59, 32.52; **IR (ν_{max}):** 3019, 2961, 2920, 1903, 1589, 1485, 1435, 1403, 1221, 1012, 826, 755 cm⁻¹.

1-(bromomethyl)-4-chlorobenzene (2d)
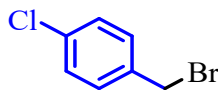
Compound **2d** was prepared according to the general procedure **S2.6**. The crude material was purified by silica gel column chromatography in hexane to provide a white solid (466 mg) with a 91% Yield. The spectra data compared with those reported in the literature.[4, 5] **Melting Point:** 46 °C; **¹H NMR (400 MHz, CDCl₃):** δ 7.32 (s, 4H), 4.45 (s, 2H); **¹³C NMR (151 MHz, CDCl₃):** δ 136.41, 134.41, 130.50, 129.12, 32.53; **IR (ν_{max}):** 3060, 1906, 1783, 1713, 1595, 1488, 1406, 1282, 122, 1087, 1014, 874, 829 759 cm⁻¹.

1-(bromomethyl)-4-benzonitrile (2e)
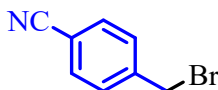
Compound **2e** was prepared according to the general procedure **S2.6**. The crude material was purified by silica gel column chromatography in hexane to provide a white solid (465 mg) with a 95% yield.

The spectra data compared with those reported in the literature.[4][5] **Melting Point:** 115 °C; **^{1}H NMR (400 MHz, CDCl$_3$):** δ 7.64 (d, J = 8.3 Hz, 2H), 7.50 (d, J = 8.3 Hz, 2H), 4.47 (s, 2H); **^{13}C NMR (101 MHz, CDCl$_3$):** δ 142.93, 132.68, 129.82, 118.47, 112.30, 31.60; **IR (ν_{max}):** 2915, 2223, 1604, 1502, 1410, 1286, 1219, 1098, 841, 816, 764 cm^{-1}.

1-(bromomethyl)-4-nitrobenzene (2f)
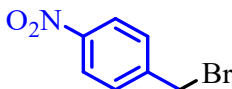
Compound **2f** was prepared according to the general procedure **S2.6**. The crude material was purified by silica gel column chromatography in hexane to provide a white solid with a 90% (486 mg) yield. The spectra data compared with those reported in the literature.[4, 5] **Melting Point:** 87 °C; **^{1}H NMR (400 MHz, CDCl$_3$):** δ 8.21 (d, J = 8.8 Hz, 2H), 7.56 (d, J = 8.7 Hz, 2H), 4.52 (s, 2H); **^{13}C NMR (126 MHz, CDCl$_3$):** δ 147.83, 144.90, 130.06, 124.19, 31.05; **IR (ν_{max}):** 2922, 2856, 1607, 1536, 1458, 1381, 1348, 1226, 1099, 858, 801, 760, 695 cm^{-1}.

1-(bromomethyl)-3-iodobenzene (2g)
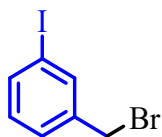
Compound **2g** was prepared according to the general procedure **S2.6**. The crude material was purified by silica gel column chromatography in hexane to provide a white solid (629 mg) with an 85% yield. The spectra data compared with those reported in the literature.[4] The spectra data compared with those reported in the literature.[6] **Melting Point:** 46 °C; **^{1}H NMR (400 MHz, CDCl$_3$):** δ 7.74 (t, J = 1.6 Hz, 1H), 7.63 (dd, J = 7.9, 1.1 Hz, 1H), 7.35 (d, J = 7.7 Hz, 1H), 7.07 (t, J = 7.8 Hz, 1H), 4.39 (s, 2H); **^{13}C NMR (126 MHz, CDCl$_3$):** δ 139.96, 137.92, 137.47, 130.48, 128.32, 94.32, 31.96; **IR (ν_{max}):** 3012, 2921, 2857, 1737, 1462, 1377, 1218, 1079, 973, 835, 764, 689 cm^{-1}.

1-(bromomethyl)-3-iodo-5-methylbenzene (2h)
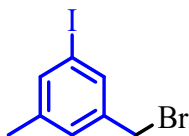
Compound **2h** was prepared according to the general procedure **S2.6**. The crude material was purified by silica gel column chromatography in hexane to provide a white solid (635 mg) with 82% yield. The spectra data compared with those reported in the literature.[4] **¹H NMR (500 MHz, CDCl₃):** δ 7.53 (s, 1H), 7.46 (s, 1H), 7.15 (s, 1H), 4.35 (s, 2H), 2.29 (s, 3H); **¹³C NMR (101 MHz, CDCl₃):** δ 140.70, 139.64, 138.14, 134.98, 129.24, 94.29, 32.16, 20.95; **IR (ν$_{max}$):** 3021, 2955, 2913, 2855, 1595, 1563, 1438, 1374, 1255, 1208, 1121, 1039, 994, 879, 851, 793, 761, 692 cm⁻¹.

1-(bromomethyl)-3,5-dimethylbenzene (2i)
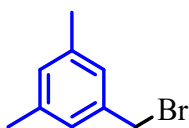
Compound **2i** was prepared according to the general procedure **S2.6**. The crude material was purified by silica gel column chromatography in hexane to provide a white solid (408 mg) with a 65% yield. The spectra data compared with those reported in the literature.[7] **¹H NMR (500 MHz, CDCl₃):** δ 7.03 (s, 2H), 6.95 (s, 1H), 4.45 (s, 2H), 2.32 (s, 6H); **¹³C NMR (126 MHz, CDCl₃):** δ 138.46, 137.65, 130.23, 126.88, 33.96, 21.24; **IR (ν$_{max}$):** 3017, 2959, 2917, 2863, 1774, 1606, 1525, 1463, 1379, 1303, 1212, 1161, 1118, 1035, 944, 849, 759, 699, 630 cm⁻¹.

1-(bromomethyl)-2-iodobenzene (2j)
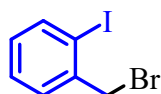
Compound **2j** was prepared according to the general procedure **S2.6**. The crude material was purified

by silica gel column chromatography in hexane to provide a white solid (600 mg) with 81% yield. The spectra data compared with those reported in the literature.[8] **Melting Point:** 53 °C; **¹H NMR (400 MHz, CDCl₃):** δ 7.86 (dd, J = 7.9, 1.1 Hz, 1H), 7.48 (dd, J = 7.7, 1.6 Hz, 1H), 7.34 (td, J = 7.5, 1.2 Hz, 1H), 6.98 (td, J = 7.7, 1.7 Hz, 1H), 4.60 (s, 2H); **¹³C NMR (101 MHz, CDCl₃):** δ 140.31, 140.20, 130.61, 130.20, 129.00, 100.18, 38.90; **IR (ν_max):** 3057, 2922, 2855, 1573, 1465, 1438, 1277, 1014, 813, 756, 721, 655 cm⁻¹.

1-(bromomethyl)-2-benzonitrile (2k)
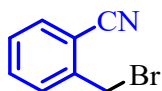
Compound **2k** was prepared according to the general procedure **S2.6**. The crude material was purified by silica gel column chromatography in hexane: EA (98:2) to provide a white solid (523 mg) with an 85% yield. The spectra data compared with those reported in the literature.[9] **Melting Point:** 74 °C; **¹H NMR (500 MHz, CDCl₃):** δ 7.66 (dd, J = 7.7, 1.0 Hz, 1H), 7.58 (dtd, J = 9.1, 7.8, 1.3 Hz, 2H), 7.42 (td, J = 7.5, 1.5 Hz, 1H), 4.64 (s, 2H); **¹³C NMR (101 MHz, CDCl₃):** δ 141.24, 133.39, 133.31, 130.59, 129.07, 116.87, 112.55, 29.45; **IR (ν_max):** 3026, 2229, 1721, 1601, 1488, 1449, 1295, 1222, 830, 764, 670 cm⁻¹.

1-(bromomethyl)-2-nitrobenzene (2l)
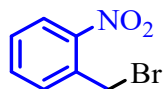
Compound **2l** was prepared according to the general procedure **S2.6**. The crude material was purified by silica gel column chromatography in hexane: EA (98:2) to provide a pale-yellow liquid (378 mg) with a 70% yield. The spectra data compared with those reported in the literature.[10] **¹H NMR (400 MHz, CDCl₃):** δ 8.02 (dd, J = 8.2, 1.2 Hz, 1H), 7.65 – 7.55 (m, 2H), 7.52 – 7.43 (m, 1H), 4.82 (s, 2H); **¹³C NMR (151 MHz, CDCl₃):** δ 148.02, 133.83, 132.85, 132.62, 129.73, 125.55, 29.01; **IR**

(v_{max}): 2924, 2859, 1574, 1529, 1440, 1349, 1308, 1225, 860, 791, 753, 700, 668, cm⁻¹.

2-bromo-1-(bromomethyl)-3-methylbenzene (2m)

Compound **2m** was prepared according to the general procedure **S2.6**. The crude material was purified by silica gel column chromatography in hexane to provide a white solid (443 mg) with a 72% yield.[11] **¹H NMR (400 MHz, CDCl₃):** δ 7.26 (t, J = 4.5 Hz, 1H), 7.21 – 7.12 (m, 2H), 4.62 (d, J = 1.0 Hz, 2H), 2.41 (s, 3H); **¹³C NMR (101 MHz, CDCl₃):** δ 139.49, 137.39, 131.06, 128.76, 127.34, 127.13, 34.75, 23.88; **IR (v_{max}):** 3054, 2973, 2853, 1578, 1447, 1382, 1262, 1212, 1166, 1026, 933, 863, 773, 718 cm⁻¹.

1-bromo-2-(bromomethyl) naphthalene (2n)
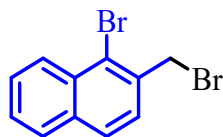
Compound **2n** was prepared according to the general procedure **S2.6**. The crude material was purified by silica gel column chromatography in hexane to provide a white solid (568 mg) with 76% yield.[12, 13] **Melting Point:** 101 °C; **¹H NMR (400 MHz, CDCl₃):** δ 8.37 – 8.28 (m, 1H), 7.84 – 7.74 (m, 2H), 7.60 (ddd, J = 8.4, 6.9, 1.4 Hz, 1H), 7.53 (ddd, J = 13.7, 7.6, 4.1 Hz, 2H), 4.85 (s, 2H); **¹³C NMR (101 MHz, CDCl₃):** δ 135.05, 134.26, 132.63, 128.44, 128.28, 127.98, 127.85, 127.75, 127.33, 125.09, 34.91; **IR (v_{max}):** 3044, 1597, 1556, 1499, 1329, 1260, 1213, 1108, 1028, 979, 861, 812, 757, 722, cm⁻¹.

9-bromo-9H-fluorene (2o)
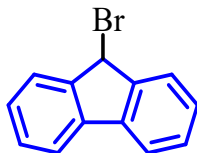
Compound **2o** was prepared according to the general procedure **S2.6**. The crude material was purified by silica gel column chromatography in hexane to provide a white solid (539 mg) with 88% yield.[14]

Melting Point: 105 °C; **^{1}H NMR (400 MHz, CDCl$_3$):** δ 7.66 (t, J = 8.1 Hz, 4H), 7.39 (td, J = 7.4, 0.9 Hz, 2H), 7.34 (td, J = 7.4, 1.2 Hz, 2H), 6.00 (s, 1H); **^{13}C NMR (126 MHz, CDCl$_3$):** δ 144.15, 139.78, 129.20, 128.07, 126.35, 120.25, 46.03; **IR (ν_{max}):** 3030, 1607, 1447, 1217, 1186, 1133, 940, 854, 764, 736, 647 cm^{-1}.

S2.7 Lab-scale solar tracker panel reactor platform for a photochemical reaction for the synthesis of 2a.

Solar radiation was crucial as early earth's primary light source. Harnessing solar energy in continuous-flow chemical processes offers the advantage of minimizing or eliminating harmful emissions during chemical and API production. While extensive research for API synthesis, the use of solar light for API intermediate synthesis still needs to be explored. This is primarily due to the challenges associated with natural variations in solar radiation, climate conditions, cloud cover, and sun positioning, all of which can impact photocatalytic performance and deter researchers in this field. Our laboratory has previously developed and reported on a solar panel tracker reactor designed to address these challenges, facilitating efficient solar reactions.[15] A solution of **1a** in ACN (0.5 M) and solution of NBS in ACN (0.505 M) and both solution were introduced into a T-mixer at a flow rate of 1.5 mL min^{-1} for each solution and then passed through the (od =1.58, id = 1mm, l = 10.2 mm, vol = 8 mL) reactor and subjected to sunlight irradiation while testing various flow rates (**Table S5, entry 1-5**). It was found that a flow rate of 5 mL min^{-1} for each solution was sufficient to achieve a yield of 96% of **2a** (**Table S5, entry 5**). Subsequently, we increased the reactor volume (od =1.58, id = 1mm, l = 20.4 mm, vol. = 16 mL) and continued to flow both solutions under sunlight irradiation, exploring various flow rates (**Table S5, entry 6-11**). A 15 mL min flow rate^{-1} for each solution was observed with an optimal 92% isolated yield of **2a** (**Table S5, entry 9**).

Table S5: Optimization of lab-scale solar tracker smart flow platform for synthesis of **2a**.
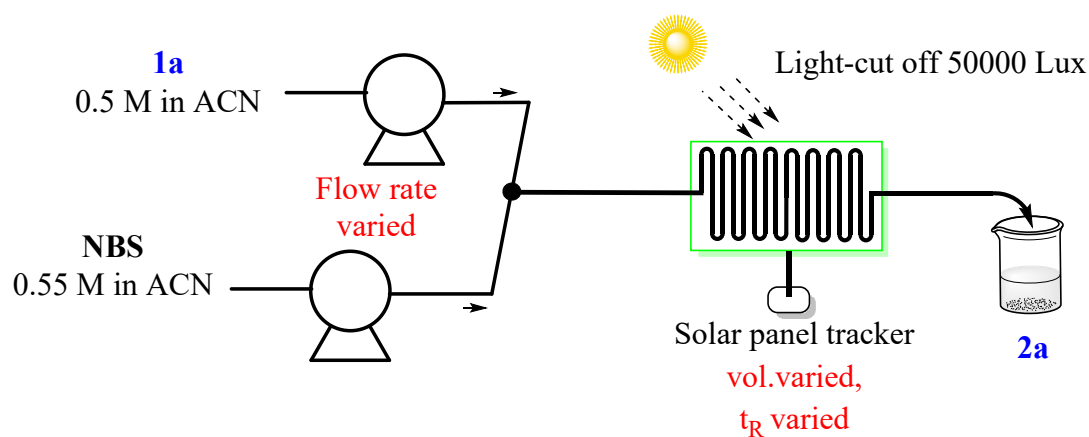
| Entry | Flow rate (mL min⁻¹) | | Res. time | Yield |
	Solution A	Solution B	(Seconds)	(%)^b
1	1.5	1.5	160	90
2	2	2	150	91
3	2.5	2.5	96	93
4	4	4	60	92
5	5	5	48	93
6^a	10	10	48	93
7^a	12.5	12.5	38	94
8^a	14	14	34	95
9^a	**15**	**15**	**32**	**97 (92)^c**
10^a	17.5	17.5	27	85

Reaction Condition: 0.5 M of **1a** in ACN, 0.505 M of NBS in ACN, (od = 1.58, id = 1mm, l = 10.2 m, v = 8 mL) solar tracker panel reactor, (a) (od = 1.58, id = 1mm, l = 20.4 m, v = 16 mL) solar tracker panel reactor; (c) yields calculated on the crude LC-MS analysis yield in parenthesis indicated isolated yield. The outdoor experiment date is 14/06/23, time 11.00-12.00 am.

S2.8 General procedure of lab-scale solar tracker smart flow platform for synthesis of 2a.

A solution of **1a** in ACN [0.5 M (724 g in 7.5L)], and a solution of NBS in ACN [0.5 M (674 g in 7.5L)]. These stock solutions were introduced into a T-mixer at a flow rate of 15 mL min^{-1} for each solution and then passed through the (od =1.58, id = 1mm, l = 20.4 mm, vol. = 16 mL) solar tracker reactor for light irradiation. The first two-min reaction mixture was discarded, then collected for 8 h (outdoor experiment date 16/06/2023, time 9.00 am to 5 pm), and ACN was distilled out from the reaction mixture up to 80%. Then, add water, get precipitated, and wash two times with hot water to remove the byproduct. Then, the precipitate dissolved in EA, dried over anhydrous Na_2SO_4, filtered, and concentrated under a vacuum. The compound was purified using silica gel column chromatography with a hexane/EA gradient (100:10) to get 92% isolated yield and 896 g product with (112 h^{-1}) productivity.

S2.9 Fabrication and Optimization of pilot-scale solar tracker panel reactor platform for a photochemical reaction.

(a)

Rorating base plate

Stepper motor

Solar tracker platform

Supported SS mesh sheet

Photoreactor volume l.0 L (od 1/4, id 4mm, 83m)

Photoreactor mounted on SS mesh sheet

Contineous flow pilot scale solar tracker reactor

(b)

1. Stock solution of reactant
2. Continuous Syringe Pumps
3. Syringes
4. Solenoid valve
5. LDR
6. T-junction
7. Mixing reactor
8. 7. 1/8 to 1/4 extender
9. Photoreactor 1L
10. Supported SS-mesh sheet
11. Tracker switch
12. Stepper motor
13. parabolic antenna
14. Product collector

Fig. S8. (a) Schematic representation of fabrication of continuous flow pilot scale solar tracker reactor; (b) Schematic representation of total assembly of pilot scale solar tracker reactor.

For the development of a pilot-scale solar tracker reactor, we have modified our previously developed solar panel tracker. Initially, for the fabrication of the solar tracker flow reactor, we utilized a parabolic dish with a rotating cylindrical base. A stepper motor with a torque of 66 Kg-cm was procured from the local market and securely attached to the rotating cylindrical base of the parabolic dish. Concurrently, we utilized a round-shaped stainless steel mesh sheet, 1 mm thick. PFA tubing reactor (od = 1/4, id = 4 mm, l = 83m, vol. = 1.0 L) incorporated over

the SS mesh sheet in circular manner. The entire assembly was then firmly affixed to the parabolic dish. Following meticulous fabrication, all components were interconnected using screws to ensure robustness and structural stability (Figure S9a). Next, the solar tracker reactor was integrated with all components, including continuous syringe pumps, a T-mixer, solenoid valve, an LDR (light-dependent resistor), and a 10 mL reactor for mixing, 1/8 to 1/4 extender as illustrated in (Figure S9b). Assured of the working of the integrated pilot-scale solar panel reactor, we were interested in testing the application of the reactor for photo-bromination. A solution of **1a** in ACN (0.5 M) and solution of NBS in ACN (0.505 M) and both solutions were introduced into a T-mixer at a varied flow rate for each solution and then passed through the (od = 1/4, id = 4 mm, l = 83m, vol. = 1.0 L) reactor and subjected to sunlight irradiation (**Table S6,**). It was found that a flow rate of 100 mL min^{-1} for each solution was sufficient to achieve a yield of 93% of **2a** (**Table S5, entry 2**). After optimization, we performed a long-term experiment to ensure the stability of the reactor. Stock solutions of **1a** in 0.5 M ACN and 0.505 M NBS in ACN were introduced into a T-mixer at a flow rate of 100 mL min-1, with each solution having a residence time of 5 minutes. The mixture then passed through the solar tracker 1.0 L reactor for light irradiation (outdoor experiment date 21/12/2023, time 10.00 am to 4 pm). The initial 10-min reaction mixture was discarded, and the subsequent reaction mixture was collected for 6 hours. ACN was then distilled from the reaction mixture until reaching 80% concentration. Water was added to precipitate the desired product, which was subsequently washed twice with hot water to remove any byproducts. After recrystallization, a yield of 93% and a productivity of 769 g h^{-1} were achieved.

Supporting video S2: The current video represent the reaction performing under the sun-light with   help   of   the   solar   panel   electromechanical   flow   reactor.

Table S5: Optimization of pilot-scale solar tracker smart flow platform for synthesis of **2a**.
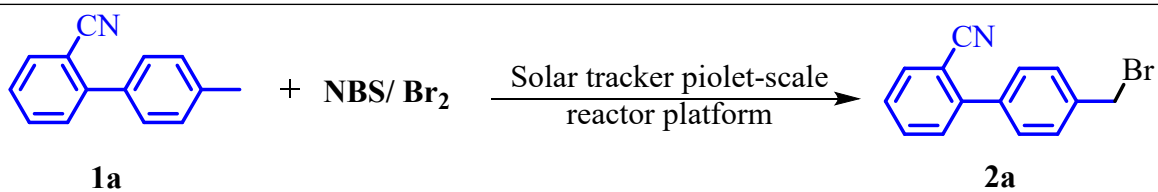
Sr No	Flow rate (mL/h)		Res. time	2a
	1a	NBS	(min)	Yield (%)
1	50	50	10	95
2	100	100	5	93

Reaction condition: 0.5 M of formula **1a** in ACN, 0.505 M of NBS in ACN, (od = 1/4, id = 4mm, l = 83 m, v = 1.0 L); yields calculated on the crude ^{1}H NMR analysis.

S2.10 Quantum efficiency (φ) calculation:

The values of the number of incident photons ($N_{photons}$) were calculated using the following equations. Here,

$$N_{photon} = \frac{P\lambda t}{hc}$$

Area of lamp (a) = 448 cm^2 = 352 x 10^{-4} m^2

Power of the light (p) = 60W = 60 $J\ s^{-1}$

λ = Wavelength of the light (420 nm) = 420 x 10^{-9} m

t = Duration of irradiation time, 1 h. = 3600 s,

h = Planck's constant = 6.626 x 10^{-34} J s

c = Velocity of light = 3 x 10^8 m s^{-1}

No of photons incident per hour

$$N_{photon} = \frac{60\ J\ s^{-1} \times 420 \times 10^{-9}\ m \times 3600\ s}{6.626 \times 10^{-34}\ J\ s \times 3 \times 10^8\ m\ s^{-1}}$$

$$N_{photon} = 4.563 \times 10^{23}$$

$$Mole's\ photons\ incident\ per\ hour = \frac{N_{photon}}{N}$$

[N = Avogadro's number (6.02214 × 10^{23})]

$$Mole's\ photons\ incident\ per\ hour = \frac{4.563 \times 10^{23}}{6.02214 \times 10^{23}}$$

$$Mole's\ photons\ incident\ per\ hour = 0.758\ mole$$

Moles of product formed per hour is:

$$Mole's\ of\ product\ formed\ per\ hour = \frac{productivity/h}{mole.wt}$$

The product formed per hour is = 9.59 g/h.

$$of\ Mole's\ of\ product\ formed\ per\ hour = \frac{9.59}{272}$$

$$Mole's\ of\ product\ formed\ per\ hour = 3.526 \times 10^{-2}$$

Quantum efficiency (ϕ):

$$Quantum\ efficiency\ (\emptyset): = \frac{Mole's\ of\ product\ formed}{Mole's\ photons\ incident} \times 100$$

$$Quantum\ efficiency\ (\emptyset): = \frac{3.526 \times 10^{-2}}{0.758} \times 100$$

$$Quantum\ efficiency\ (\emptyset): = 4.65\ \%$$

S3.0 Nucleophilic substitution reaction for C-N coupling

S3.1 Optimization of Nucleophilic substitution reaction for the synthesis of Losartan intermediates (4a).
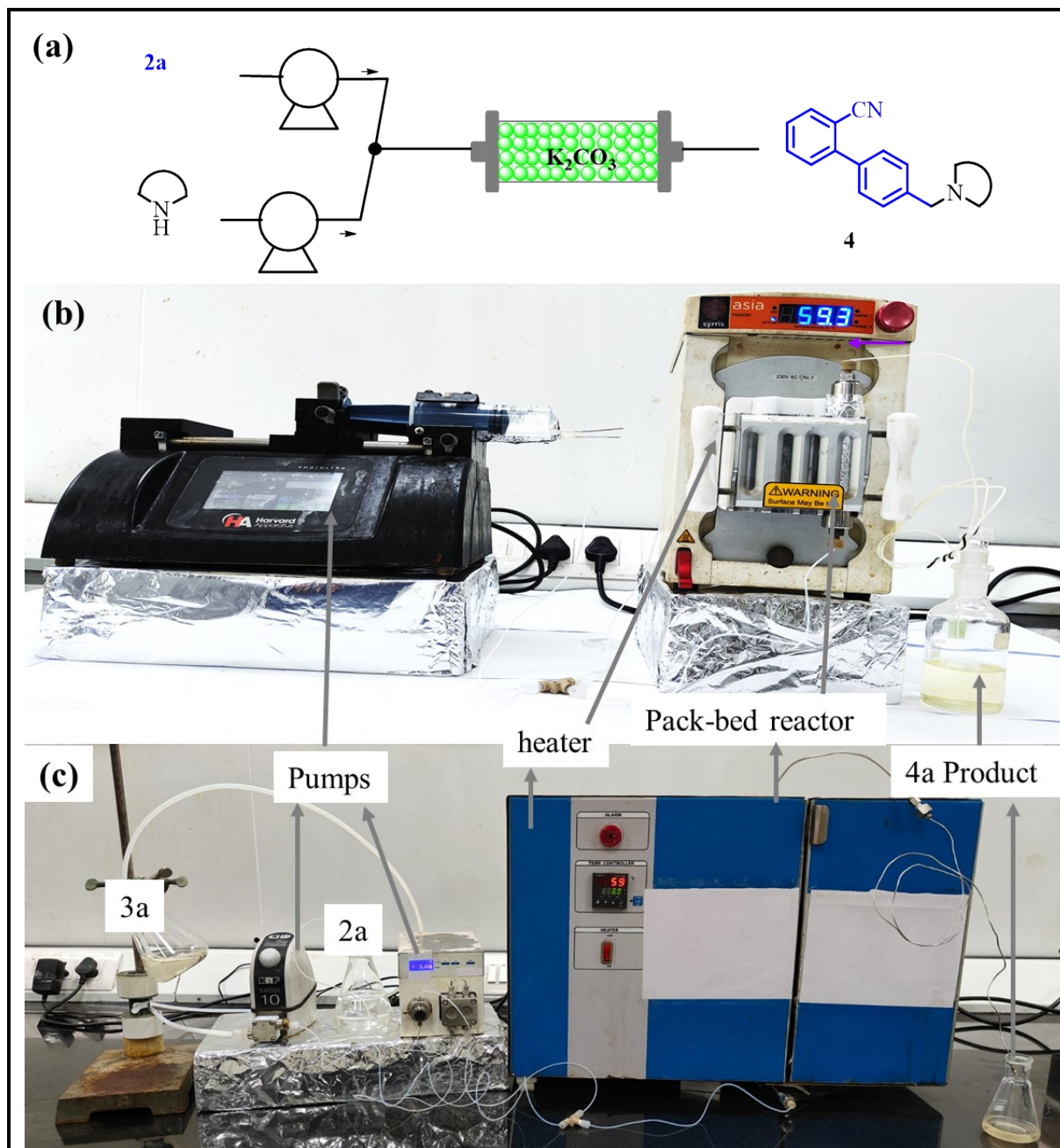
Fig. S9: (a) Blueprint of set-up for the nucleophilic substitution reaction (b) digital photograph of set-up for the nucleophilic substitution reaction using 7 mL packed bed reactor; (c) digital photograph of set-up for the nucleophilic substitution using 100 mL packed bed reactor.

A stock solution **2a** in EA (0.1 M) and **3a** in DMF (0.105 M) and these two solutions were introduced into a T-mixer with variable flow rates to maintain the stoichiometric ratio passed through to a packed bead reactor containing K_2CO_3 (id = 7 mm, l = 150 mm, vol. = 7 mL free vol. 2.0 mL) with varied residence time, temperature, base and packed bed reactor size, etc. for the reaction to occur. After optimization, we obtained a flow rate of 5 mL min^{-1} for both solutions passing through a 100 mL SS-packed bed reactor (id = 22 mm, l = 270 mm, v = 100 mL, free vol. K_2CO_3 filling = 34 mL), at 60 °C temperature and a 3.4 min residence time was enough to give a maximum isolated yield of 89% for compound **4a**, with a 10 g/h productivity **(Table S7, entry 13)**.

Table S7 Optimization table of the nucleophilic substitution for the synthesis of **3a**.
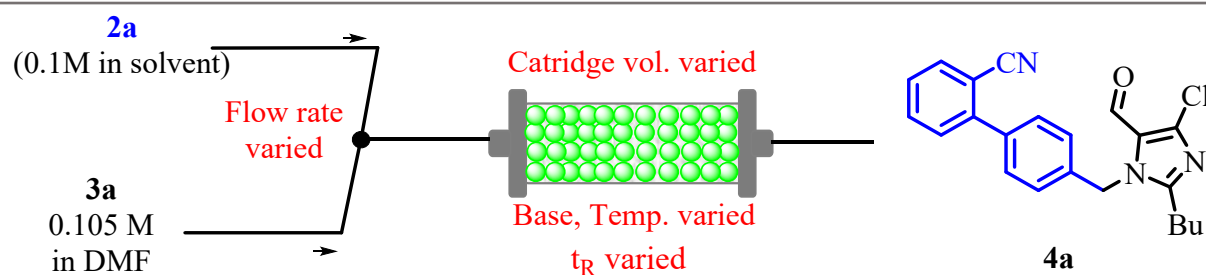
Entry	Flow rate (mL min⁻¹)		Temp ºC	Res. time (min)	Yield (%)
	2a	3a			
1	0.2	0.2	25	5.0	40
2	0.2	0.2	50	5.0	70
3	0.2	0.2	60	5.0	80
4	0.2	0.2	80	5.0	80
5	0.15	0.15	60	6.67	96
6[a]	0.15	0.15	25	6.67	30
7[b]	0.15	0.15	60	6.67	30
8[c]	0.15	0.15	60	6.67	53
9[d]	0.15	0.15	60	6.67	92
10[e]	0.15	0.15	60	6.67	65
11[f]	0.15	0.15	60	6.67	50
12[g]	3.0	3.0	60	5.67	95
13[g]	4.0	4.0	60	4.25	96
14[g]	**5.0**	**5.0**	**60**	**3.4**	**95 (89)**
15[g]	7.5	7.5	60	2.27	70

Reaction condition: 0.1 M of **2a** in EA and 0.105 M of **3a** in DMF, 7.0 mL SS packed bed reactor (id = 6 mm, l = 150 mm, free vol. 2.0 mL), K_2CO_3; (a) KOH, (b) Na_2CO_3; (c) Amberlyst 15 hydroxide; (d) toluene; (e) acetone; (f) ACN; (g) 100 mL SS packed bed reactor (id = 22 mm, l = 270 mm, v = 100 mL, free vol. K_2CO_3 filling 34 mL),); yield based on the crude LC-MS analysis; yield in parenthesis indicated isolated yield.

S3.2 Pilot scale synthesis of 4a..

Initially, we take a solution of **2a** (0.25 M in DMF), and **3a** (1.05 eq.). and pass this solution with a flow rate of 100 mL min^{-1} into the 1.0L SS-packed bed reactor (od id = 22 mm, l = 270 mm, v = 100 mL, free volume after 1 kg K_2CO_3 filling = approx. 400 mL) for the nucleophilic substitution reaction we get 82% yield of **4a**. Then we performed various reaction conditions with variable flow rate and concentration of the solution. (Table S8) After optimization, we obtained a **2a** (0.5 M in DMF), and **3a** (1.05 eq.) solution with a flow rate of 70 mL min^{-1} passing through a 1L SS-packed bed reactor (id = 22 mm, l = 270 mm, v = 100 mL, free vol. K_2CO_3 filling = 400 mL), at 60 °C temperature and a 5.71 min residence time was enough to give a maximum isolated yield of 96% for compound **4a**, with a g/h productivity (**Table S8, entry 4**).

Table S8. Optimization of large-scale synthesis of losartan intermediates **4a**.
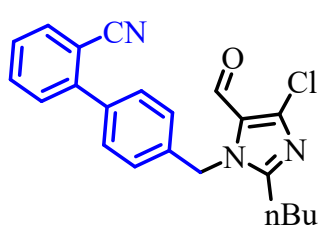
Entry	Flow rate (mL.min⁻¹)	Res. time (min)	4a Yield (%)
1	100	4.0	82
2	75	5.33	94
3[a]	75	5.33	92
4[a]	70	5.710	96

Reaction Condition: 2a (0.25 M in DMF), and **3a** (1.05 eq.). and pass this solution with a flow rate of 100 mL min⁻¹ into the SS-packed bed reactor (od 74mm id = 64 mm, l = 300 mm, v = 1.0 L, free volume after 1 kg K_2CO_3 filling = approx. 400 mL); a) **2a** (0.5 M in DMF), and **3a** (1.05 eq.); yield based on crude ^1H NMR analysis.

S3.3 Long-term experiment of K$_2$CO$_3$.
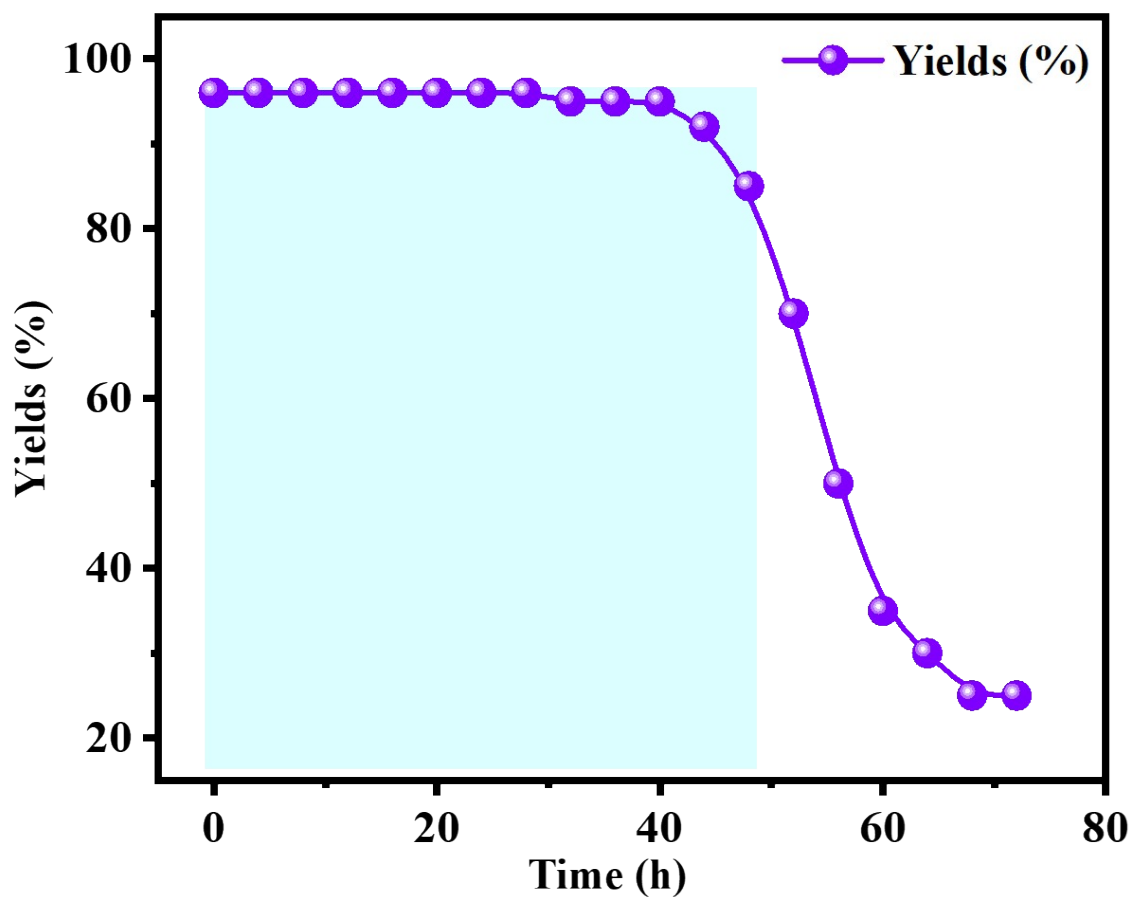
Fig. S10 Schematic presentation of intermediate **4a** syntheses in continuous catalytic manner: reaction condition: stock solution of **2a** (0.1 M in EA; stock solution of 3a (0.105 M in DMF); packed bead K$_2$CO$_3$ cartridge (K$_2$CO$_3$ weight = 7.2 gm) (id = 7 mm, l = 150 mm, vol. = 7 mL) at 60 $^\circ$C; yields are determined by LC-MS analysis, at least three measurements were taken to obtain an average yield.

S3.4 General procedures for the continuous flow nucleophilic substitution for the synthesis of various sartan intermediates (4).

A stock solution **2a** in EA (0.1 M) and **3** in DMF (0.105 M) these two solutions were introduced into a T-mixer with each flow rate of 5 mL min^{-1} to maintain the stoichiometric ratio and then passed through a 100 mL SS-packed bed reactor (id = 22 mm, l = 270 mm, v = 100 mL, free vol. K_2CO_3 filling 34 mL) at 60 °C temperature and a 3.4 min residence time was a complete reaction. The product was collected in a cold-water reservoir and extracted with EA. The organic layer was washed twice with water, dried over anhydrous Na_2SO_4, filtered, and concentrated under a vacuum. The compound was further purified by silica gel column chromatography.
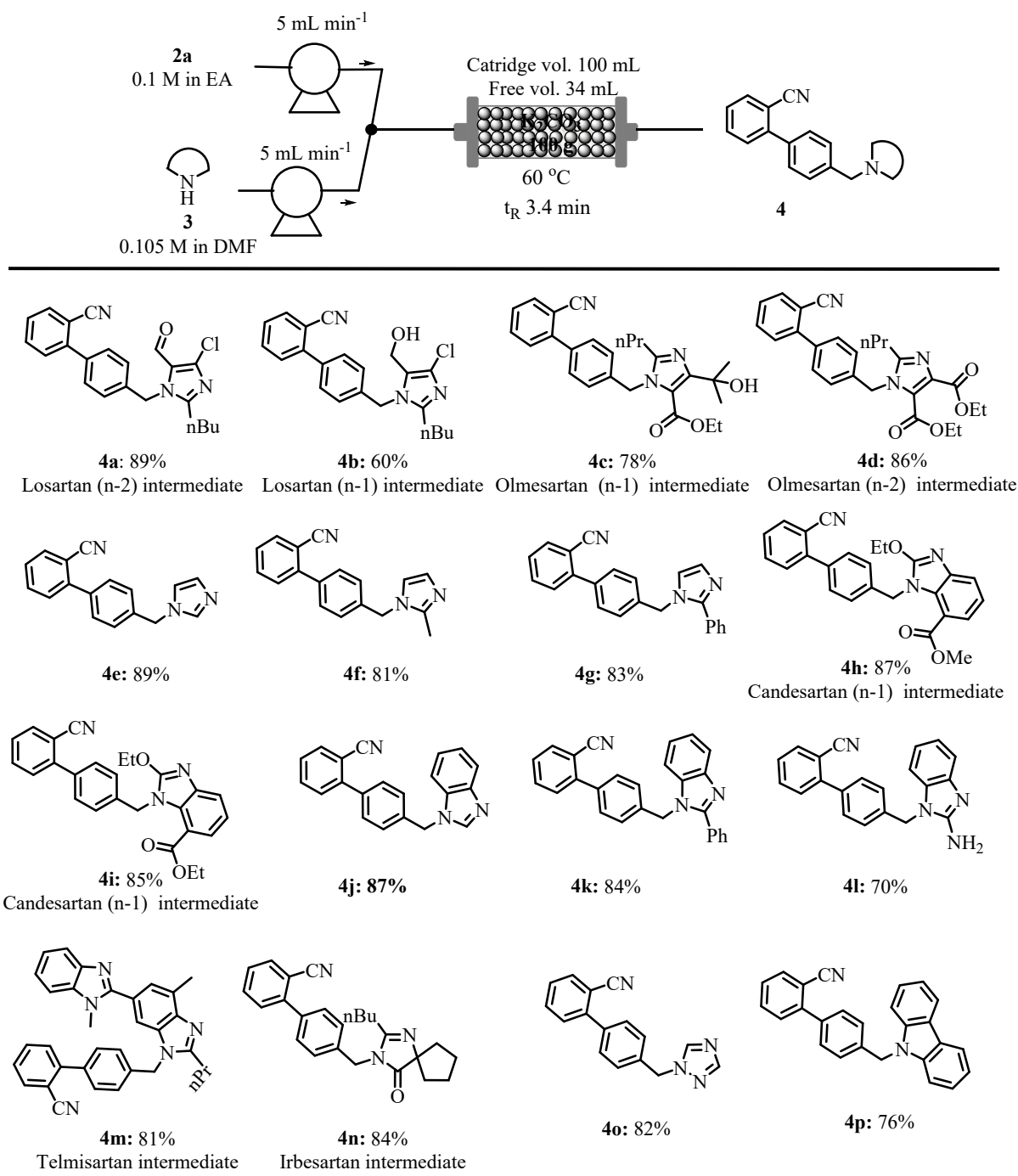
Fig. S11 Various scope of substrates of nucleophilic substitution; reaction condition: 0.1 M of **2a** in EA, 0.105 M of **3** in DMF, a 100 mL SS-packed bed (id = 22 mm, l = 270 mm, v = 100 mL, free vol. K_2CO_3 filling 34 mL) reactor, t_R of 3.4 min, temp. 25 °C ± 5 °C, yield based on the   isolated   yield.

S4.1 Fully integrated continuous flow platform for the synthesis of losartan intermediates (4a).

Using two separate pumps, the outflowing crude mixture from separator **2a** in EA (approximately 0.13M) and stock solution **3a** in DMF (0.136 M) were introduced into a T-mixer (T_3). The combined mixture passed through a 100 mL SS-packed bed (id = 22 mm, l = 270 mm, v = 100 mL, free vol. K_2CO_3 filling 34 mL) reactor for the nucleophilic substitution reaction. The flow rates of **2a** & **3a** have varied to maintain the stoichiometry (Table S9). A residence time of 3.8 min and a temperature of 60 °C were enough to synthesize compound **4a**. The regular extraction and purification process provided compound **4a** in 82% isolated yield.

Table S9. Optimization of an integrated platform for the Wohl Ziglar Bromination and Nucleophilic Substitution.
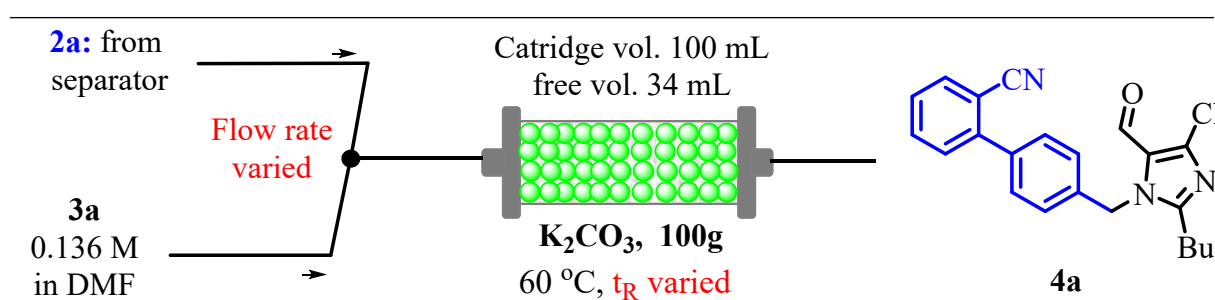
Entry	Flow rate (mL/min)		Res. time (min)	4a Yield (%)
	2a	3a		
1	4.0	4.0	4.25	84
2	5.0	5.0	3.4	77
3	**4.5**	**4.5**	**3.8**	**82**
4	6.0	6.0	2.8	71

Reaction Condition: 2a from separator (approximately 0.13 M in EA); **3a** (0.136M) in DMF; 100 mL SS-packed bed (id = 22 mm, l = 270 mm, v = 100 mL, free vol. K_2CO_3 filling 34 mL) reactor; yield based on isolated yield.

S4.2 General procedure of fully integrated continuous flow platform the synthesis of various sartan intermediates (4a).

A stock solution of **1** (0.25 M in EA) and a solution of NBS [0.253 M in EA: ACN (4:1)] was introduced flow rate each solution at 2.5 mL min^{-1} into T-mixer (T$_1$) using syringe pumps pass through a 5.0 mL PFA reactor for the blue light exposure using a 60 W blue LED with 1 min residence time. After completion of the reaction, water was introduced into a T-mixer (T$_2$) to remove succinimide impurities. Complete removal of succinimide byproduct was observed with 0.4 min residence time by flowing through a PTFE coil (od = 3.18, id = 2.0 mm, l =2.0 m, v = 6 mL) reactor. Further, the organic-aqueous segment was separated by passing through the above-designed homemade membrane-based liquid-liquid separator, and complete separation was achieved with a residence time (2.0 min) and flow rate of water (10 mL min^{-1}) at 25°C. After extraction and separation, the outflowing crude solution of product **2a** was connected to one pump, while another was connected to the stock solution of **3** [0.136 M in DMF]. Both solutions were introduced at T-mixer (T$_3$), each flowing at a 4.5 mL min^{-1} flow rate. The combined mixture then passed through a 100 mL SS-packed bed reactor (id = 22 mm, l = 270 mm, v = 100 mL, reaction volume after K$_2$CO$_3$ filling = 34 mL) for the nucleophilic substitution reaction. A residence time of 3.8 min at a temperature of 60 °C was sufficient for synthesizing compound **4a**. The first 20 min reaction mixture was discarded and then collected for 1.5 h (810 mL). The organic layer was washed twice with water, dried over anhydrous Na$_2$SO$_4$, filtered, and concentrated under a vacuum. The crude mixture was purified by silica gel column chromatography.
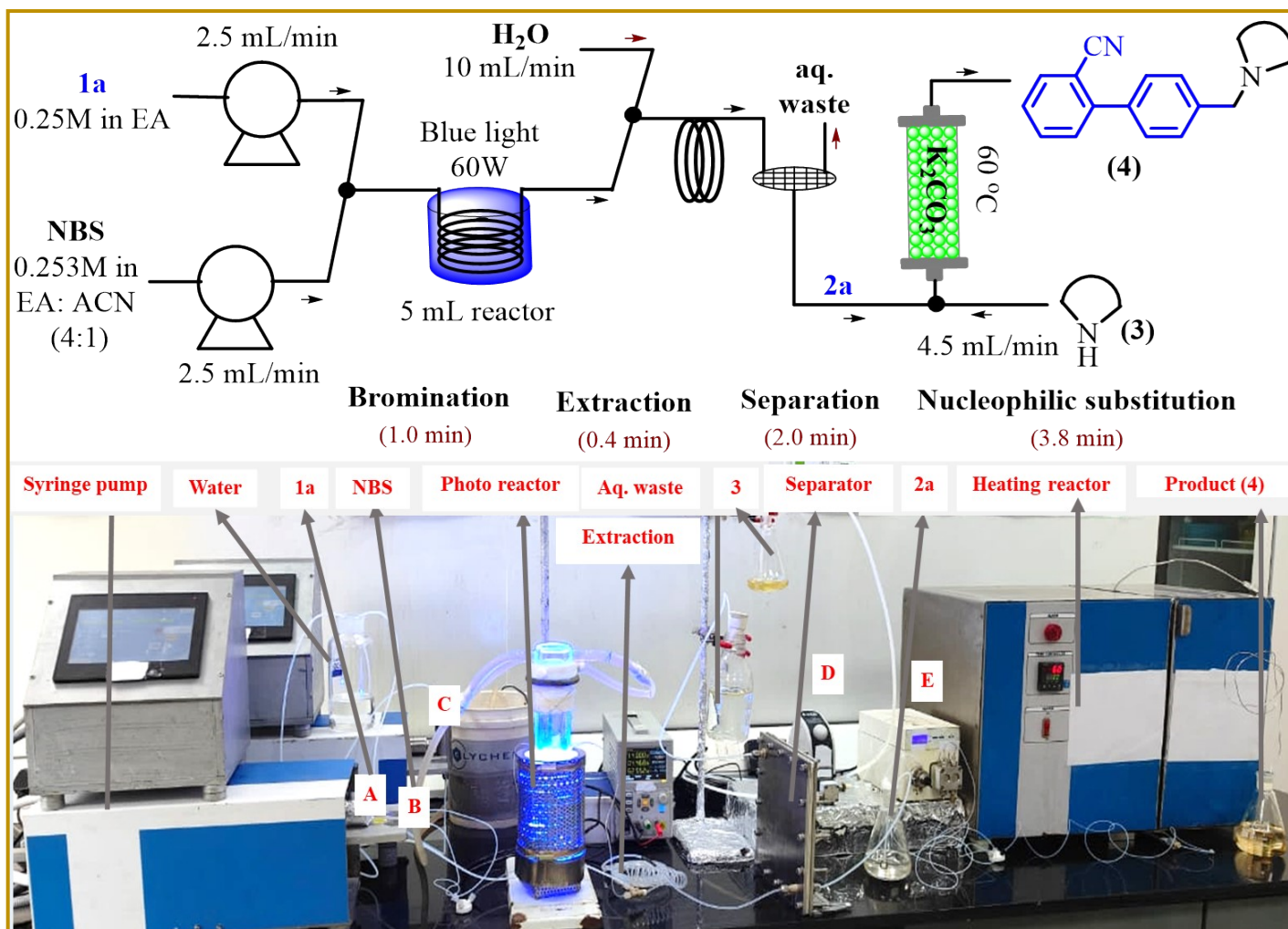
Fig. S12 Fully integrated platform for the synthesis of sartan intermediates.

Supporting video S3: The current video represent the integrated continuous flow set-up for the sartan intermediate.

4'-((2-Butyl-4-chloro-5-formyl-1*H*-imidazol-1-yl) methyl)-[1,1'-biphenyl]-2-carbonitrile (Losartan intermediate) (4a)
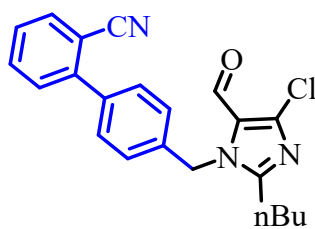
A stock solution of **1a** [0.25 M in EA (24.12 g in 500 mL)] and solution of NBS [0.253 M in EA: ACN (4:1) (23.36 g in 500 mL)] was introduced flow rate each solution at 2.5 mL min^{-1} into T-mixer (T$_1$) using syringe pumps pass through a 5.0 mL PFA reactor for the blue light exposure using a 60 W blue LED with 1 min residence time. To remove the byproduct, 10 mL min-1 water was introduced into a T-mixer (T$_2$) to the outflow of the photo-flow reactor. Further, the aqueous and EA continuous flow droplets were separated through the abovementioned liquid-liquid separator. A residence time of extraction (0.4 min) and separation (2.0 min) at 1 bar pressure was enough for the aqueous waste removal of the crude organic solution of **2a** collected. The collected solution **2a** was connected to one pump, while another was connected to the stock solution **3** [0.136 M in DMF (12.65 g, 500 mL)]. Both solutions were introduced at T-mixer (T$_3$), each flowing at a 4.5 mL min^{-1} flow rate. The combined mixture then passed through a 100 mL SS-packed bed reactor for the nucleophilic substitution reaction. A residence time of 3.8 min at a temperature of 60 °C was sufficient for synthesizing compound **4a**. The first 20 min reaction mixture was discarded and then collected for 1.5 h (810 mL). The organic layer was washed twice with water, dried over anhydrous Na$_2$SO$_4$, filtered, and concentrated under a vacuum. The crude mixture was purified by silica gel column chromatography in hexane: EA (70:30) to provide a pale-yellow solid with an 82 % (16.28 g) isolated yield. The spectra data compared with those reported in the literature.[16]

Melting Point: 104 °C; **^{1}H NMR (400 MHz, CDCl$_3$):** δ 9.77 (s, 1H), 7.76 (dd, *J* = 7.7, 0.9 Hz, 1H), 7.64 (td, *J* = 7.7, 1.4 Hz, 1H), 7.58 – 7.51 (m, 2H), 7.50 – 7.39 (m, 2H), 7.18 (d, *J* = 8.3

Hz, 2H), 5.62 (s, 2H), 2.71 – 2.64 (m, 2H), 1.78 – 1.66 (*m*, 2H), 1.37 (dd, *J* = 15.0, 7.5 Hz, 2H), 0.90 (t, *J* = 7.3 Hz, 3H**); ^{13}C NMR (101 MHz, CDCl$_3$):** δ 177.98, 154.68, 144.58, 143.21, 137.92, 136.19, 133.82, 132.95, 130.02, 129.38, 127.84, 126.78, 124.33, 118.56, 111.19, 47.97, 29.28, 26.56, 22.41, 13.71; **IR (ν$_{max}$):** 2956, 2865, 2226, 1664, 1516, 1471, 1423, 1376, 1273, 763, cm^{-1}; **HRMS(ESI):** *m/z* calcd for **C$_{22}$H$_{21}$N$_3$OCl** [M+H]$^+$ 378.1373, found 378.1360.

4'-((2-Butyl-4-chloro-5-(hydroxymethyl)-1*H*-imidazol-1-yl)   methyl)-[1,1'-biphenyl]-2-carbonitrile (Losartan intermediate) (4b)
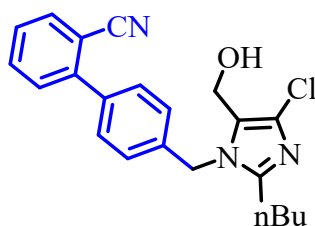
Compound **4b** was prepared according to the general procedure **S4.2**. The crude material was purified by silica gel column chromatography in hexane: EA (30:70) to provide a white liquid with a 54% yield. The spectra data compared with those reported in the literature.[17]

Melting Point: 159 °C; **^{1}H NMR (400 MHz, DMSO):** δ 7.94 (dd, *J* = 7.7, 1.0 Hz, 1H), 7.78 (td, *J* = 7.7, 1.3 Hz, 1H), 7.64 – 7.53 (m, 4H), 7.25 (d, *J* = 8.3 Hz, 2H), 5.36 (s, 2H), 5.30 (*t*, *J* = 4.9 Hz, 1H), 4.39 (d, *J* = 4.5 Hz, 2H), 2.55 – 2.50 (*m*, 2H), 1.47 (d, *J* = 7.5 Hz, 2H), 1.23 (q, *J* = 7.4 Hz, 2H), 0.78 (t, *J* = 7.3 Hz, 3H); **^{13}C NMR (126 MHz, CDCl$_3$):** δ 148.65, 144.63, 137.79, 136.80, 133.82, 132.96, 130.00, 129.41, 127.83, 127.26, 126.29, 125.00, 118.57, 111.19, 53.06, 47.22, 29.71, 26.75, 22.41, 13.74; **IR (ν$_{max}$):** 3223, 2956, 2866, 2226, 1574, 1454, 1417, 1353, 1252, 1073, 1011, 827, 755 cm^{-1}; **HRMS(ESI):** *m/z* calcd for C$_{22}$H$_{23}$N$_3$OCl [M+H]$^+$ 380.1530, found 380.1522.

Ethyl 1-((2'-cyano-[1,1'-biphenyl]-4-yl) methyl)-4-(2-hydroxypropan-2-yl)-2-propyl-1H-imidazole-5-carboxylate (Olmesartan intermediate) (4c)
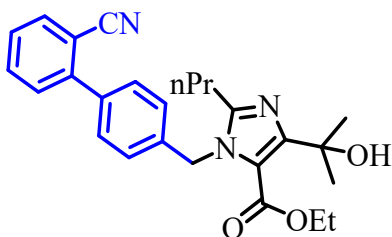
Compound **4c** was prepared according to the general procedure **S4.2**. The crude material was purified by silica gel column chromatography in hexane: EA (30:70) to provide a white solid with a 70% yield. The spectra data compared with those reported in the literature. **Melting Point:** 94 °C; **^{1}H NMR (400 MHz, CDCl3):** δ 7.77 (dd, J = 7.7, 0.9 Hz, 1H), 7.65 (td, J = 7.7, 1.4 Hz, 1H), 7.56 – 7.42 (m, 4H), 7.05 (d, J = 8.3 Hz, 2H), 5.83 (s, 1H), 5.52 (s, 2H), 4.23 (q, J = 7.1 Hz, 2H), 2.81 – 2.53 (m, 2H), 1.75 – 1.72 (m, 2H), 1.65 (s, 6H), 1.16 (t, J = 7.1 Hz, 3H), 0.97 (t, J = 7.4 Hz, 3H); **^{13}C NMR (126 MHz, CDCl$_3$):** δ 161.62, 159.03, 151.49, 144.78, 137.80, 137.38, 133.81, 132.92, 129.99, 129.27, 127.76, 125.73, 118.59, 117.02, 111.27, 70.41, 61.34, 48.88, 29.38, 21.42, 13.92; **IR (ν_{max}):** 3388, 2974, 2227, 1670, 1529, 1462, 1389, 1289, 1215, 1166, 1053, 747 cm^{-1}; **HRMS(ESI):** m/z calcd for **C$_{26}$H$_{30}$N$_3$O$_3$** [M+H]$^+$ 432.2287, found 432.2299.

Diethyl 1-((2'-cyano-[1,1'-biphenyl]-4-yl)methyl)-2-propyl-1H-imidazole-4,5-dicarboxylate (Olmesartan intermediate) (4d)
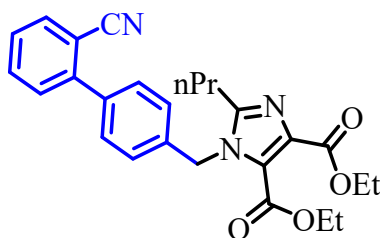
Compound **4d** was prepared according to the general procedure **S4.2**. The crude material was purified by silica gel column chromatography in hexane: EA (70:30) to provide a pale yellow liquid with a 78% isolated yield. The spectra data compared with those reported in the literature.[18] **^{1}H NMR (400 MHz, CDCl$_3$):** δ 7.80 – 7.73 (m, 1H), 7.64 (td, J = 7.8, 1.3 Hz, 1H),

7.52 (d, J = 8.3 Hz, 2H), 7.50 – 7.42 (m, 2H), 7.13 (d, J = 8.3 Hz, 2H), 5.48 (s, 2H), 4.40 (q, J = 7.1 Hz, 2H), 4.27 (q, J = 7.1 Hz, 2H), 2.73 – 2.64 (m, 2H), 1.75 (dq, J = 15.0, 7.4 Hz, 2H), 1.39 (t, J = 7.1 Hz, 3H), 1.25 (t, J = 7.1 Hz, 3H), 0.96 (t, J = 7.4 Hz, 3H); **^{13}C NMR (126 MHz, CDCl$_3$):** δ 163.11, 160.49, 151.96, 144.63, 137.84, 136.48, 136.34, 133.83, 132.92, 130.00, 129.34, 127.82, 126.54, 124.88, 118.53, 111.27, 61.65, 61.34, 48.02, 29.16, 21.39, 14.33, 13.92; **IR (ν_{max}):** 2971, 2226, 1716, 1455, 1287, 1203, 1110, 1022, 764, 629 cm^{-1} ; **HRMS(ESI):** *m/z* calcd for C$_{26}$H$_{28}$N$_3$O$_4$ [M+H]$^+$ 446.2080 found 446.2092.

4'-((1H-Imidazol-1-yl) methyl)-[1,1'-biphenyl]-2-carbonitrile (4e)
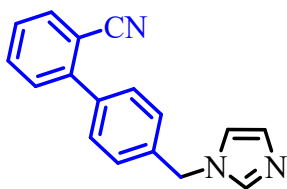
Compound **4e** was prepared according to the general procedure **S4.2**. The crude material was purified by silica gel column chromatography in hexane: EA (50:50) to provide a white solid with an 83% yield. The spectra data compared with those reported in the literature.[19] **Melting Point:** 202 °C; **^{1}H NMR (400 MHz, CDCl$_3$):** δ 7.77 (m, 1H), 7.65 (m, 1H), 7.60 (s, 1H), 7.55 (d, J = 8.2 Hz, 2H), 7.51 – 7.44 (m, 2H), 7.32 – 7.22 (m, 2H), 7.13 (*s*, 1H), 6.96 (*s*, 1H), 5.20 (*s*, 2H); **^{13}C NMR (101 MHz, CDCl$_3$):** δ 144.66, 138.17, 137.55, 136.86, 133.80, 132.96, 130.00, 129.42, 127.88, 127.50, 119.42, 118.59, 111.28, 50.43; **IR (ν_{max}):** 3063, 2964, 2225, 1654, 1471, 1413, 1362, 1275, 1117, 1024, 928, 825, 766, 704, cm^{-1}; **HRMS(ESI):** *m/z* calcd for **C$_{17}$H$_{14}$N$_3$** [M+H]$^+$ 260.1188, found 260.1187.

4'-((2-Methyl-1H-imidazol-1-yl) methyl)-[1,1'-biphenyl]-2-carbonitrile (4f)
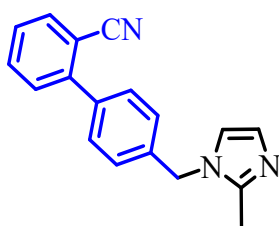
Compound **4f** was prepared according to the general procedure **S4.2**. The crude material was purified by silica gel column chromatography in hexane: EA (50:50) to provide a white solid with a 72% isolated yield. **Melting point:** 155 °C; **^{1}H NMR (500 MHz, CDCl$_3$):** δ 7.79 – 7.74 (m, 1H), 7.65 (td, *J* = 7.7, 1.4 Hz, 1H), 7.55 – 7.52 (m, 2H), 7.51 – 7.43 (m, 2H), 7.17 (d, *J* = 8.5 Hz, 2H), 7.00 (d, *J* = 1.3 Hz, 1H), 6.90 (d, *J* = 1.4 Hz, 1H), 5.13 (s, 2H), 2.38 (s, 3H). **^{13}C NMR (126 MHz, CDCl$_3$):** δ 145.02, 144.71, 137.88, 137.05, 133.81, 132.94, 130.00, 129.40, 127.83, 127.59, 126.91, 119.99, 118.60, 77.31, 77.05, 76.80, 49.40, 13.17; **IR (ν$_{max}$):** 2924, 2855, 2224, 1597, 1473, 1420, 1355, 1278, 1129, 1077, 990, 761 cm^{-1}. **HRMS(ESI):** *m/z* calcd for **C$_{18}$H$_{16}$N$_3$** [M+H]$^+$ 274.1344, found 274.1339.

4'-((2-Phenyl-1H-imidazol-1-yl) methyl)-[1,1'-biphenyl]-2-carbonitrile (4g)
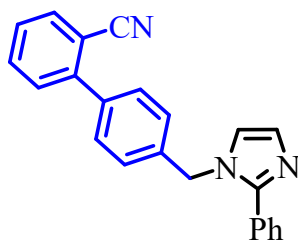
Compound **4g** was prepared according to the general procedure **S4.2**. The crude material was purified by silica gel column chromatography in hexane to provide a pale-yellow viscous liquid with a 75% isolated yield. **^{1}H NMR (500 MHz, CDCl$_3$):** δ 7.77 – 7.74 (m, 1H), 7.64 (td, *J* = 7.7, 1.2 Hz, 1H), 7.59 – 7.52 (m, 4H), 7.49 (d, *J* = 7.7 Hz, 1H), 7.47 – 7.39 (m, 4H), 7.23 – 7.18 (m, 3H), 7.02 (d, *J* = 1.2 Hz, 1H), 5.29 (s, 2H). **^{13}C NMR (126 MHz, CDCl$_3$):** δ 148.36, 144.67, 137.83, 137.64, 133.82, 132.97, 130.49, 130.03, 129.41, 129.20, 128.96, 128.83, 128.69, 127.85, 126.92, 121.35, 118.64, 111.22, 50.07. **IR (ν$_{max}$):** 3060, 2924, 28961, 2226, 1610, 1491, 1368, 1273, 1197, 1118, 1009, 825, cm^{-1}. **HRMS(ESI):** *m/z* calcd for **C$_{23}$H$_{18}$N$_3$** [M+H]$^+$ 336.1501, found 336.1494.

Methyl 1-((2'-cyano-[1,1'-biphenyl]-4-yl) methyl)-2-ethoxy-1H-benzo[d]imidazole-7-carboxylate (candesartan intermediate) (4h)
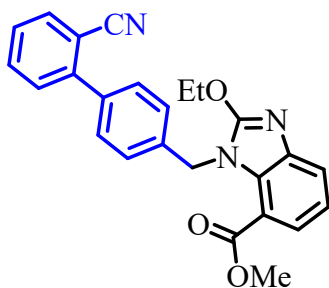
Compound **4h** was prepared according to the general procedure **S4.2**. The crude material was purified by silica gel column chromatography in hexane: EA (70:30) to provide a white solid with a 78% isolated yield. The spectra data compared with those reported in the literature.[20]

Melting Point: 165 °C; **^{1}H NMR (400 MHz, CDCl$_3$):** δ 7.74 (dd, J = 7.9, 1.0 Hz, 2H), 7.58 (ddd, J = 16.7, 7.7, 1.2 Hz, 2H), 7.45 – 7.38 (m, 4H), 7.18 (t, J = 7.9 Hz, 1H), 7.10 (d, J = 8.4 Hz, 2H), 5.69 (s, 2H), 4.67 (q, J = 7.1 Hz, 2H), 3.75 (s, 3H),1.49 (t, J = 7.1 Hz, 3H). **^{13}C NMR (101 MHz, CDCl$_3$):** δ 166.86, 158.75, 144.98, 141.95, 138.08, 137.05, 133.78, 132.82, 131.51, 129.99, 128.90, 127.59, 126.86, 123.64, 121.99, 120.96, 118.64, 115.85, 111.21, 66.82, 52.33, 47.05, 14.69; **IR (v$_{max}$):** 3020, 2981, 2225, 1708, 1615, 1548, 1478, 1427, 1351, 1279, 1249, 1215, 1129, 1038, 741, 666 cm^{-1} **HRMS(ESI):** m/z calcd for **C$_{25}$H$_{22}$N$_3$O$_3$** [M+H]$^+$ 412.1661, found 412.1669.

Ethyl 1-((2'-cyano-[1,1'-biphenyl]-4-yl) methyl)-2-ethoxy-1H-benzo[d]imidazole-7-carboxylate (candesartan intermediate) (4i)
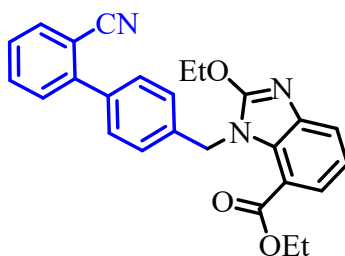
Compound **4i** was prepared according to the general procedure **S4.2**. The crude material was purified by silica gel column chromatography in hexane: EA (70:30) to provide a white solid with a 75% isolated yield. The spectra data compared with those reported in the literature.[21]

Melting Point: 135°C; **^{1}H NMR (400 MHz, CDCl$_3$):** δ 7.74 (dd, J = 7.9, 1.1 Hz, 2H), 7.63 –

7.55 (m, 2H), 7.46 – 7.39 (m, 4H), 7.18 (t, J = 7.9 Hz, 1H), 7.10 (d, J = 8.4 Hz, 2H), 5.71 (s, 2H), 4.67 (q, J = 7.1 Hz, 2H), 4.23 (q, J = 7.1 Hz, 2H), 1.49 (t, J = 7.1 Hz, 3H), 1.24 (t, J = 7.1 Hz, 3H); **^{13}C NMR (101 MHz, CDCl$_3$):** δ 166.42, 158.71, 144.97, 141.93, 138.17, 137.01, 133.80, 132.82, 131.50, 129.97, 128.91, 127.57, 126.84, 123.62, 121.88, 120.92, 118.63, 116.25, 111.19, 66.79, 61.26, 47.00, 14.69, 14.22; **IR (ν_{max}):** 2982, 2226, 1709, 1613, 1548, 1468, 1423, 1356, 1314, 1250, 1122, 1033, 747 cm^{-1}; **HRMS(ESI):** m/z calcd for **C$_{26}$H$_{24}$N$_3$O$_3$** [M+H]$^+$ 426.1818, found 426.1815.

4'-((1*H*-Benzo[d]imidazol-1-yl) methyl)-[1,1'-biphenyl]-2-carbonitrile (4j)
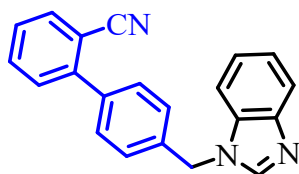
Compound **4j** was prepared according to the general procedure **S4.2**. The crude material was purified by silica gel column chromatography in hexane: EA (60:40) to provide a white solid with a 79% isolated yield. The spectra data compared with those reported in the literature.[22]

Melting point: 122 °C; **^{1}H NMR (400 MHz, CDCl$_3$):** δ 8.00 (s, 1H), 7.89 – 7.81 (m, 1H), 7.79 – 7.71 (m, 1H), 7.62 (td, J = 7.8, 1.4 Hz, 1H), 7.57 – 7.49 (m, 2H), 7.48 – 7.41 (m, 2H), 7.37 – 7.22 (m, 5H), 5.42 (s, 2H); **^{13}C NMR (101 MHz, CDCl$_3$):** δ 144.57, 143.95, 143.32, 138.11, 136.24, 133.92, 133.80, 132.99, 130.00, 129.44, 127.89, 127.34, 123.29, 122.43, 120.48, 118.64, 111.16, 110.11, 48.39; **IR (ν_{max}):** 3060, 2924, 28961, 2226, 1610, 1491, 1368, 1273, 1197, 1118, 1009, 754, cm^{-1}; **HRMS(ESI):** m/z calcd for **C$_{21}$H$_{16}$N$_3$** [M+H]$^+$ 310.1344, found 310.1333.

4'-((2-Phenyl-1*H*-benzo[d]imidazol-1-yl) methyl)-[1,1'-biphenyl]-2-carbonitrile (4k)
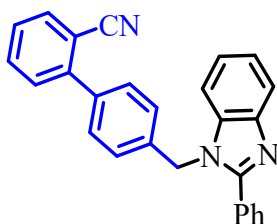
Compound **4k** was prepared according to the general procedure **S5.2**. The crude material was purified by silica gel column chromatography in hexane: EA (60:40) to provide a white solid liquid with a 75% isolated yield. **Melting point:** 181 °C; **¹H NMR (500 MHz, CDCl₃):** δ 7.89 (dt, *J* = 8.1, 0.9 Hz, 1H), 7.77 (dd, *J* = 7.8, 1.0 Hz, 1H), 7.73 – 7.69 (m, 2H), 7.64 (td, *J* = 7.7, 1.4 Hz, 1H), 7.55 – 7.52 (m, 2H), 7.51 – 7.47 (m, 4H), 7.45 (td, *J* = 7.6, 1.2 Hz, 1H), 7.34 (ddd, *J* = 8.1, 5.5, 2.9 Hz, 1H), 7.28 – 7.26 (m, 2H), 7.23 (d, *J* = 8.5 Hz, 2H), 5.53 (s, 2H); **¹³C NMR (101 MHz, CDCl₃):** δ 154.22, 144.68, 143.23, 137.72, 137.04, 136.02, 133.86, 132.95, 130.05, 129.50, 129.30, 128.89, 127.81, 126.43, 123.22, 122.84, 120.09, 118.67, 111.20, 110.55, 48.18; **IR (ν$_{max}$):** 3023, 2924, 2861, 2225, 1574, 1450, 1389, 1339, 1214, 1160, 927, 749 cm^{-1}; **HRMS (ESI)** *m/z* calcd for **C$_{27}$H$_{20}$N$_3$** [M+H]$^+$ 386.1630, found 386.1646.

4'-((2-Amino-1*H*-benzo[d]imidazol-1-yl) methyl)-[1,1'-biphenyl]-2-carbonitrile (4l):
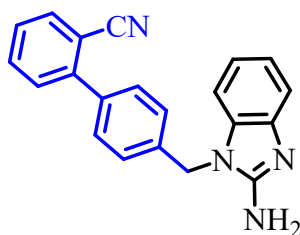
Compound **4l** was prepared according to the general procedure **S4.2**. The crude material was purified by silica gel column chromatography in hexane: EA (30:70) to provide a pale brown with a 62% isolated yield. **Melting point:** 142 °C; **¹H NMR (500 MHz, CDCl₃):** ¹H NMR (400 MHz, CDCl₃) δ 7.76 (dd, *J* = 8.3, 1.3 Hz, 1H), 7.64 (td, *J* = 7.9, 1.4 Hz, 1H), 7.55 – 7.43 (m, 5H), 7.29 (*d, J* = 8.4 Hz, 2H), 7.21 – 7.07 (m, 3H), 5.23 (s, 2H), 4.58 (s, 2H); **¹³C NMR (101 MHz, CDCl₃):** ¹³C NMR (101 MHz, CDCl₃) δ 153.34, 144.62, 141.86, 138.12, 135.97, 134.57, 133.78, 132.95, 129.96, 129.62, 127.88, 126.81, 121.93, 120.32, 118.59, 116.88, 111.25, 107.83, 77.34, 77.23, 45.82; **IR (ν$_{max}$):** 3343, 3186, 2926, 2859, 2225, 1633, 1556, 1476, 1353, 1202, 1025,763 cm^{-1}; **HRMS (ESI)** *m/z* calcd for **C$_{21}$H$_{17}$N$_4$**[M+H]$^+$ 325.1453, found 325.1440.

4'-((1,7'-Dimethyl-2'-propyl-1*H*,3'*H*-[2,5'-bibenzo[d]imidazol]-3'-yl) methyl)-[1,1'-biphenyl]-2-carbonitrile (Telmisartan intermediate) (4m)
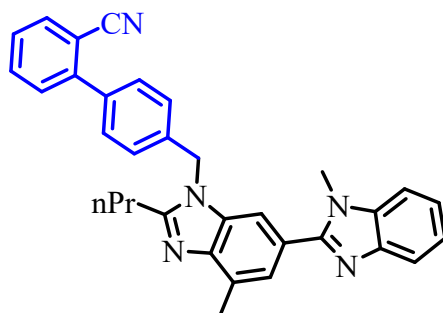
Compound **4m** was prepared according to the general procedure **S4.2**. The crude material was purified by silica gel column chromatography in hexane: EA (20:80) to provide a white solid with a 73% isolated yield. The spectra data compared with those reported in the literature.[23]

Melting Point: 193 °C; **¹H NMR (500 MHz, CDCl₃):** δ 7.81 – 7.77 (m, 1H), 7.74 (dd, *J* = 7.7, 0.8 Hz, 1H), 7.65 – 7.59 (m, 1H), 7.52 – 7.48 (m, 2H), 7.47 – 7.41 (m, 4H), 7.35 (ddd, *J* = 8.0, 3.1, 1.6 Hz, 1H), 7.31 – 7.27 (m, 2H), 7.17 (d, *J* = 8.4 Hz, 2H), 5.47 (s, 2H), 3.78 (s, 3H), 2.94 (dd, *J* = 8.6, 7.2 Hz, 2H), 2.78 (s, 3H), 1.89 (dd, *J* = 15.5, 7.6 Hz, 2H), 1.06 (t, *J* = 7.4 Hz, 3H); **¹³C NMR (151 MHz, CDCl₃):** δ 156.48, 154.68, 144.60, 143.18, 142.91, 137.90, 136.70, 136.49, 134.97, 133.81, 132.96, 130.01, 129.59, 129.48, 127.83, 126.50, 124.05, 124.01, 122.53, 122.33, 119.57, 118.59, 111.18, 109.59, 108.89, 46.96, 31.88, 29.86, 21.94, 16.95, 14.14; **IR (ν_{max}):** 2960, 2226, 1601, 1519, 1450, 1403, 1327, 1279, 1234, 1090, 753 cm⁻¹; **HRMS(ESI):** *m/z* calcd for C₃₃H₃₀N₅ [M+H]⁺ 496.2501 found 496.2507.

4'-((2-butyl-4-oxo-1,3-diazaspiro[4.4]non-1-en-3-yl)methyl)-[1,1'-biphenyl]-2-carbonitrile (Irbesartan precursor) (4n)
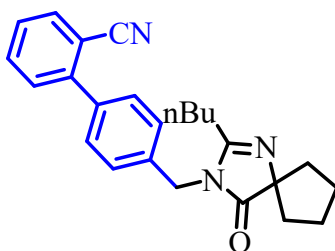
Compound **4n** was prepared according to the general procedure **S4.2**. The crude material was purified by silica gel column chromatography hexane: EA (30:70) to provide a pale-yellow solid with 77% isolated yields. The spectra data compared with those reported in the literature.[24] **Melting point:** 97 °C; **^{1}H NMR (500 MHz, CDCl$_3$):** δ 7.69 (d, J = 7.7 Hz, 1H), 7.57 (td, J = 7.7, 1.3 Hz, 1H), 7.47 (d, J = 8.2 Hz, 2H), 7.42 (d, J = 7.8 Hz, 1H), 7.37 (td, J = 7.7, 1.1 Hz, 1H), 7.21 (d, J = 8.2 Hz, 2H), 4.67 (s, 2H), 2.32 – 2.23 (m, 2H), 1.98 – 1.74 (m, 8H), 1.52 (d, J = 7.6 Hz, 2H), 1.27 (d, J = 7.4 Hz, 2H), 0.80 (t, J = 7.4 Hz, 3H); **^{13}C NMR (101 MHz, CDCl$_3$):** δ 186.78, 161.55, 144.73, 137.70, 137.22, 133.83, 132.92, 130.03, 129.38, 127.76, 127.08, 118.59, 111.22, 76.60, 43.32, 37.47, 28.86, 27.80, 26.14, 22.35, 13.75; **IR (ν$_{max}$):** 2949, 2867, 2225, 1718, 1631, 1441, 1397, 1345, 1176, 1103, 1022, 951, 760 cm^{-1}; **HRMS(ESI):** m/z calcd for C$_{25}$H$_{28}$N$_3$O [M+H]$^+$ 386.2154, found 386. 2150.

4'-((1H-1,2,4-Triazol-1-yl) methyl)-[1,1'-biphenyl]-2-carbonitrile (4o)
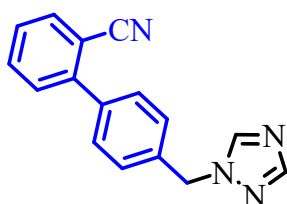
Compound **4o** was prepared according to the general procedure **S4.2**. The crude material was purified by silica gel column chromatography in hexane: EA (40:60) to provide a white solid with a 73% isolated yield. The spectra data compared with those reported in the literature.[19] **Melting point:** 238 °C; **^{1}H NMR (400 MHz, CDCl$_3$):** δ 8.00 (s, 1H), 7.88 – 7.81 (m, 1H), 7.74 (dd, J = 7.7, 0.8 Hz, 1H), 7.62 (td, J = 7.8, 1.4 Hz, 1H), 7.55 – 7.49 (m, 2H), 7.48 – 7.42 (m, 2H), 7.33 – 7.26 (m, 5H), 5.42 (s, 2H); **^{13}C NMR (101 MHz, CDCl$_3$):** δ 152.39, 144.59, 143.27, 138.53, 135.24, 133.82, 132.96, 130.02, 129.51, 128.27, 127.93, 118.55, 111.30, 53.18; **IR (ν$_{max}$):** 3021, 2927, 2226, 1509, 1442, 1354, 1274, 1213, 1138, 1015, 959,756 cm^{-1}; **HRMS(ESI):** m/z calcd for C$_{16}$H$_{13}$N$_4$ [M+H]$^+$ 261.1140, found 261.1130.

4'-((9H-Carbazol-9-yl) methyl)-[1,1'-biphenyl]-2-carbonitrile (4p)
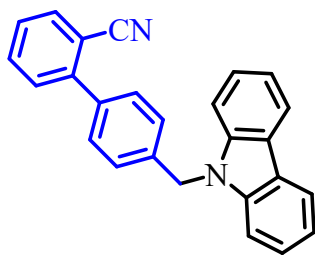
Compound **4p** was prepared according to the general procedure **S4.2**. The crude material was purified by silica gel column chromatography in hexane: EA (90:10) to provide a white solid with a 68% isolated yield. The spectra data compared with those reported in the literature.

Melting point: 120 °C. **^{1}H NMR (400 MHz, CDCl$_3$):** δ 8.15 (d, J = 7.8 Hz, 2H), 7.79 – 7.71 (m, 1H), 7.64 – 7.56 (m, 1H), 7.50 – 7.36 (m, 8H), 7.29 – 7.26 (*m*, 2H), 7.26 – 7.24 (*m*, 2H), 5.59 (*s*, 2H); **^{13}C NMR (101 MHz, CDCl$_3$);** δ 144.96, 140.65, 137.90, 137.36, 133.79, 132.88, 130.00, 129.23, 127.62, 126.79, 126.01, 123.12, 120.49, 119.40, 118.73, 111.19, 108.93, 46.29. **IR (ν$_{max}$):** 2921, 2852, 2226, 1579, 1460, 1376, 1188, 1080, 965,752 cm^{-1}; **HRMS (ESI):** *m/z* calcd for **C$_{26}$H$_{19}$N$_2$** [M+H]$^+$ 359.1548, found 359.1537.

S4.3 Comparative data for the synthesis of sartan intermediates.

Table S9. Comparative table for the synthesis of sartan intermediates.

Entry	Product formula 1	Comparative result
1		82%, 7.2 min (our study) DBDMH, AIBN, DCM, reflux, 24 h;.K$_2$CO$_3$, DMF, -8 to -12 °C, 2 h 80% (ref.[17]) NBS, AIBN, CCl$_4$, 80 °C, 3 h; K$_2$CO$_3$, DMF, 40 °C,6h 84% (ref.[25])
2		54%, 7.2 min (our study) DBDMH, AIBN, DCM, reflux, 24 h; K$_2$CO$_3$, DMF, -8 to -12 °C, 2 h; NaBH, Methanol, rt, 1 h, 71.2 (ref.[17]) Sodium methoxide, DMF, rt, 24 h 40% (ref.[26])
3		83%, 7.2 min (our study) K$_2$CO$_3$, acetone, rt, 2h; 60–75% (ref.[19])
4		70%, 7.2 min (our study) K$_2$CO$_3$, acetone, rt, 2h; 60–75% (ref.[19])

S5. Spectra
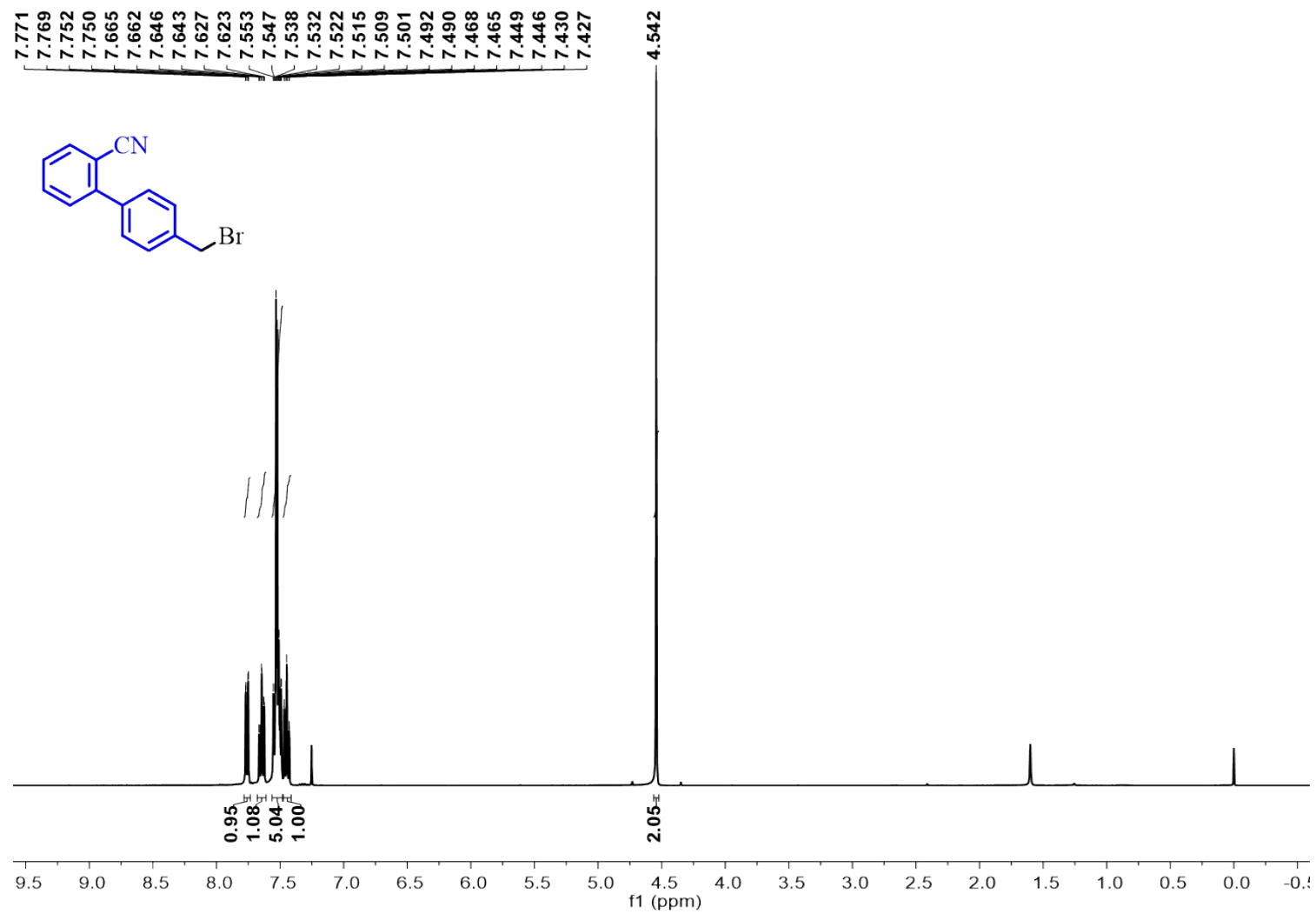
Fig. S13 ^{1}H NMR spectra of 4'-(bromomethyl)-[1,1'-biphenyl]-2-carbonitrile **(2a)**.
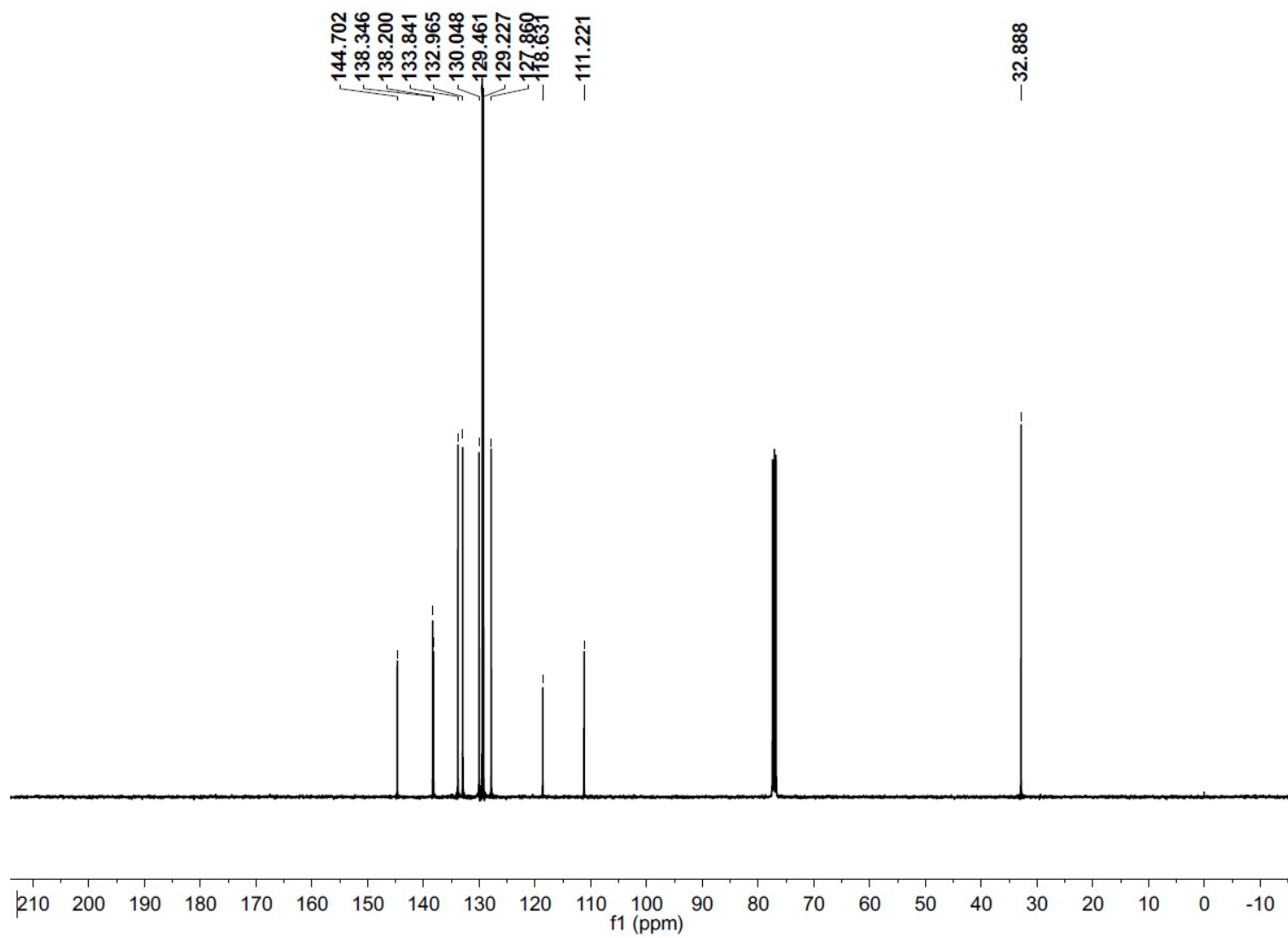
Fig. S14 ^{13}C NMR spectra of 4'-(bromomethyl)-[1,1'-biphenyl]-2-carbonitrile **(2a)**.
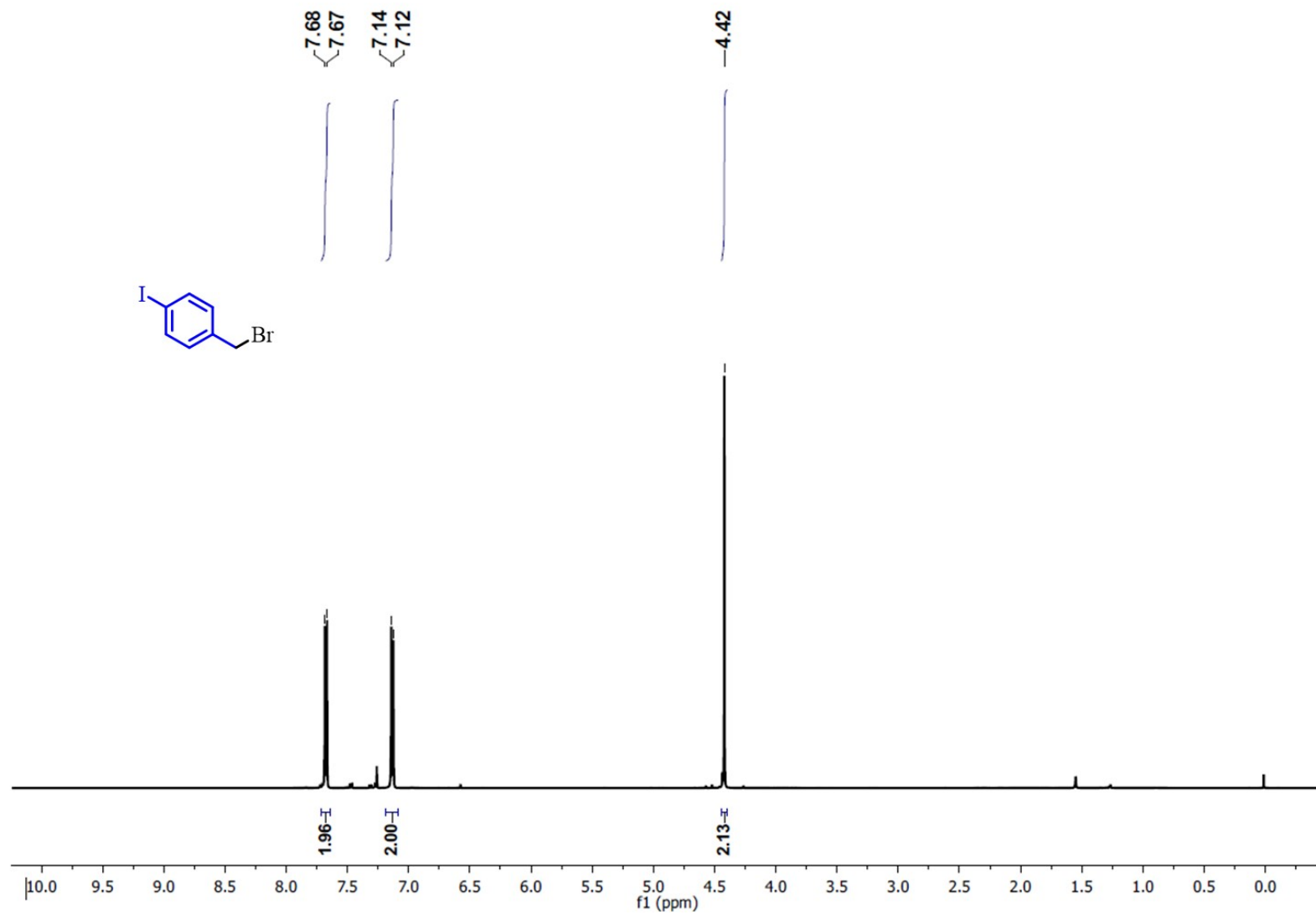
Fig. S15 ^{1}H NMR spectra of 1-(bromomethyl)-4-iodobenzene **(2b).**
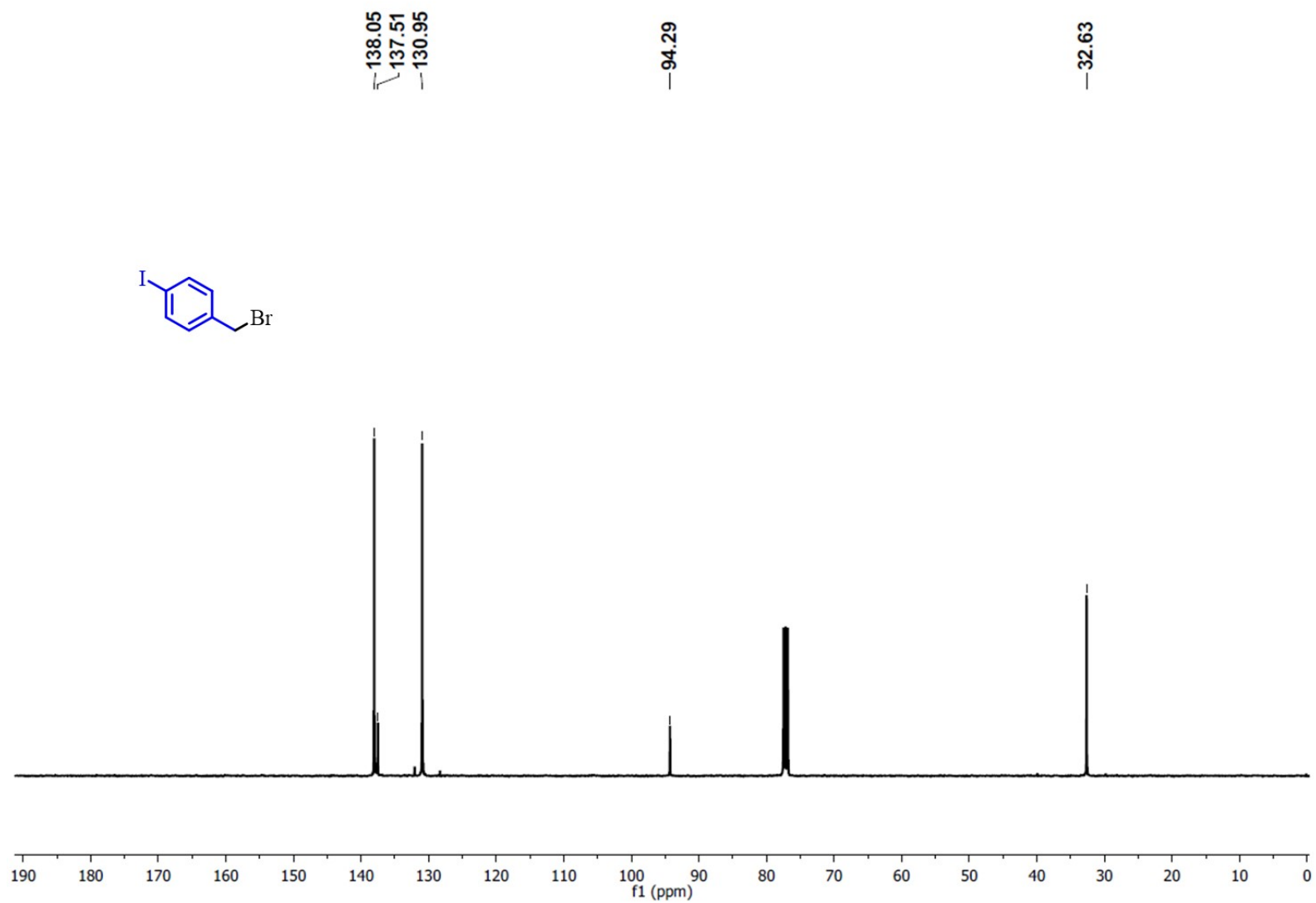
Fig. S16 ^{13}C NMR spectra of 1-(bromomethyl)-4-iodobenzene **(2b).**
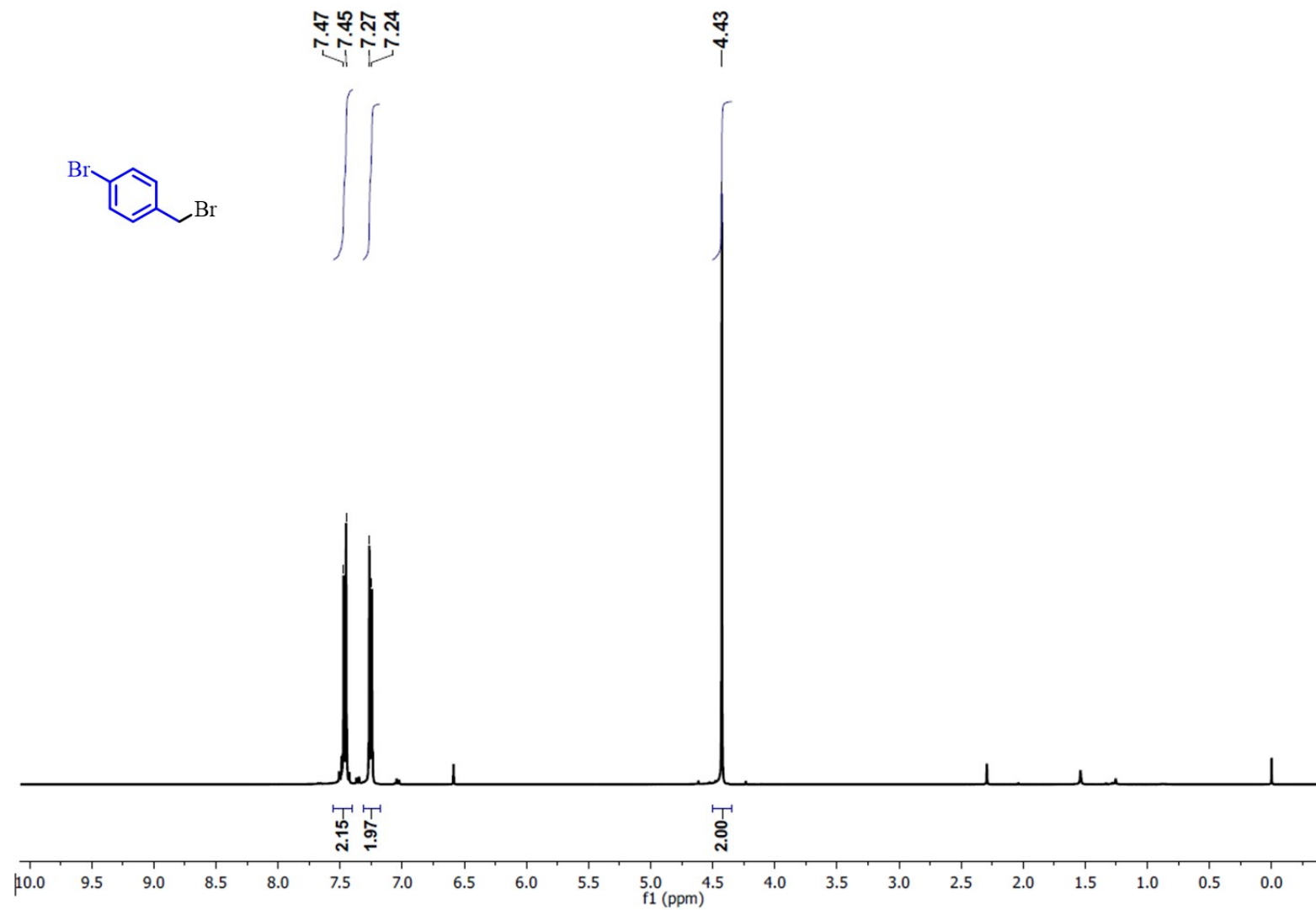
Fig. S17 ^{1}H NMR spectra of 1-bromo-4-(bromomethyl) benzene **(2c).**
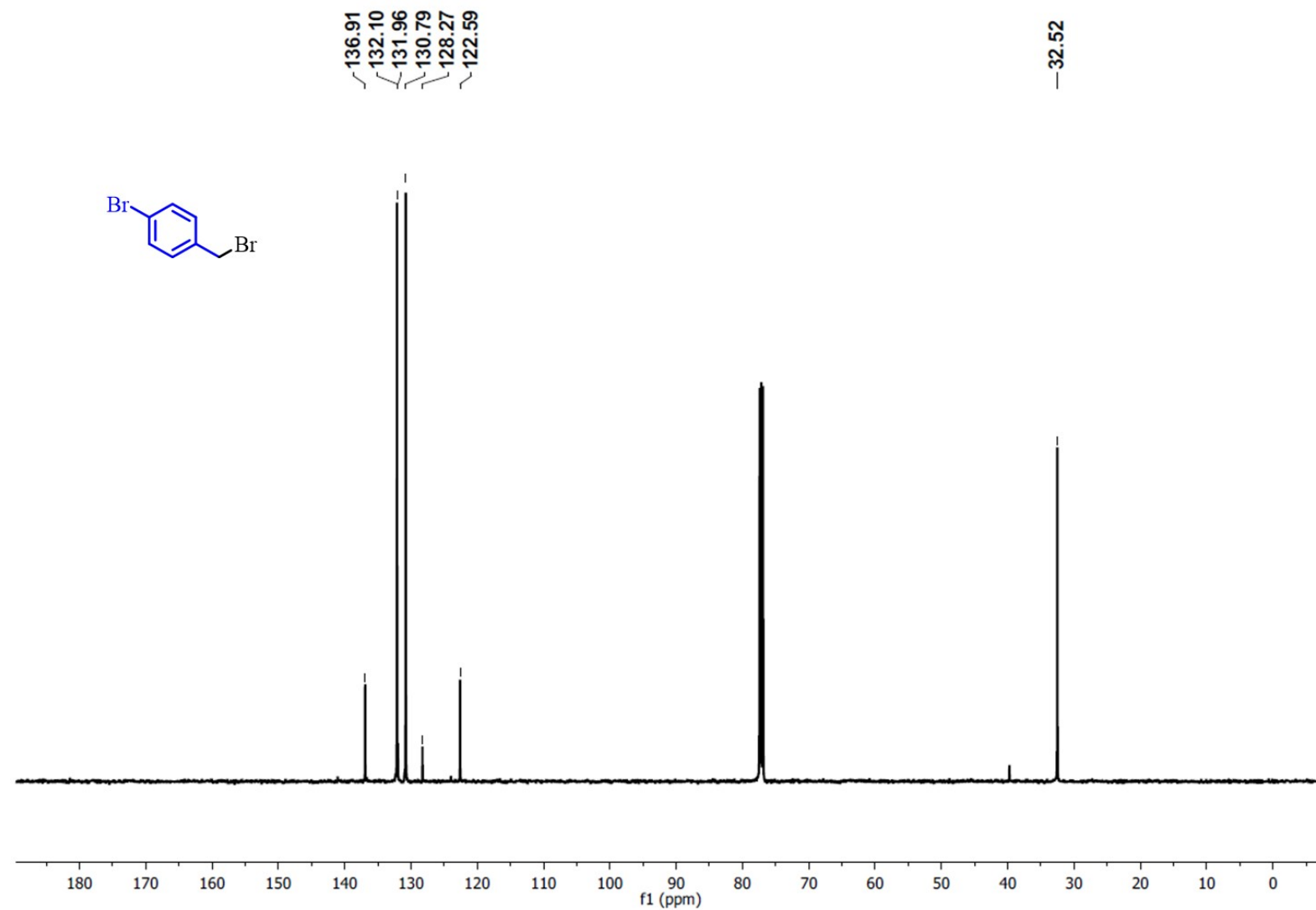
Fig. S18 ^{13}C NMR spectra of 1-bromo-4-(bromomethyl) benzene **(2c).**
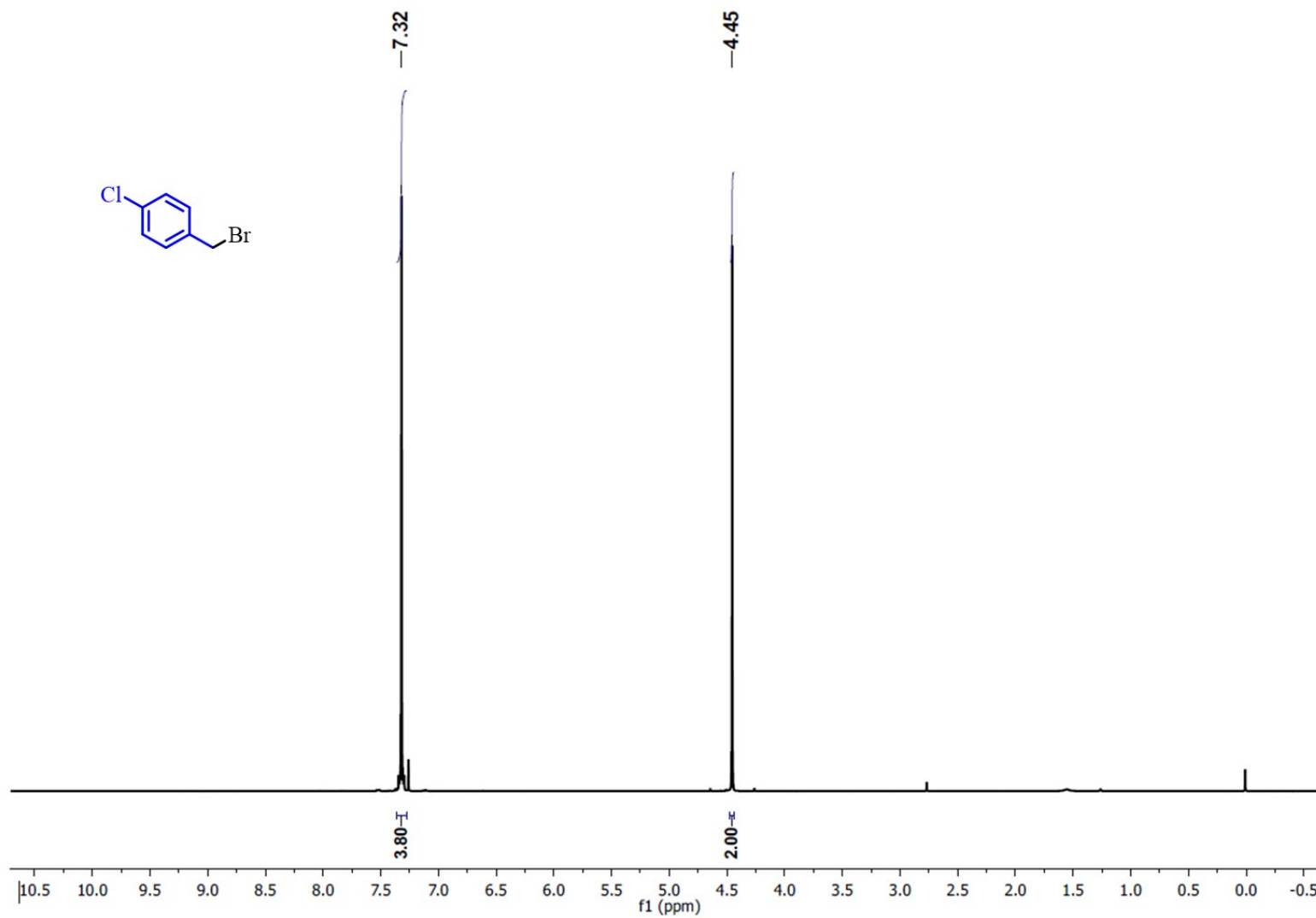
Fig. S19 ^{1}H NMR spectra of 1-(bromomethyl)-4-chlorobenzene **(2d).**
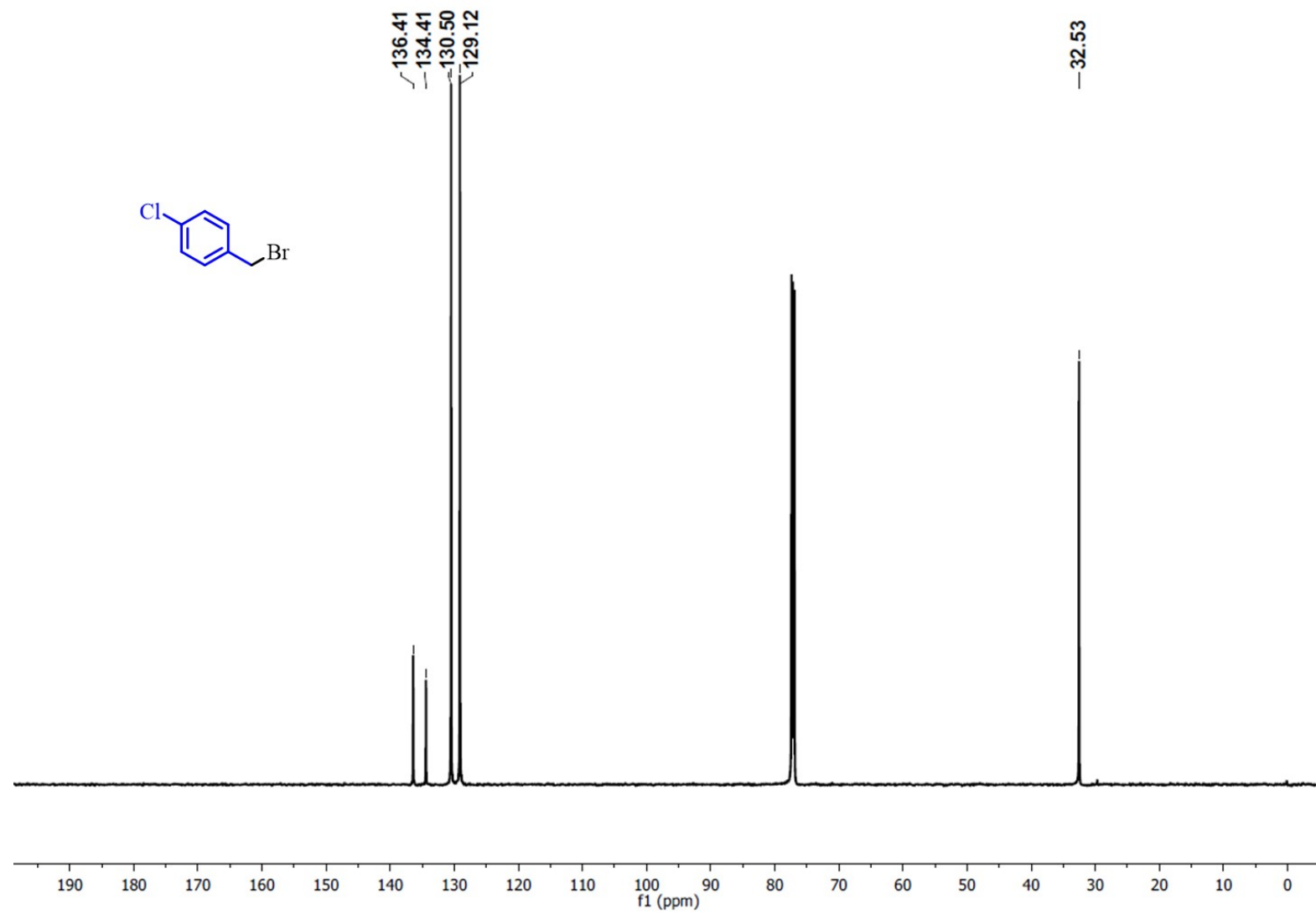
Fig. S20 ^{13}C NMR spectra of 1-(bromomethyl)-4-chlorobenzene **(2d).**
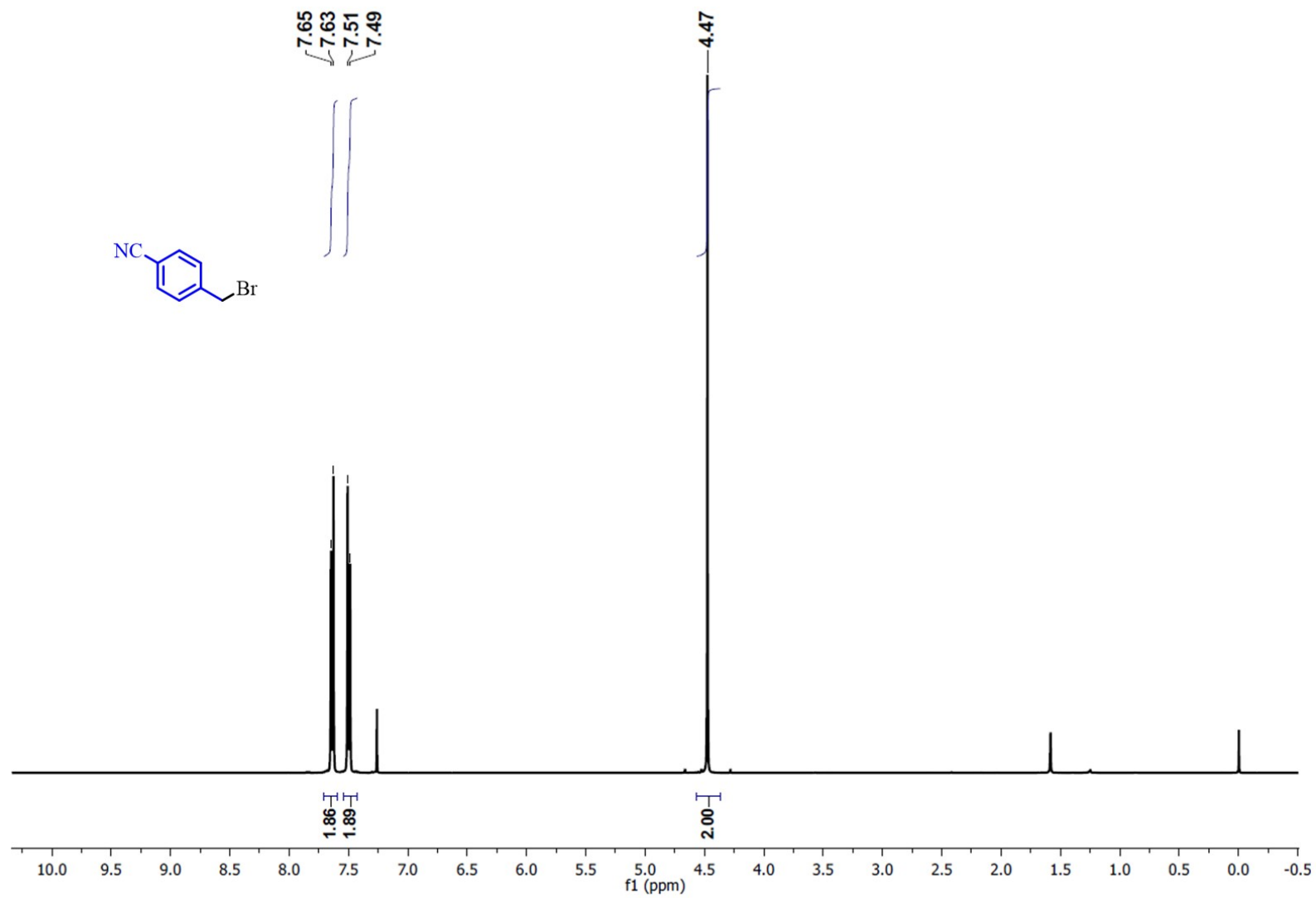
Fig. S21 ^{1}H NMR spectra of 4-(bromomethyl) benzonitrile **(2e)**.
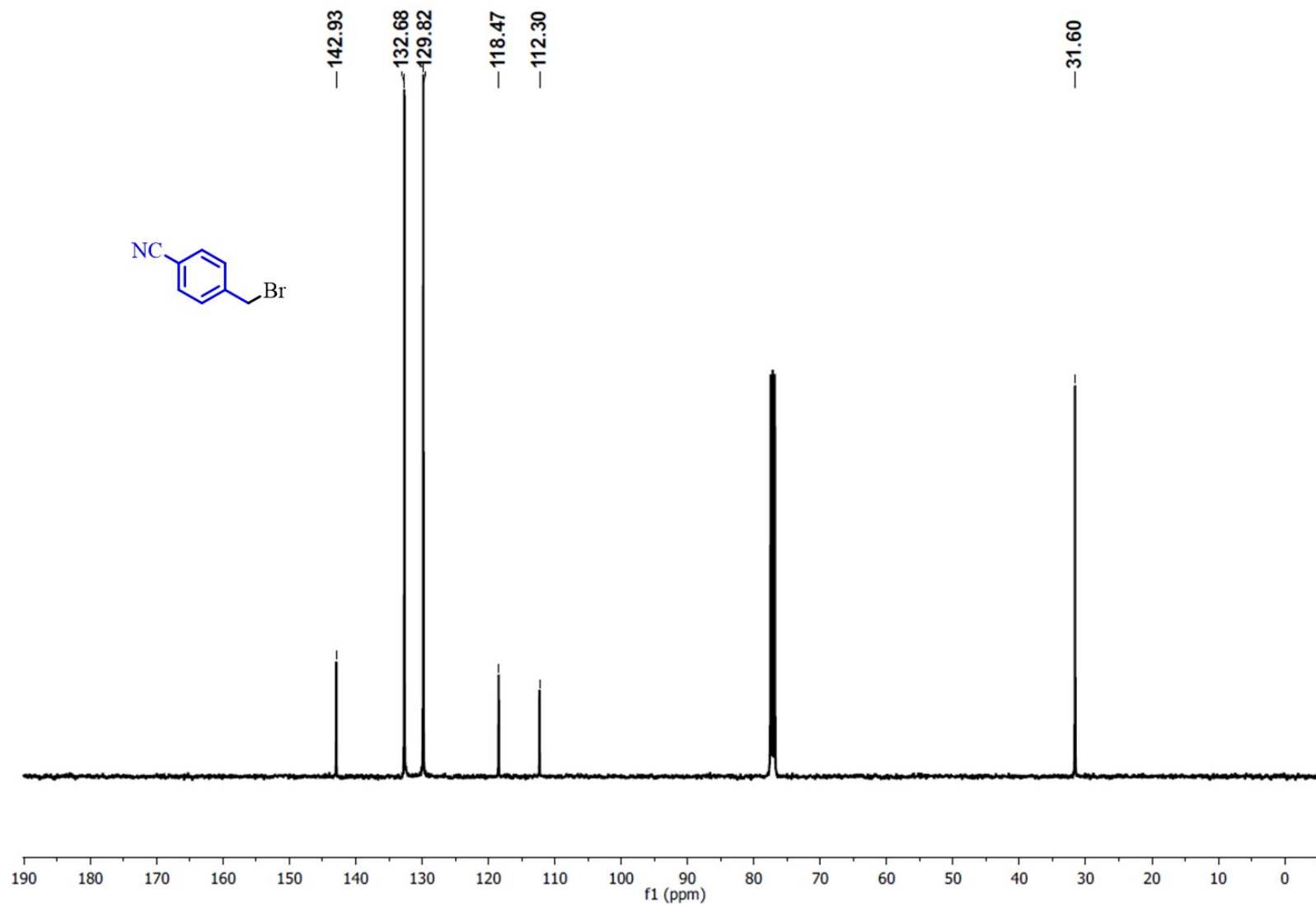
Fig. S22 ^{13}C NMR spectra of 4-(bromomethyl) benzonitrile **(2e).**
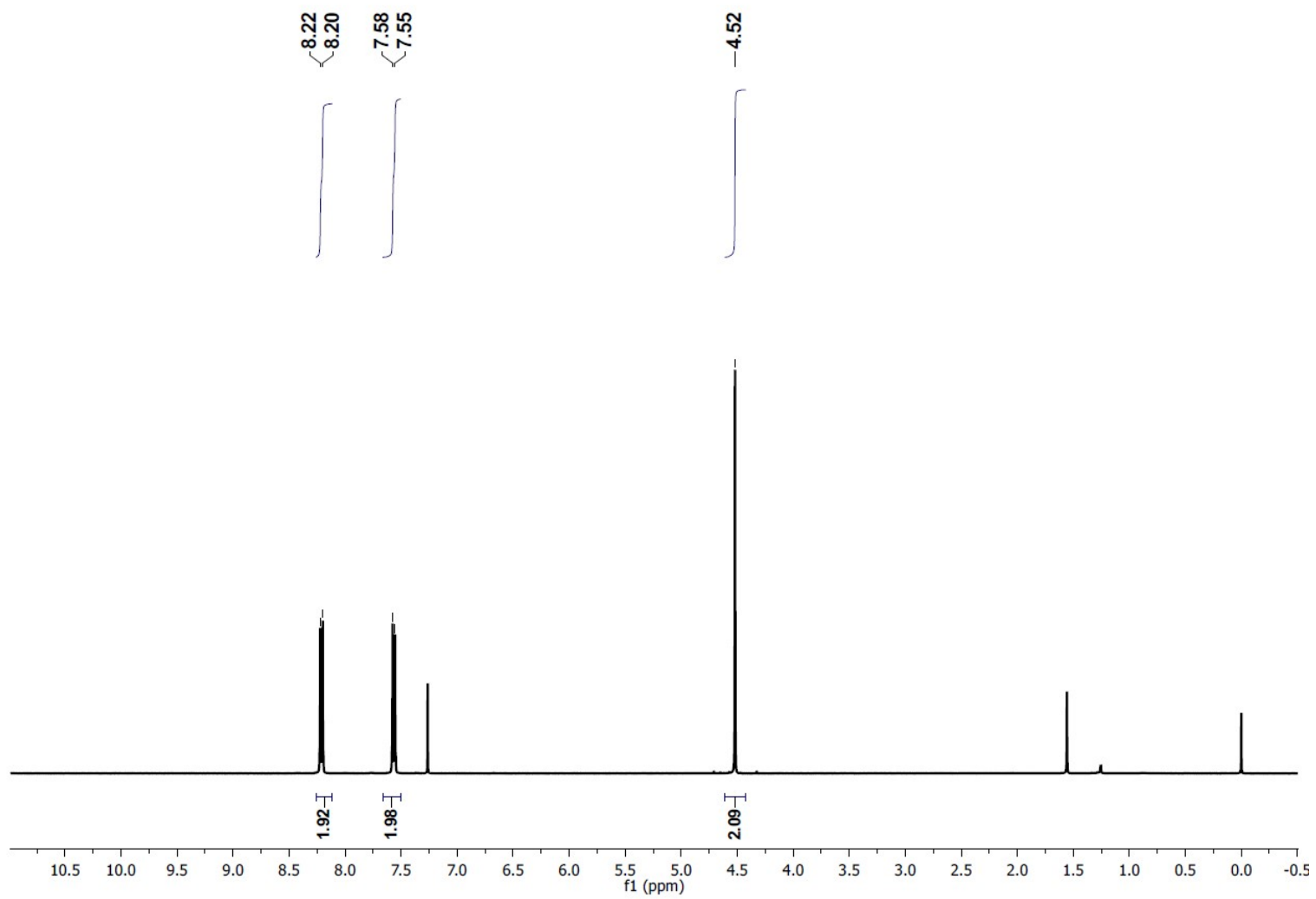
Fig. S23 ^{1}H NMR spectra of 1-(bromomethyl)-4-nitrobenzene **(2f).**
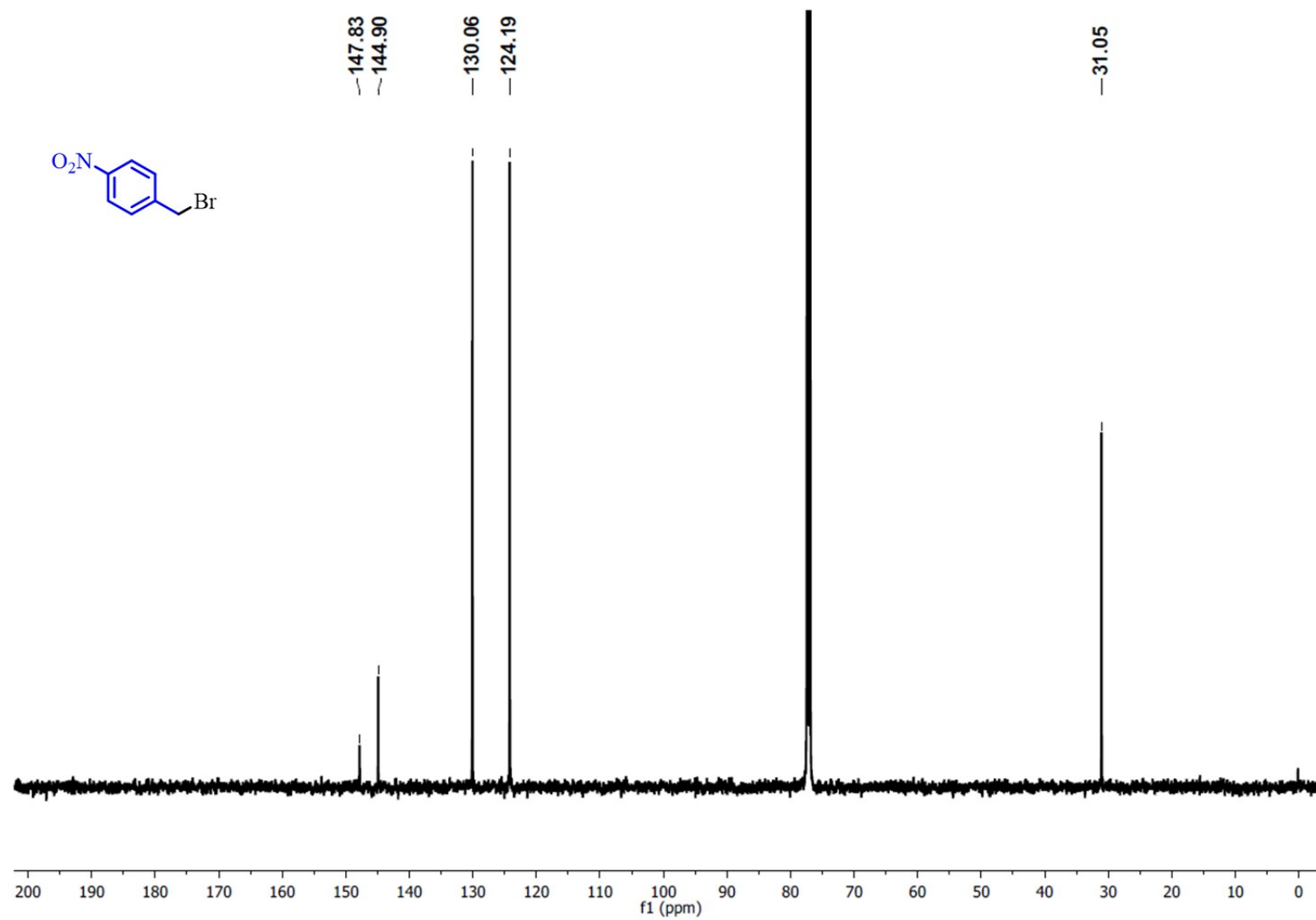
Fig. S24 ^{13}C NMR spectra of 1-(bromomethyl)-4-nitrobenzene **(2f).**

Fig. S25 ^{1}H NMR spectra of 1-(bromomethyl)-3-iodobenzene **(2g).**

139.96
137.92
137.47
130.48
128.32

94.32

31.96

f1 (ppm)
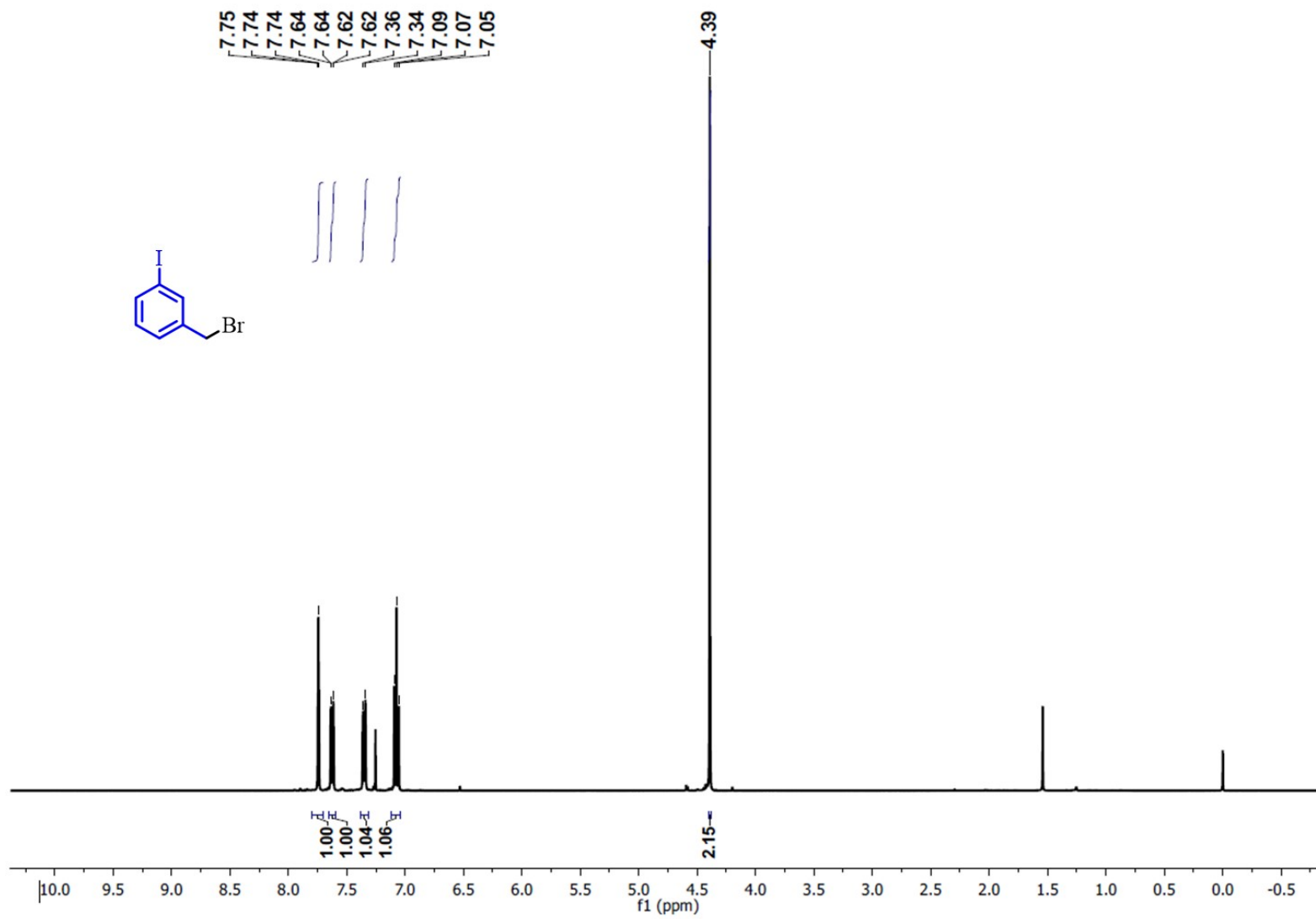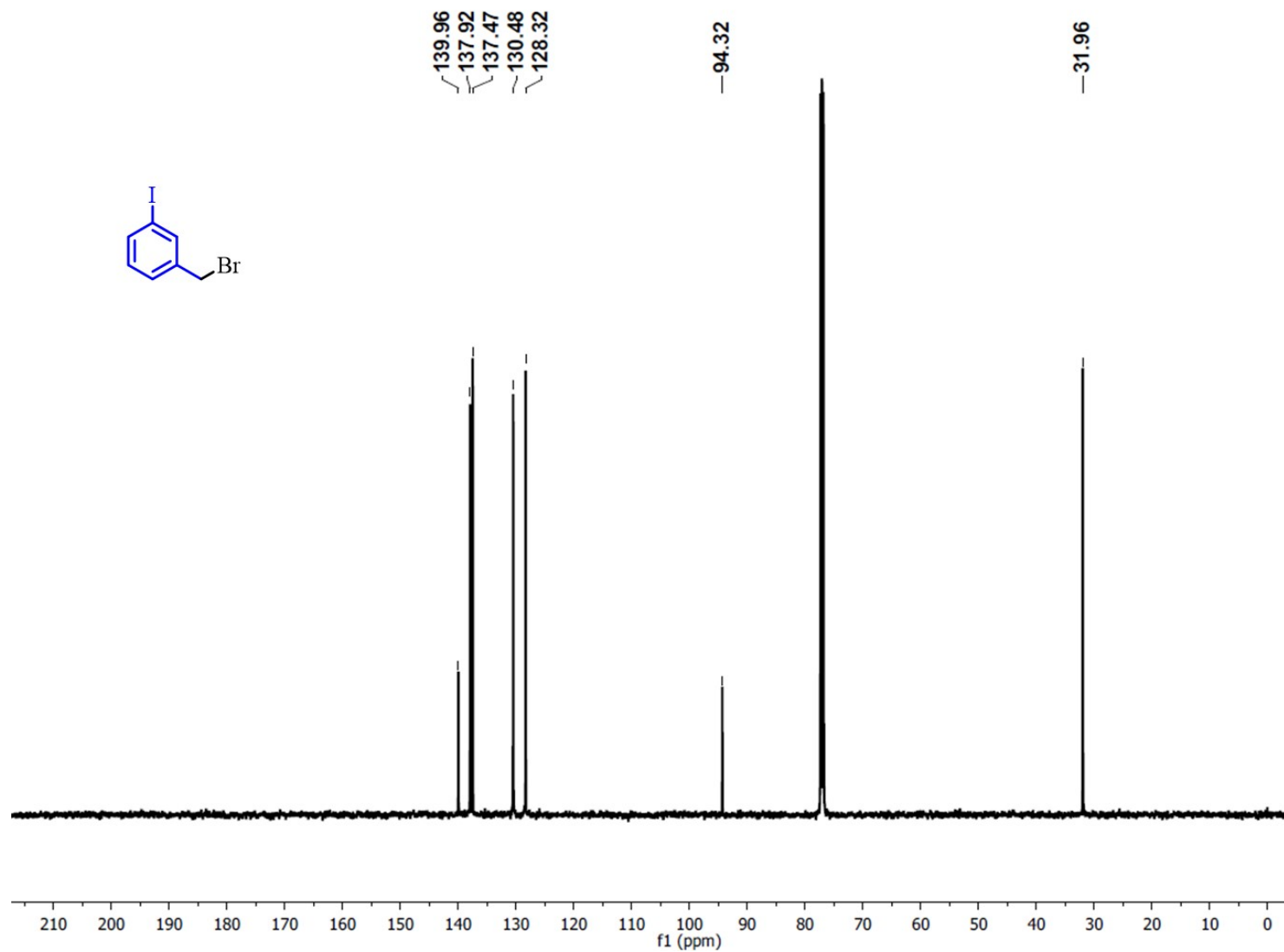
Fig. S26 ^{13}C NMR spectra of 1-(bromomethyl)-3-iodobenzene **(2g)**.
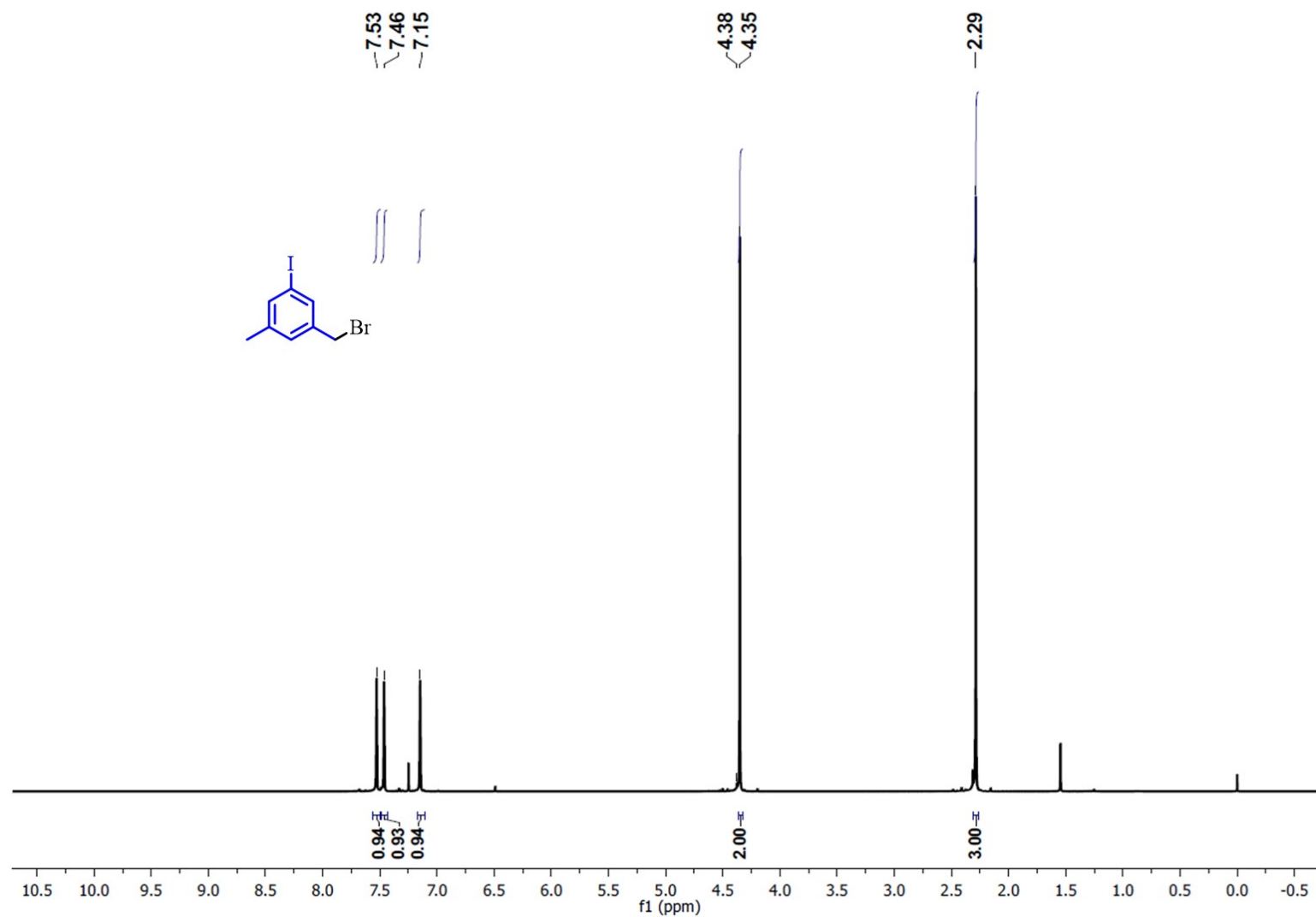
Fig. S27 ¹H NMR spectra of 1-(bromomethyl)-3-iodo-5-methylbenzene **(2h).**
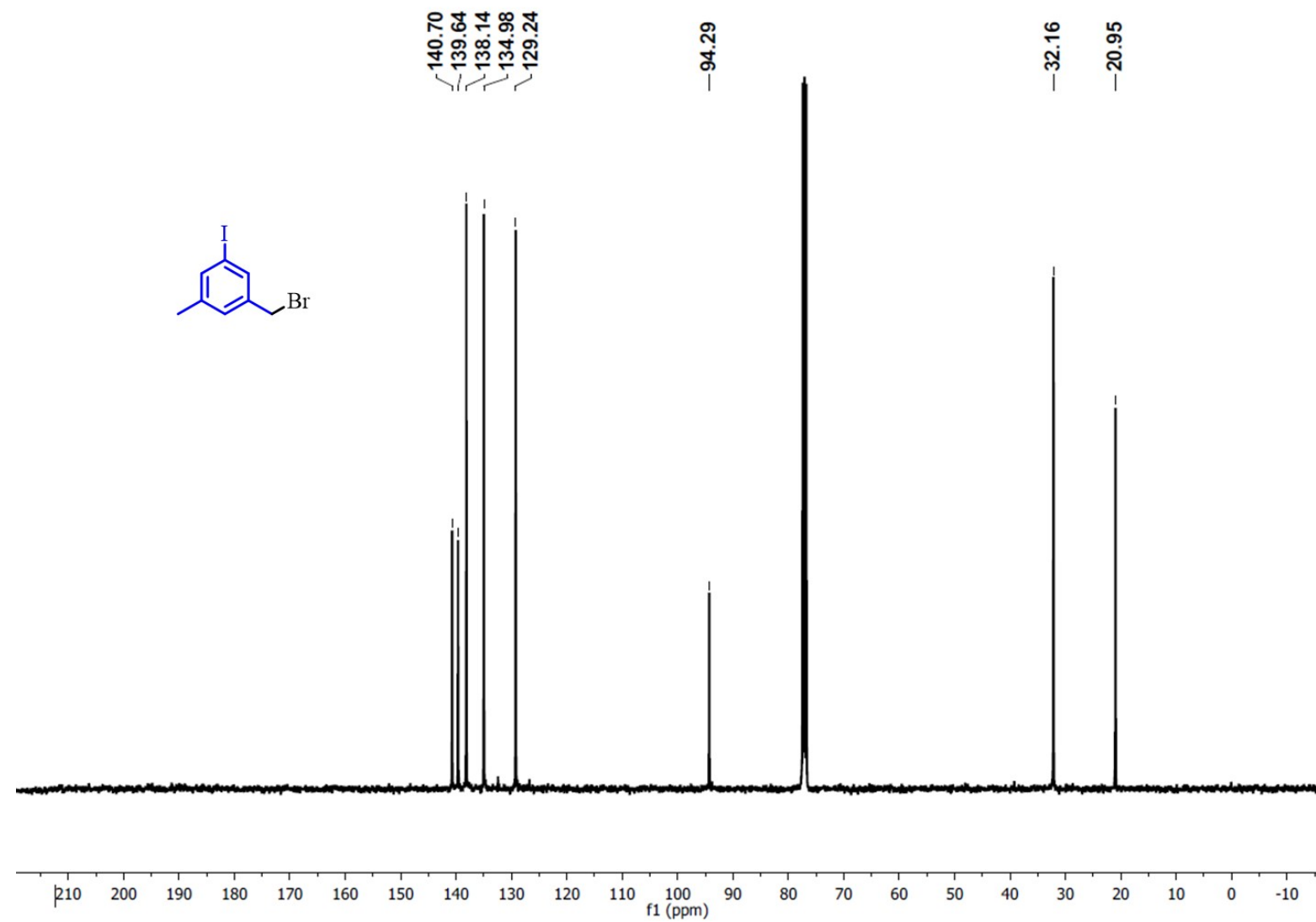
Fig. S28 ^{13}C NMR spectra of 1-(bromomethyl)-3-iodo-5-methylbenzene **(2h).**
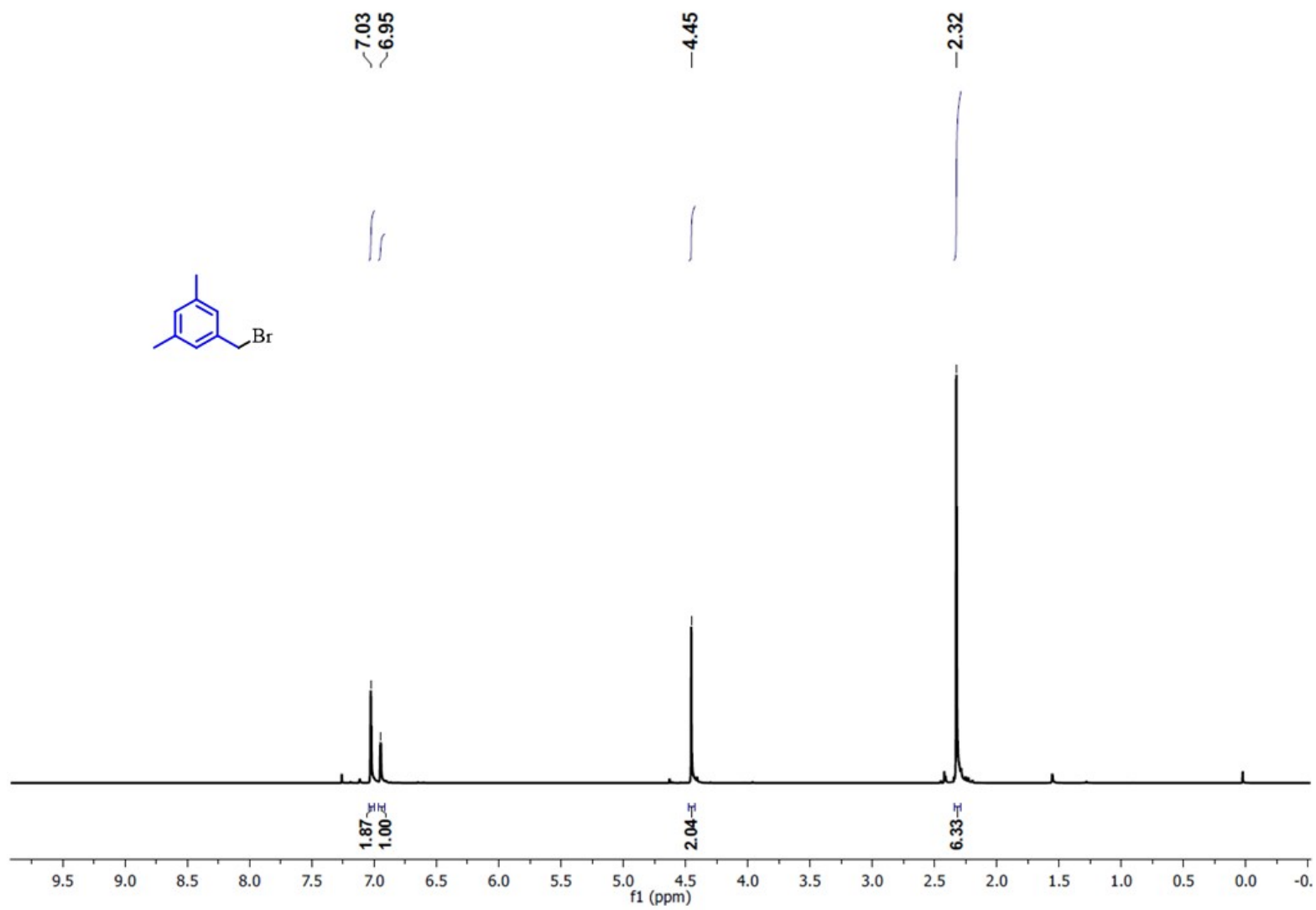
Fig. S29 ¹H NMR spectra of 1-(bromomethyl)-3,5-dimethylbenzene **(2i).**
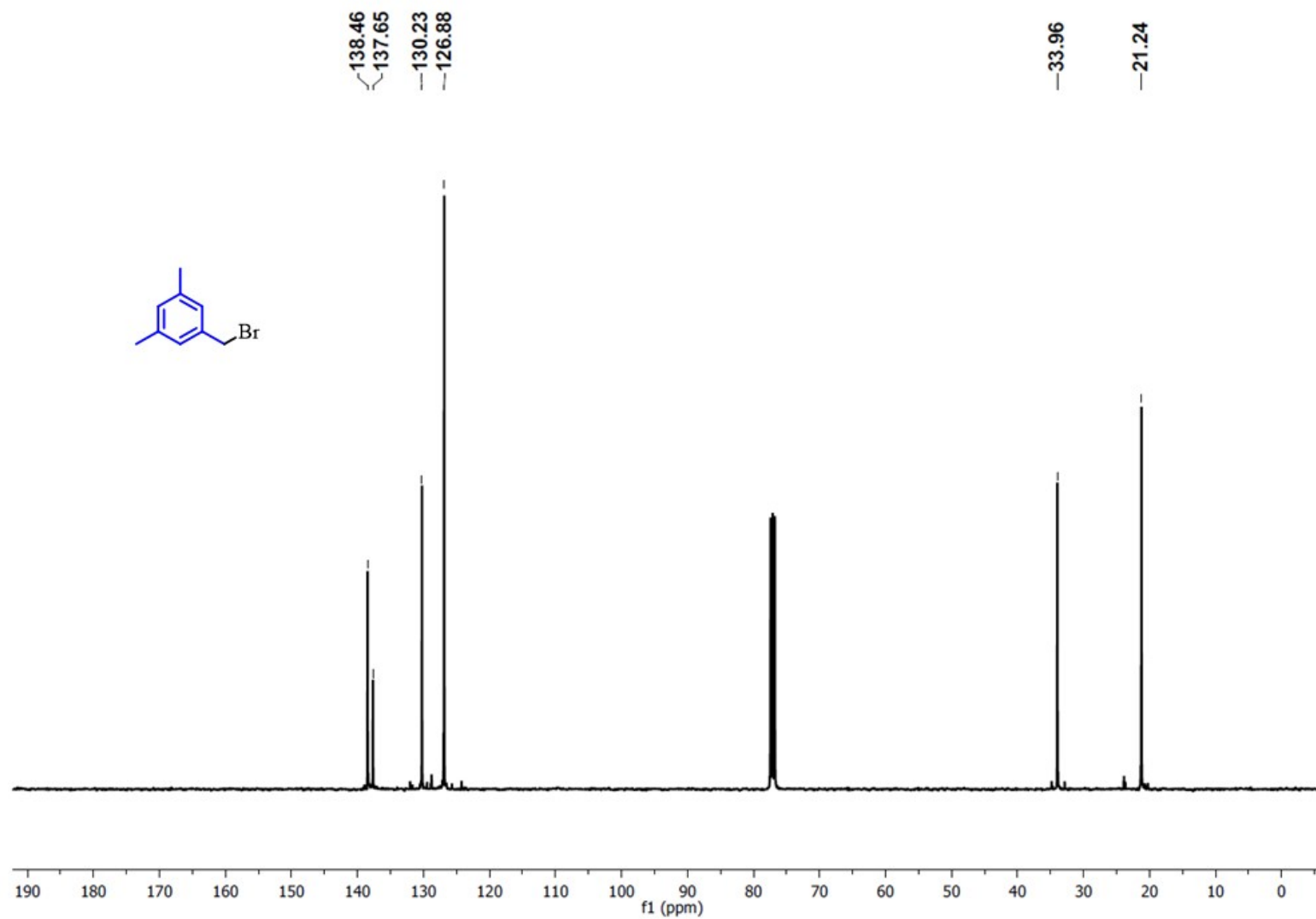
Fig. S30 ^{13}C NMR spectra of 1-(bromomethyl)-3,5-dimethylbenzene **(2i).**
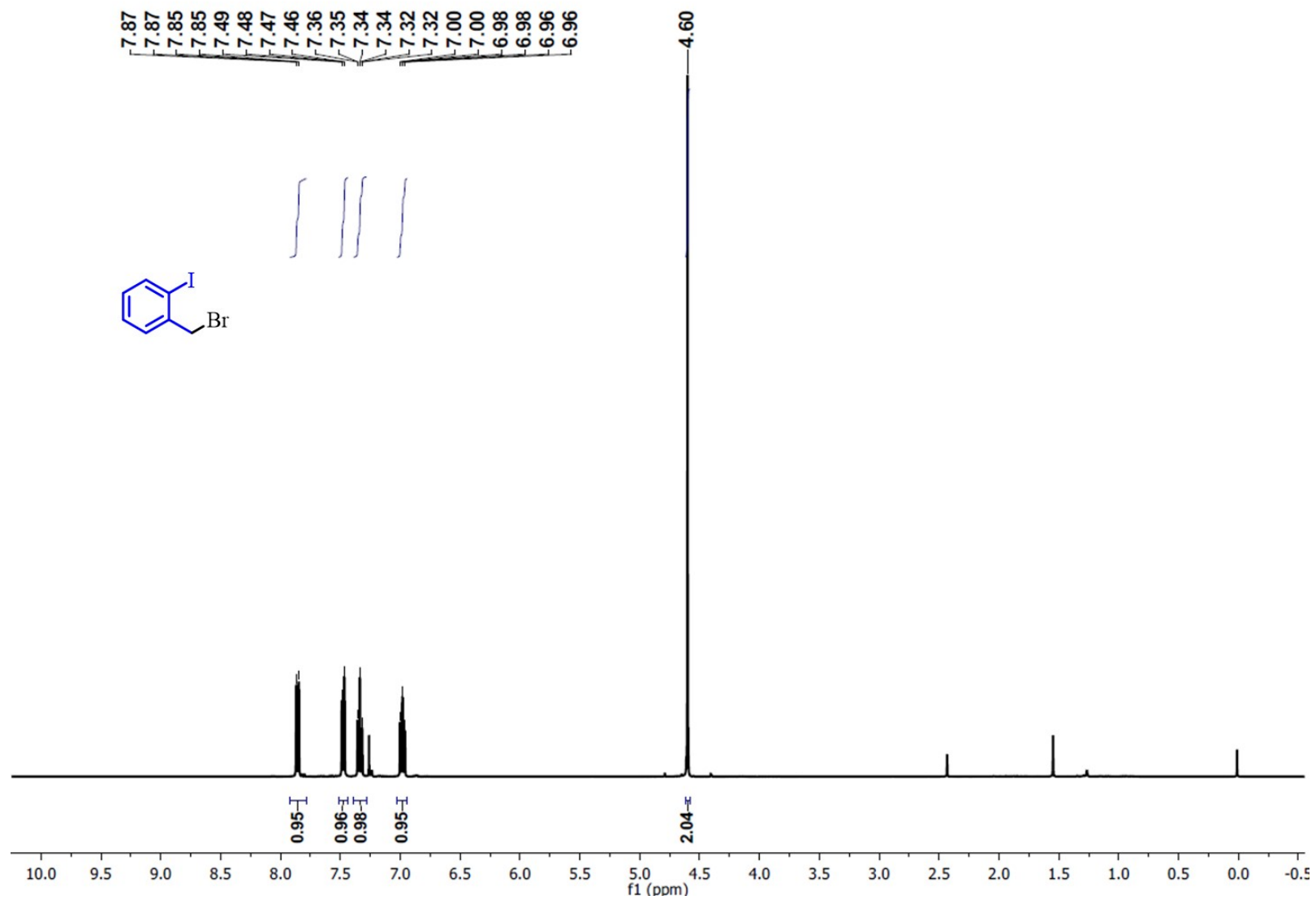
Fig. S31 ^{1}H NMR spectra of 1-(bromomethyl)-2-iodobenzene **(2j).**
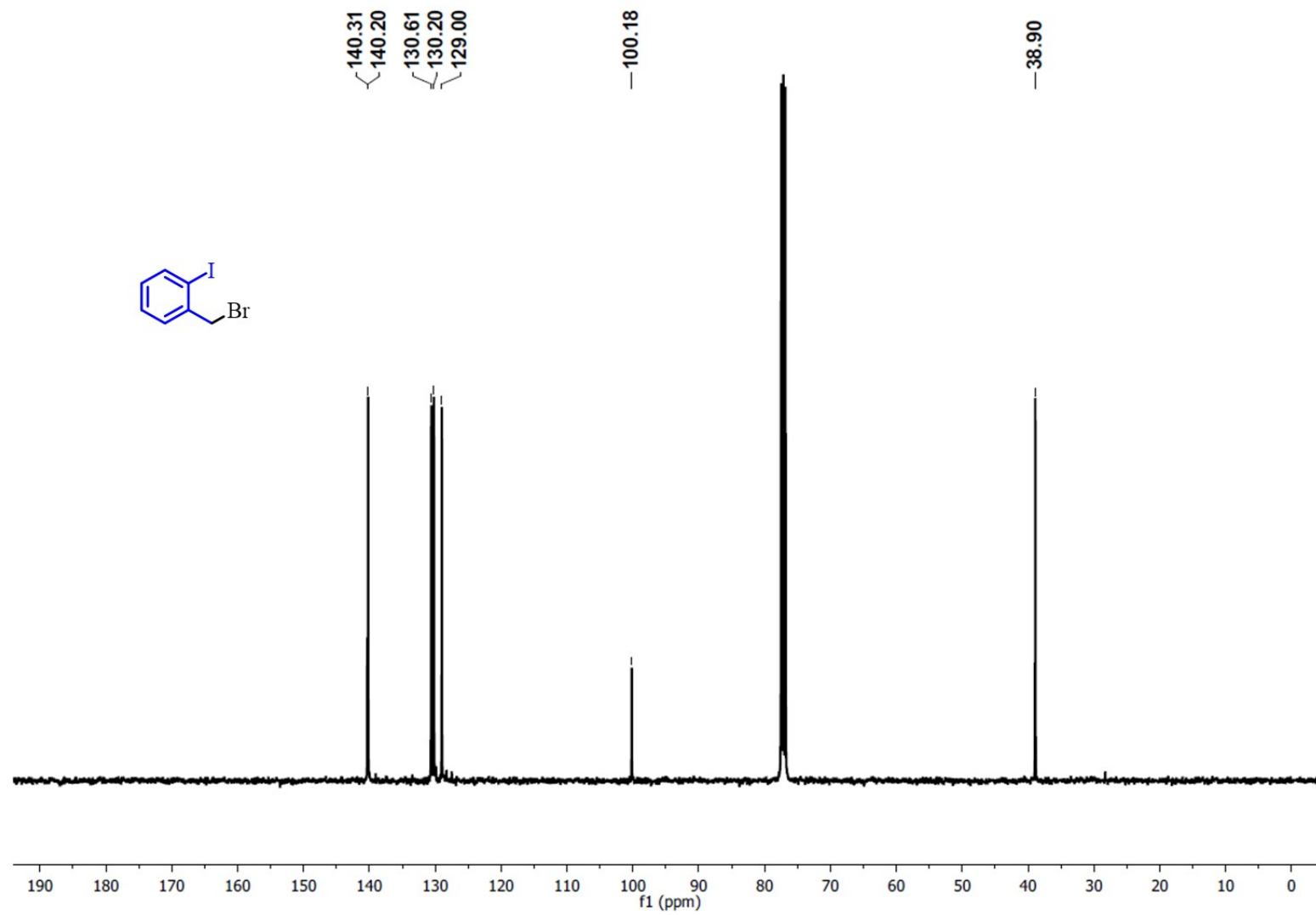
Fig. S32 ¹³C NMR spectra of 1-(bromomethyl)-2-iodobenzene **(2j).**
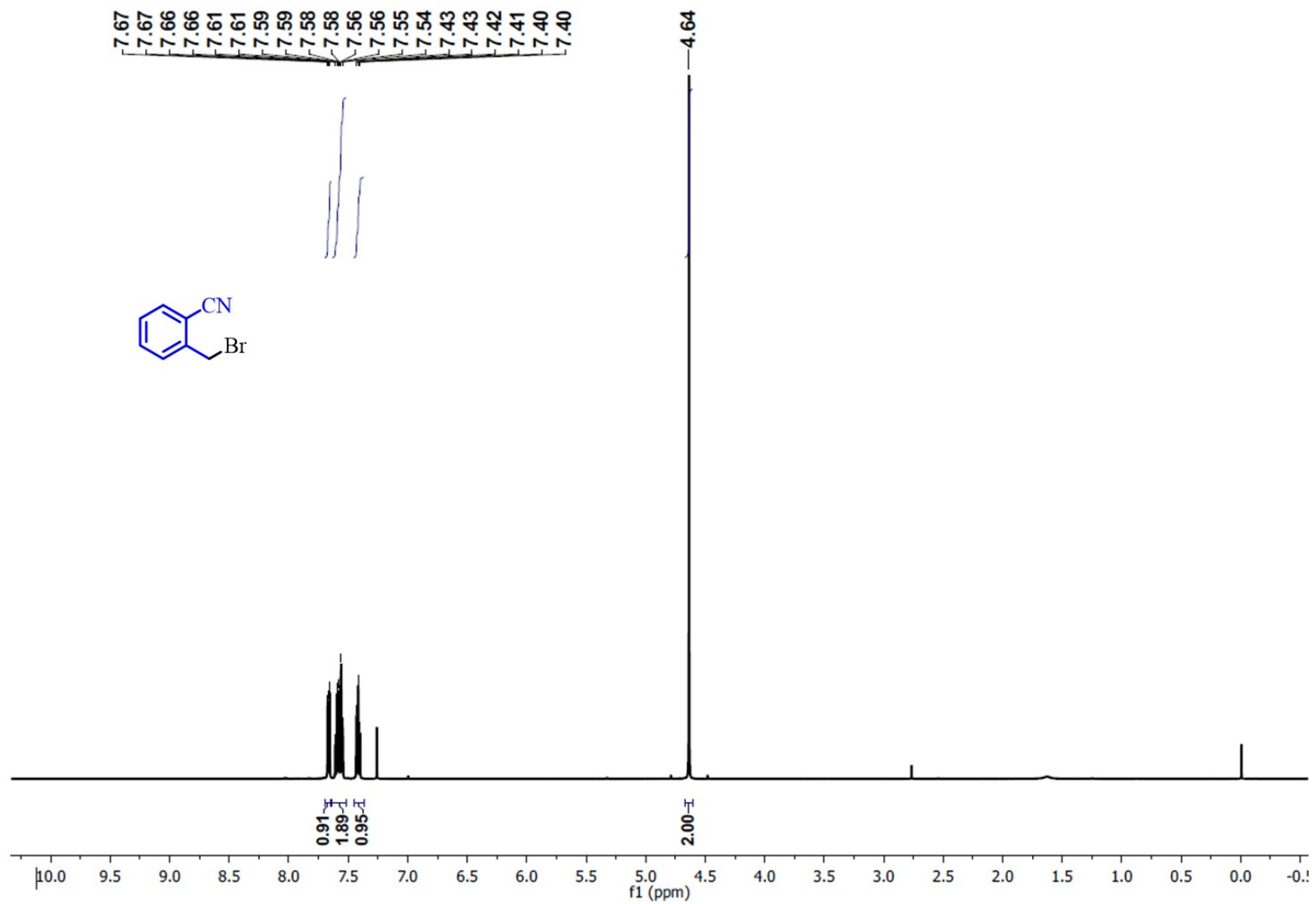
Fig. S33 ¹H NMR spectra of 2-(bromomethyl) benzonitrile **(2k).**
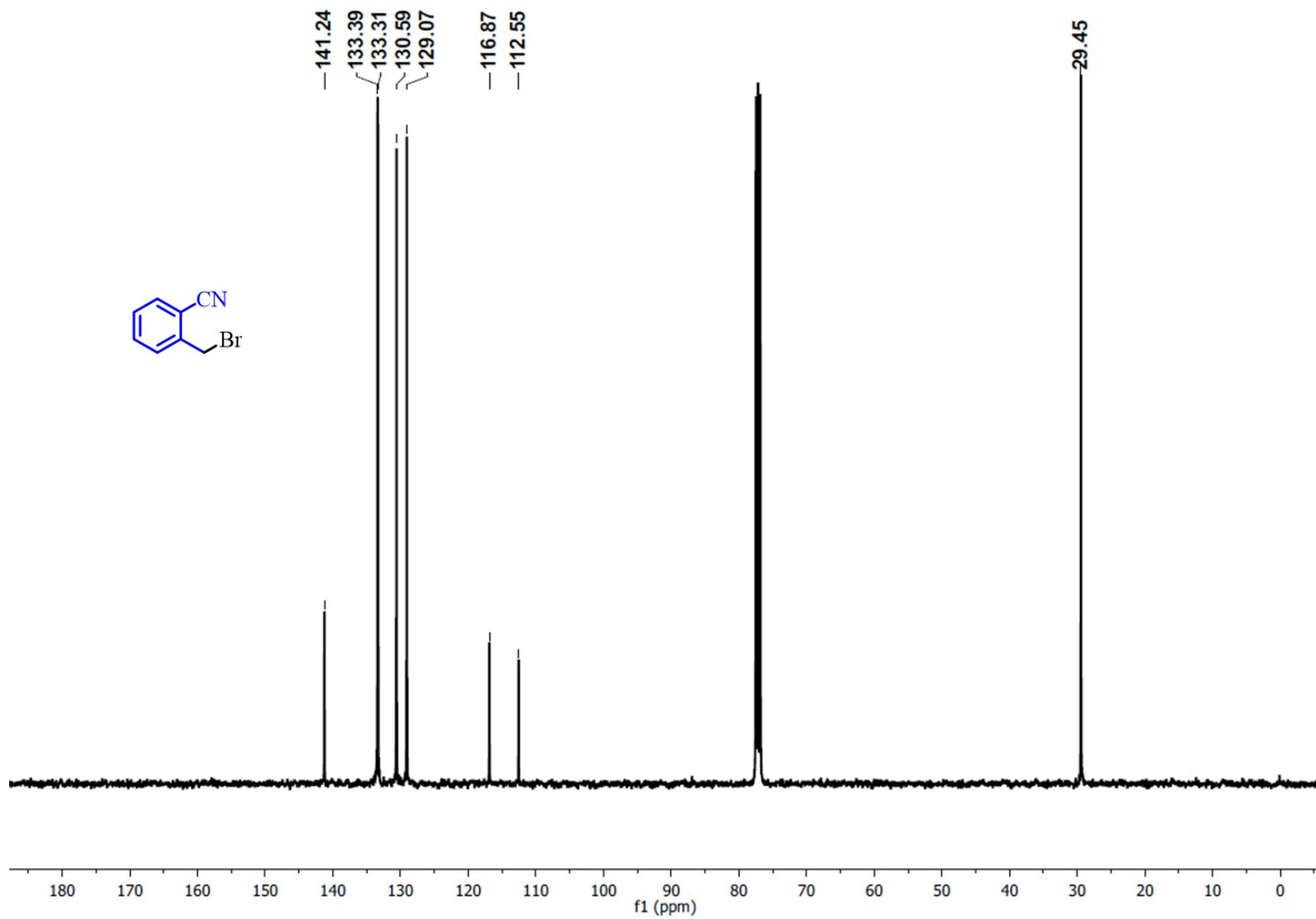
Fig. S34 ^{13}C NMR spectra of 2-(bromomethyl) benzonitrile **(2k).**

8.04, 8.03, 8.02, 8.01
7.61, 7.61, 7.59, 7.59, 7.58, 7.57, 7.56, 7.55, 7.51, 7.50, 7.49, 7.49, 7.48, 7.47
4.82

1.02

2.14
1.07

2.15

Fig. S35 ^{1}H NMR spectra of 1-(bromomethyl)-2-nitrobenzene **(2l).**

148.02

133.83
132.85
132.62
129.73
125.55

29.01

NO₂

Br

190 180 170 160 150 140 130 120 110 100 90 80 70 60 50 40 30 20 10 0
f1 (ppm)
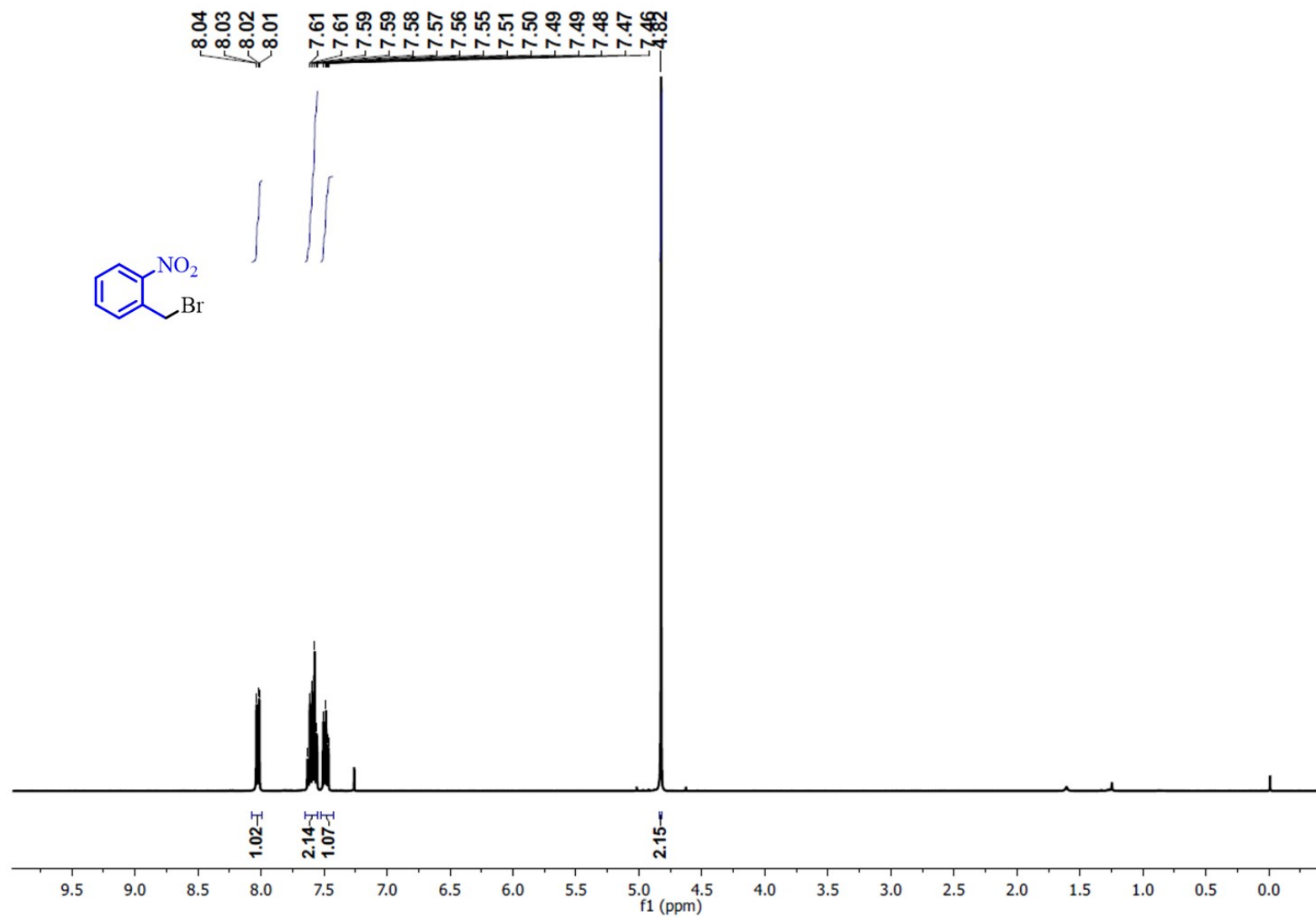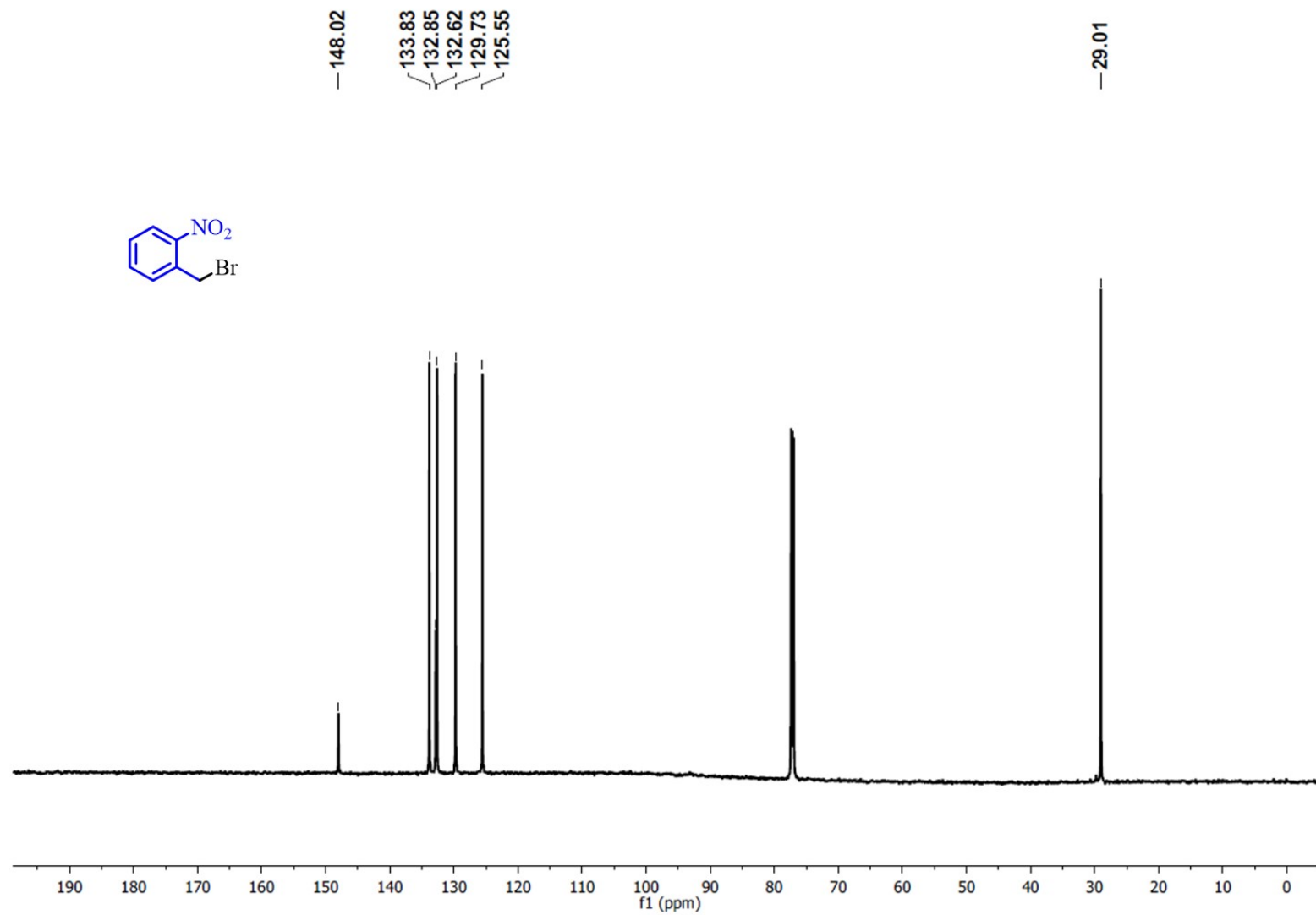
Fig. S36 ^{13}C NMR spectra of 1-(bromomethyl)-2-nitrobenzene **(2l).**
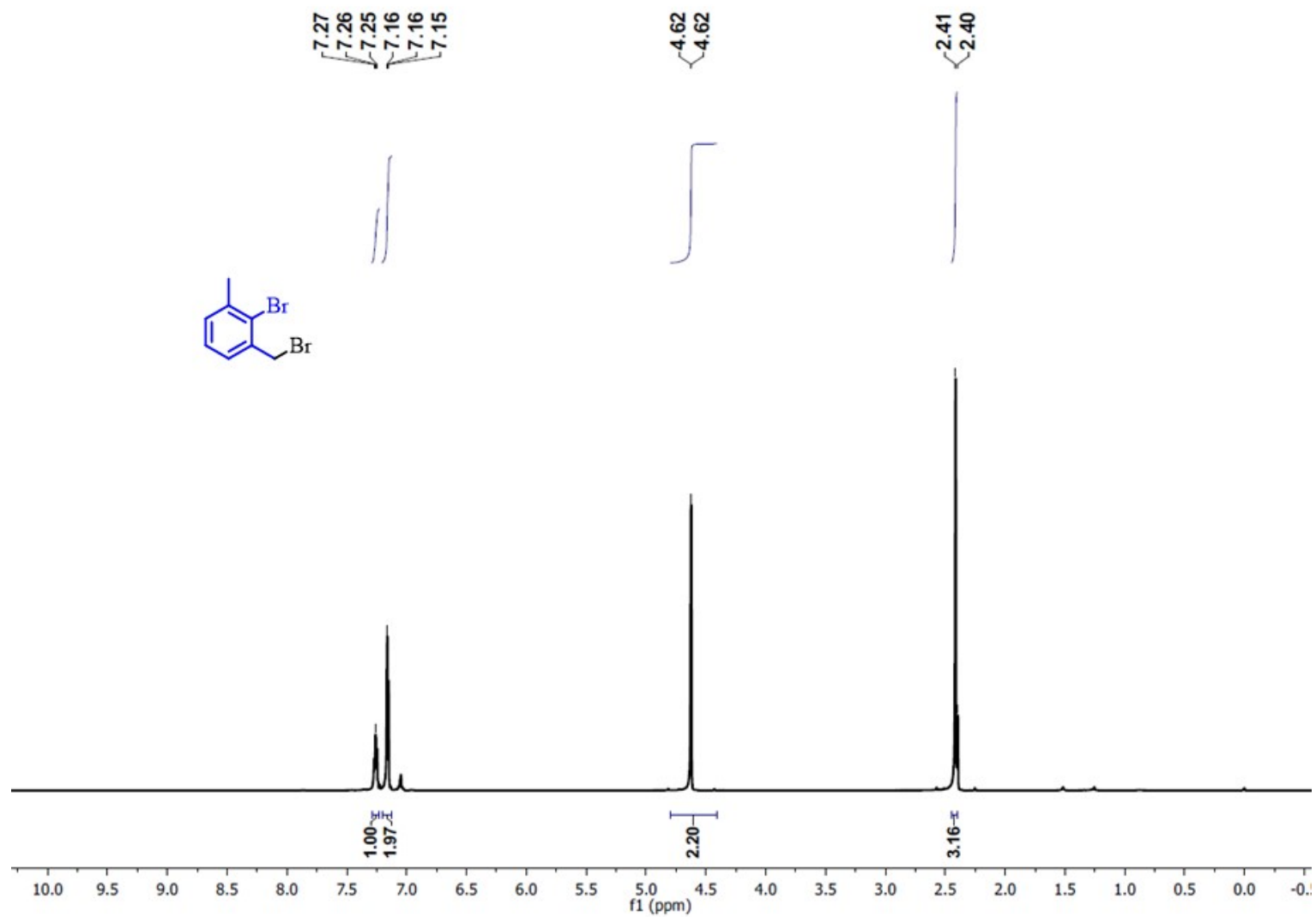
Fig. S37 ^{1}H NMR spectra of 2-bromo-1-(bromomethyl)-3-methylbenzene **(2m).**

139.49
137.39
131.06
128.76
127.34
127.13

34.75

23.88
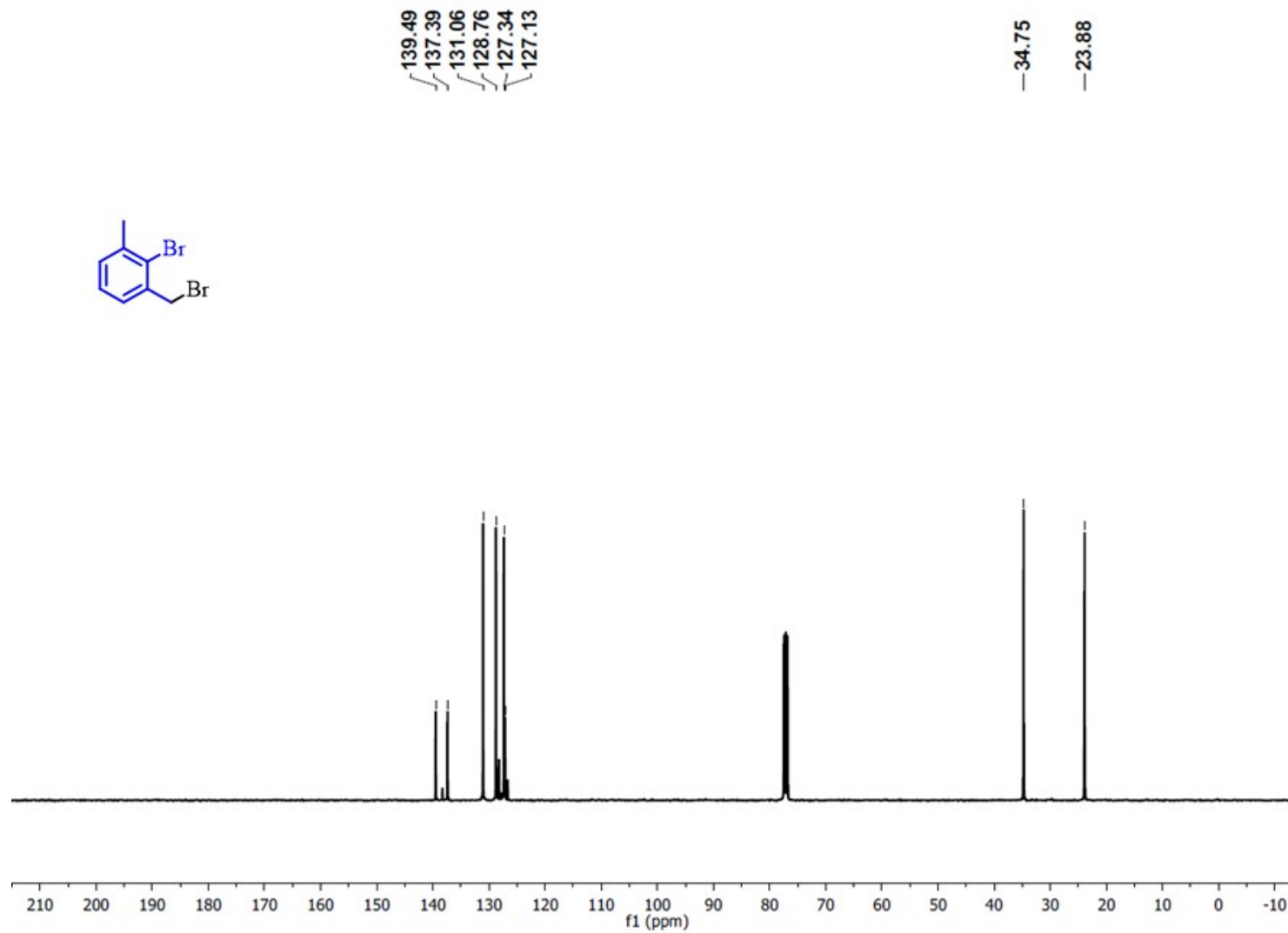
Fig. S38 ^{13}C NMR spectra of 2-bromo-1-(bromomethyl)-3-methylbenzene **(2m).**
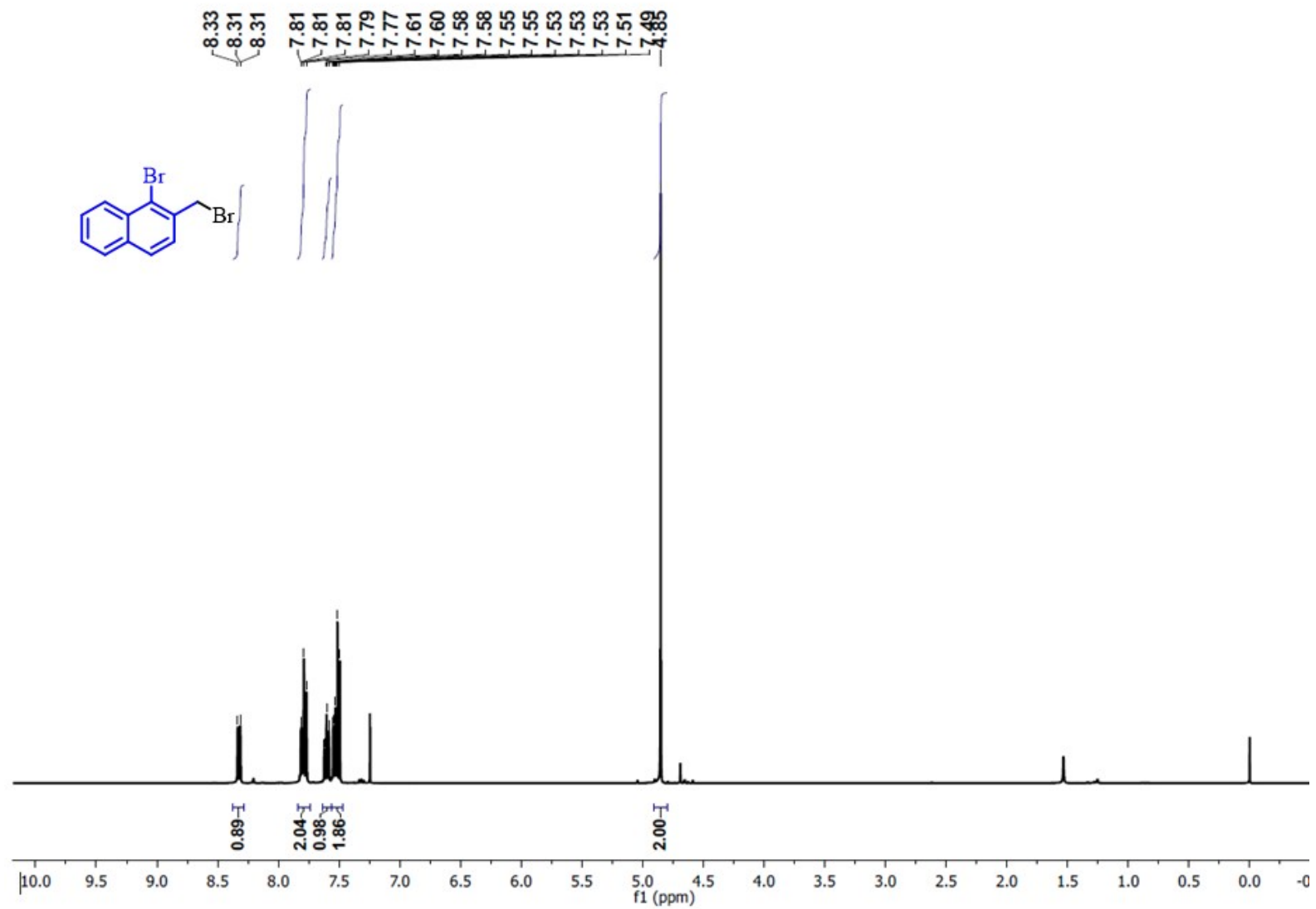
Fig. S39 ^{1}H NMR spectra of 1-bromo-2-(bromomethyl) naphthalene **(2n).**
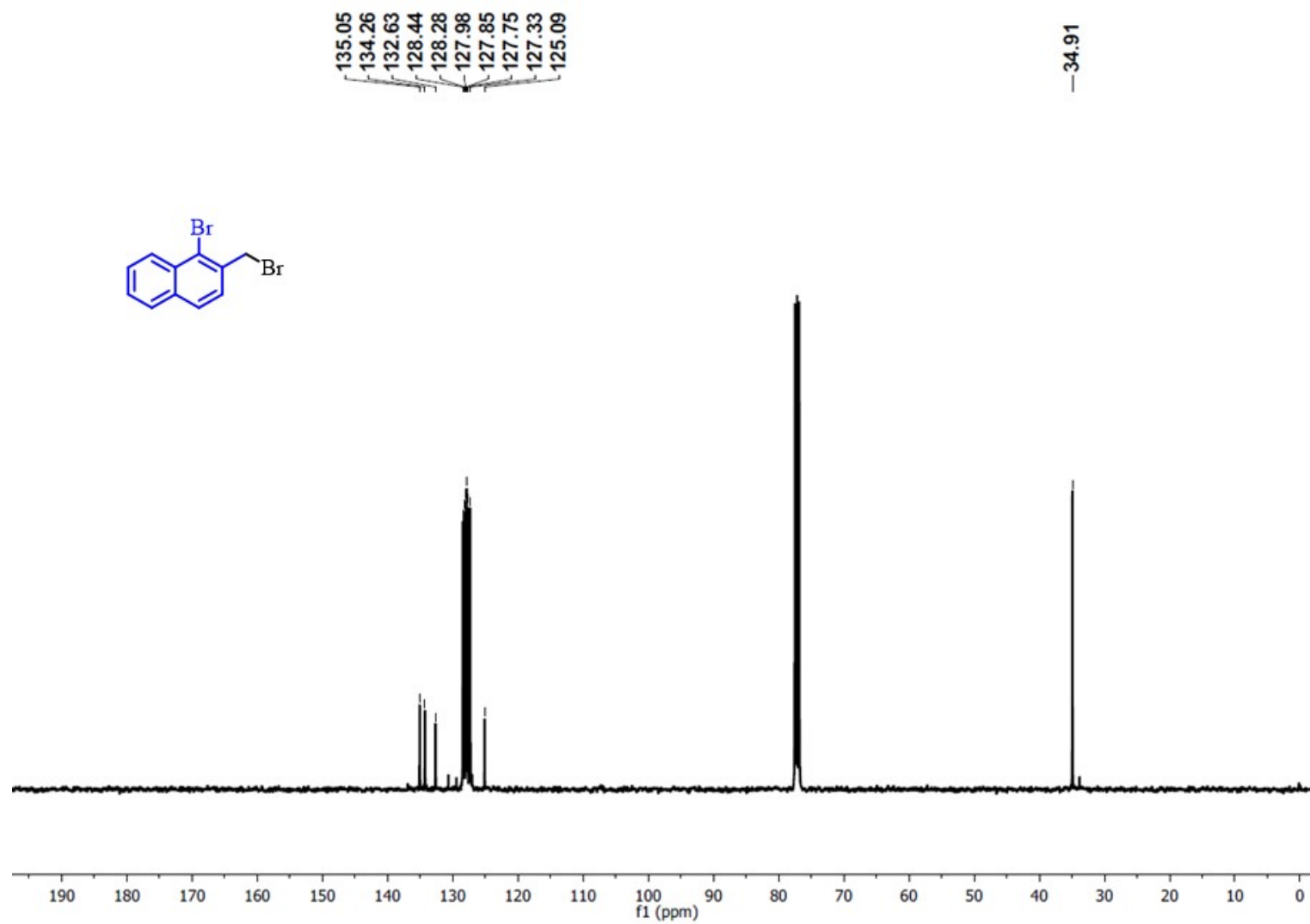
Fig. S40 ^{13}C NMR spectra of 1-bromo-2-(bromomethyl) naphthalene **(2n).**
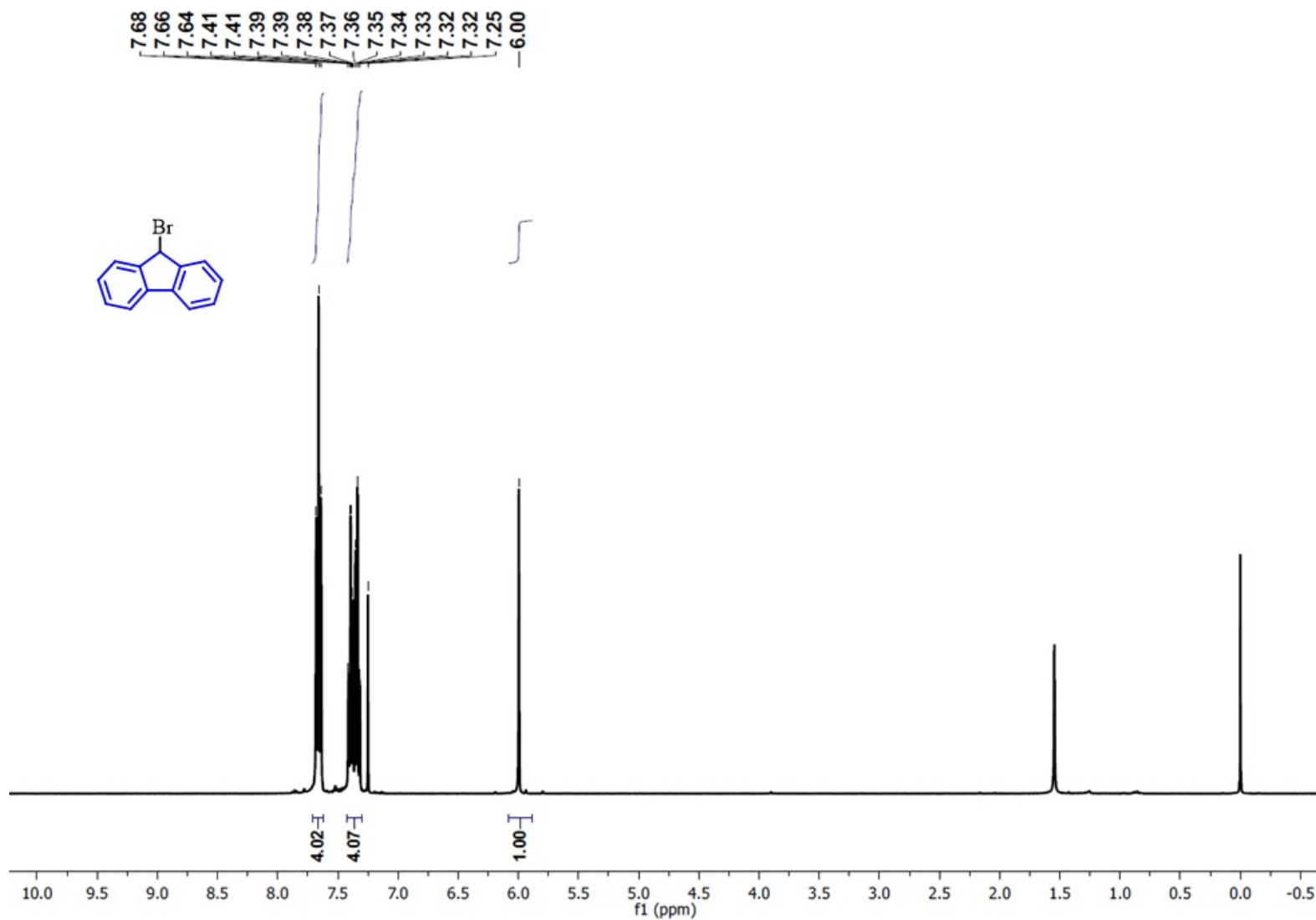
Fig. S41 ^{1}H NMR spectra of 9-bromo-9*H*-fluorene **(2o).**
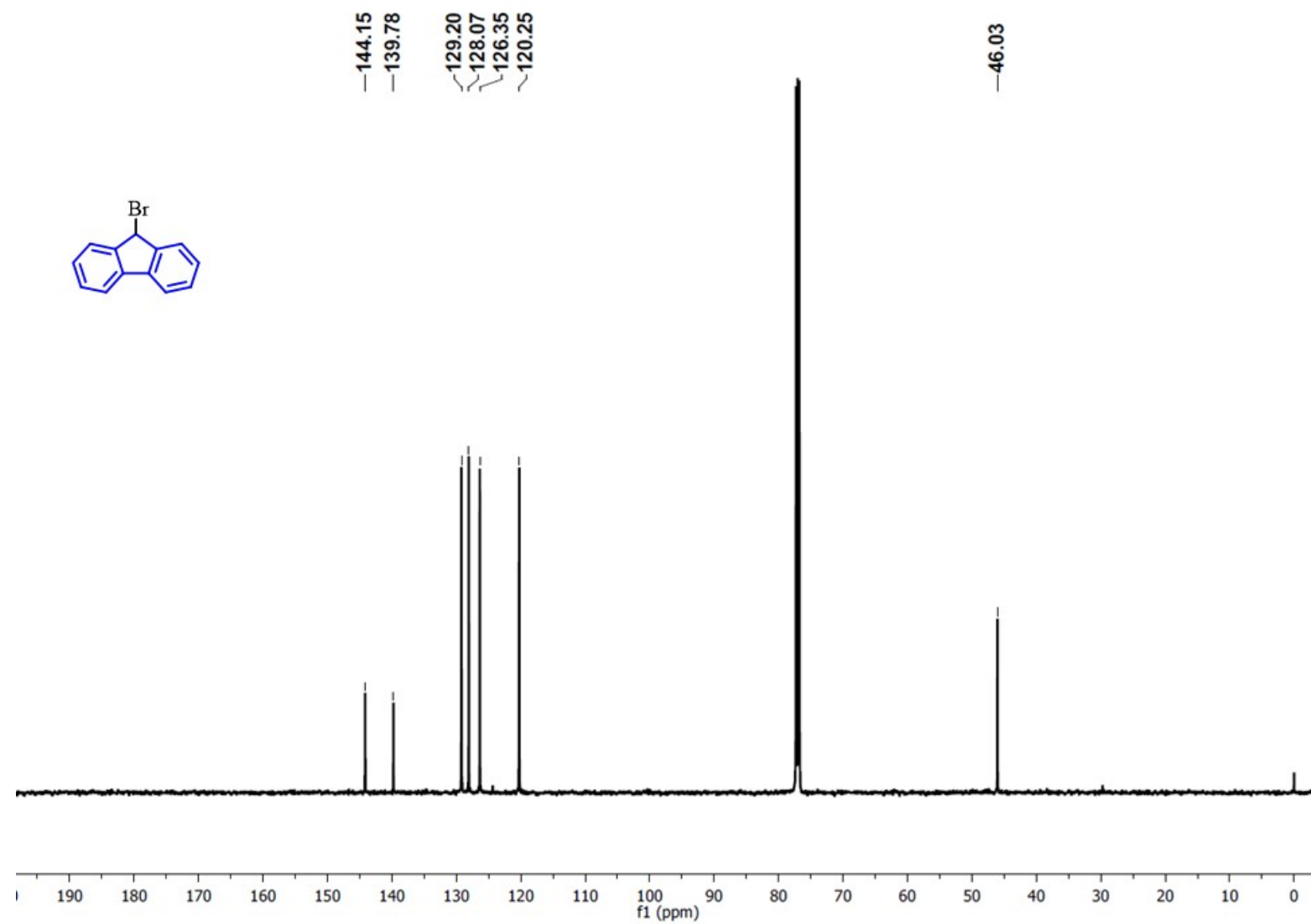
Fig. S42 ^{13}C NMR spectra of 9-bromo-9*H*-fluorene **(2o).**
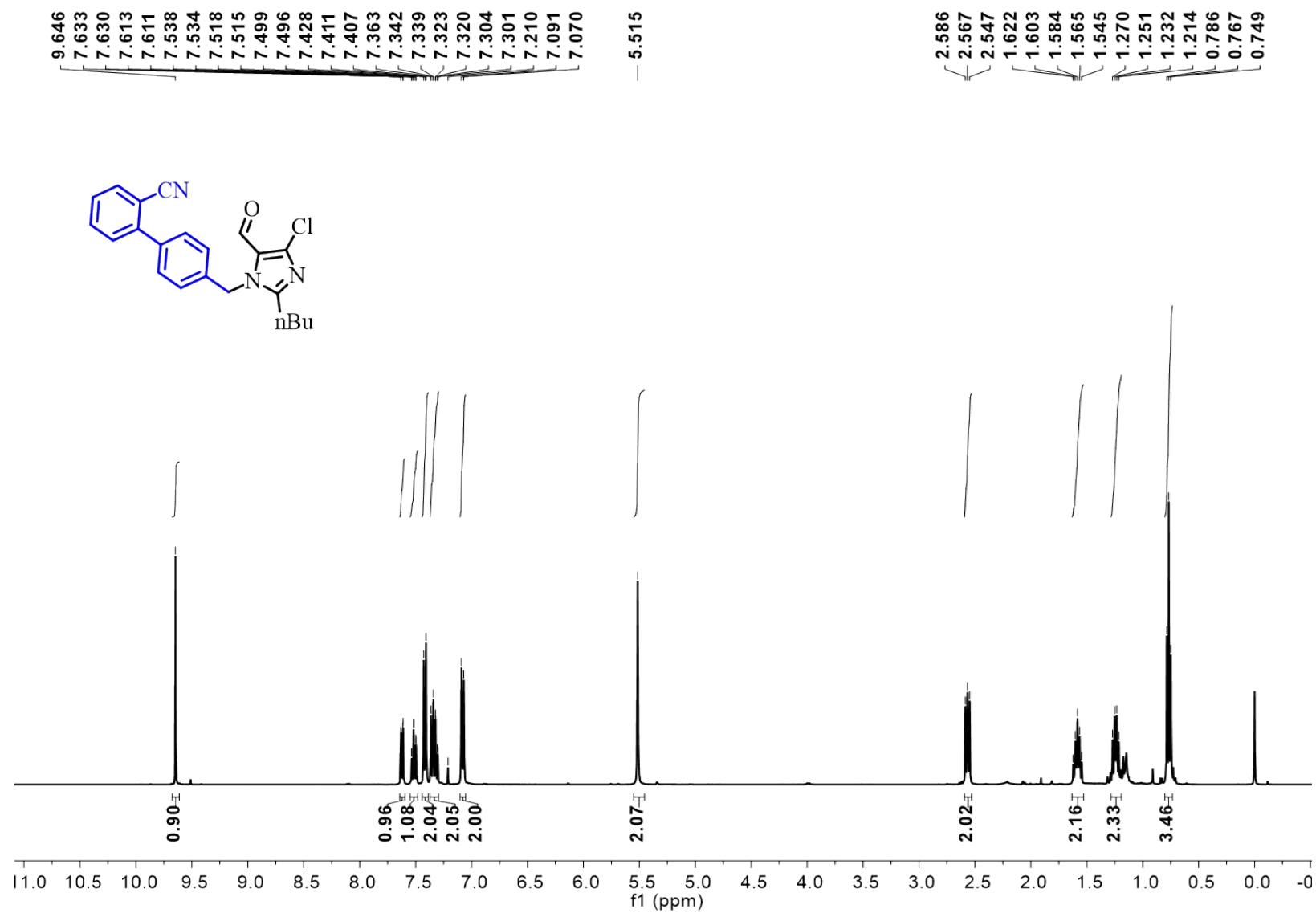
Fig. S43 ^{1}H NMR spectra of 4'-((2-butyl-4-chloro-5-formyl-1H-imidazol-1-yl) methyl)-[1,1'-biphenyl]-2-carbonitrile **(4a)**.
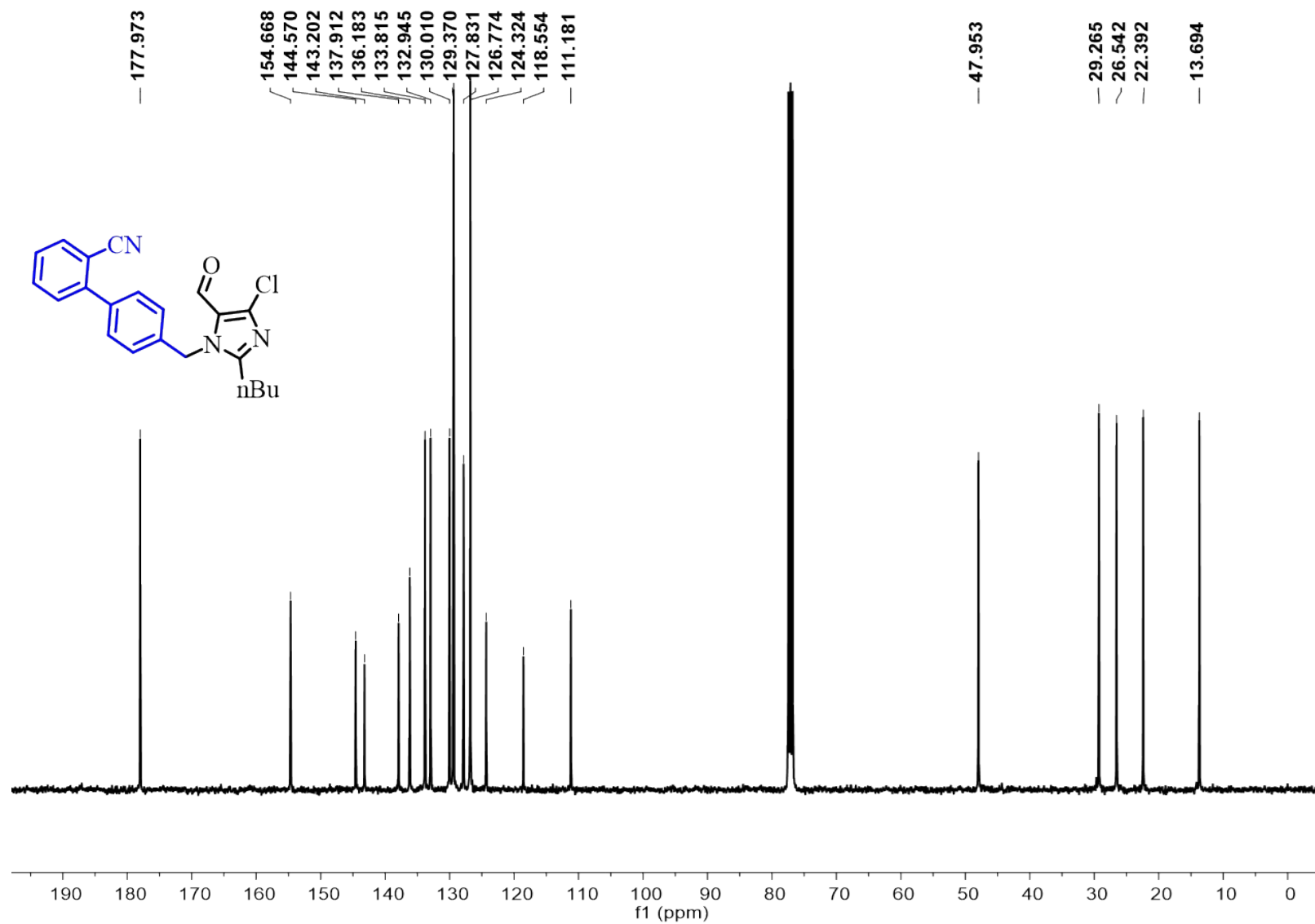
Fig. S44 ^{13}C NMR spectra of 4'-((2-butyl-4-chloro-5-formyl-1*H*-imidazol-1-yl) methyl)-[1,1'-biphenyl]-2-carbonitrile **(4a)**.
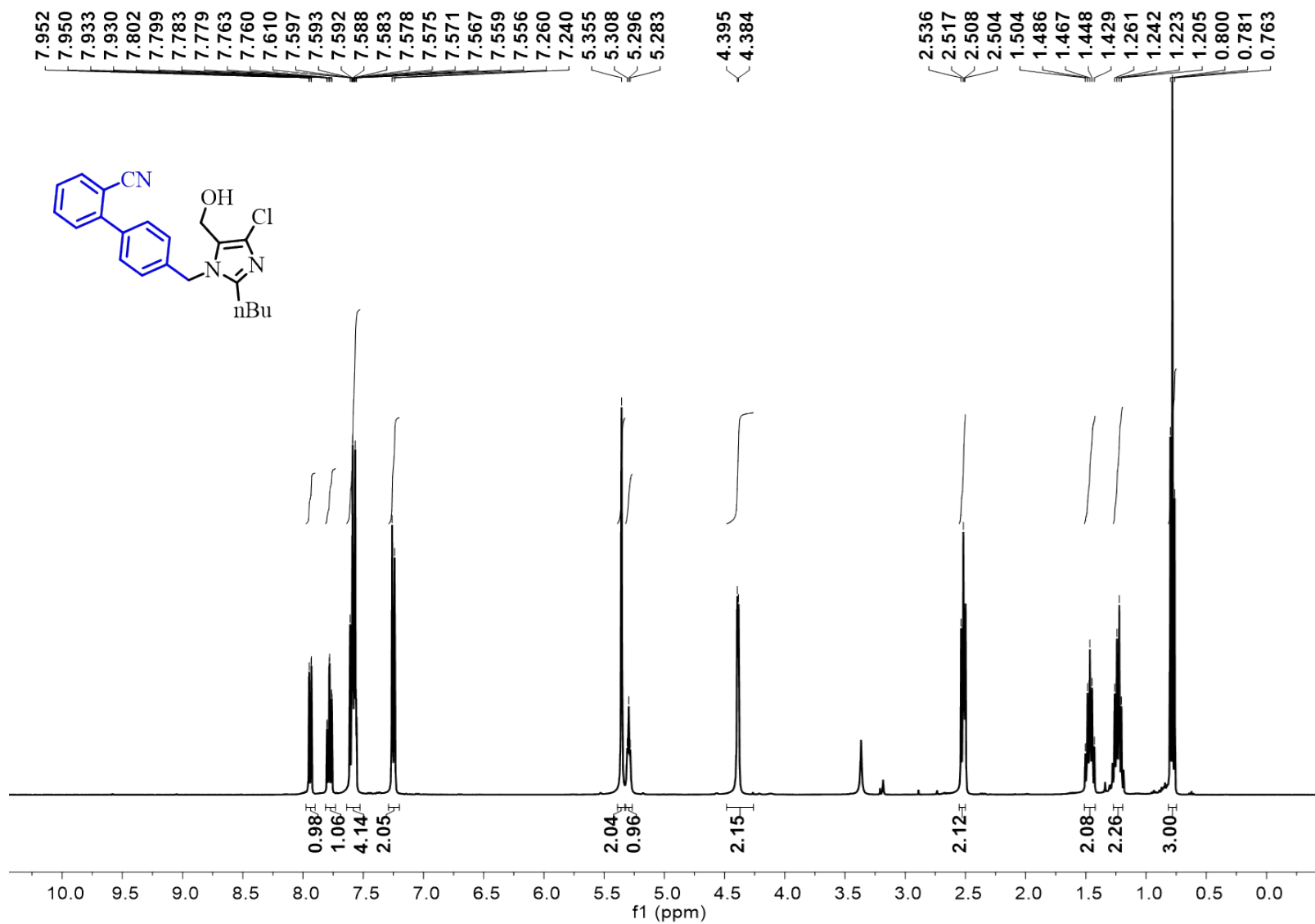
Fig. S45 ^{1}H NMR spectra of 4'-((2-butyl-4-chloro-5-(hydroxymethyl)-1H-imidazol-1-yl) methyl)-[1,1'-biphenyl]-2-carbonitrile **(4b)**.
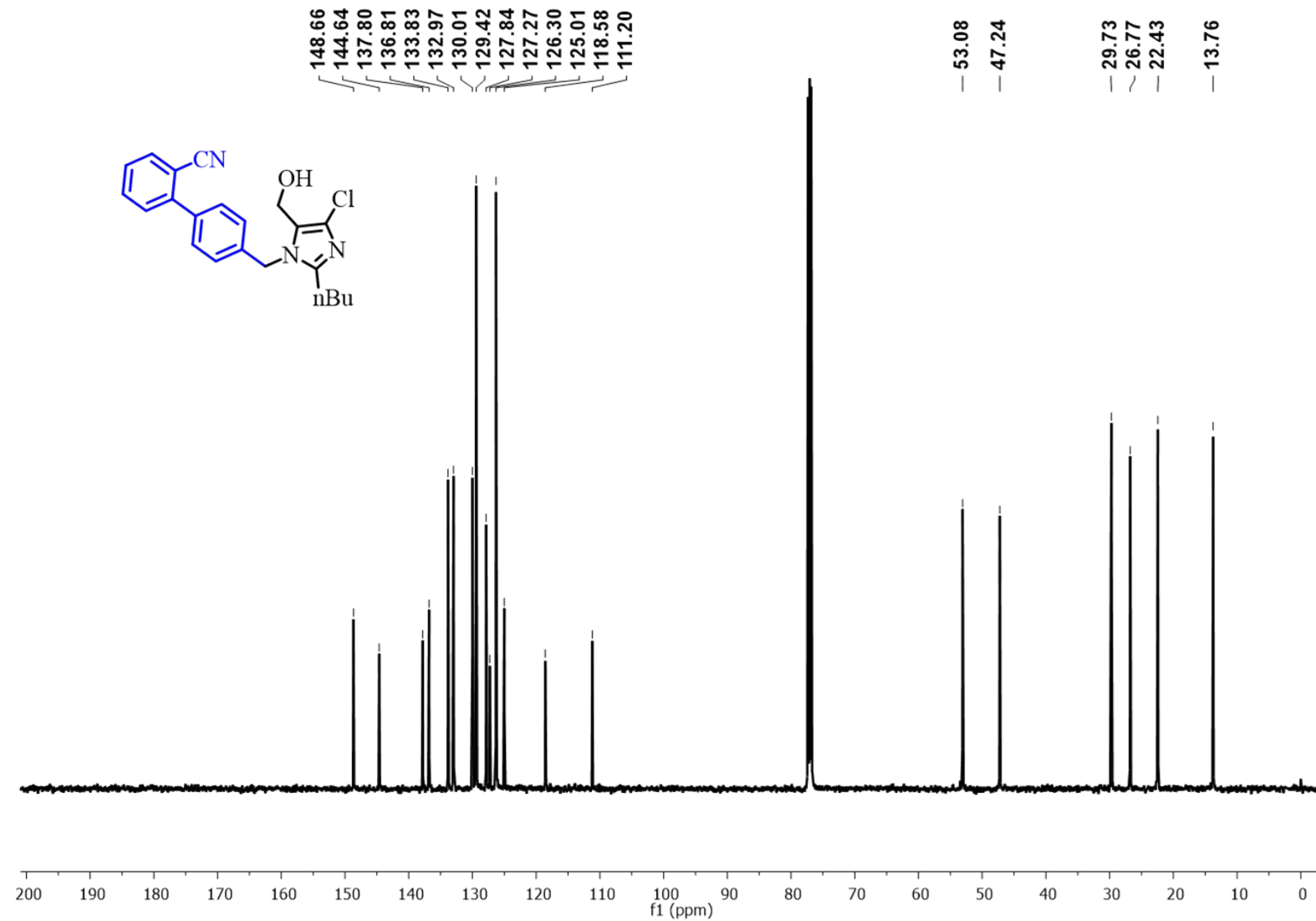
Fig. S46 ^{13}C NMR spectra of 4'-((2-butyl-4-chloro-5-(hydroxymethyl)-1*H*-imidazol-1-yl) methyl)-[1,1'-biphenyl]-2-carbonitrile **(4b)**.
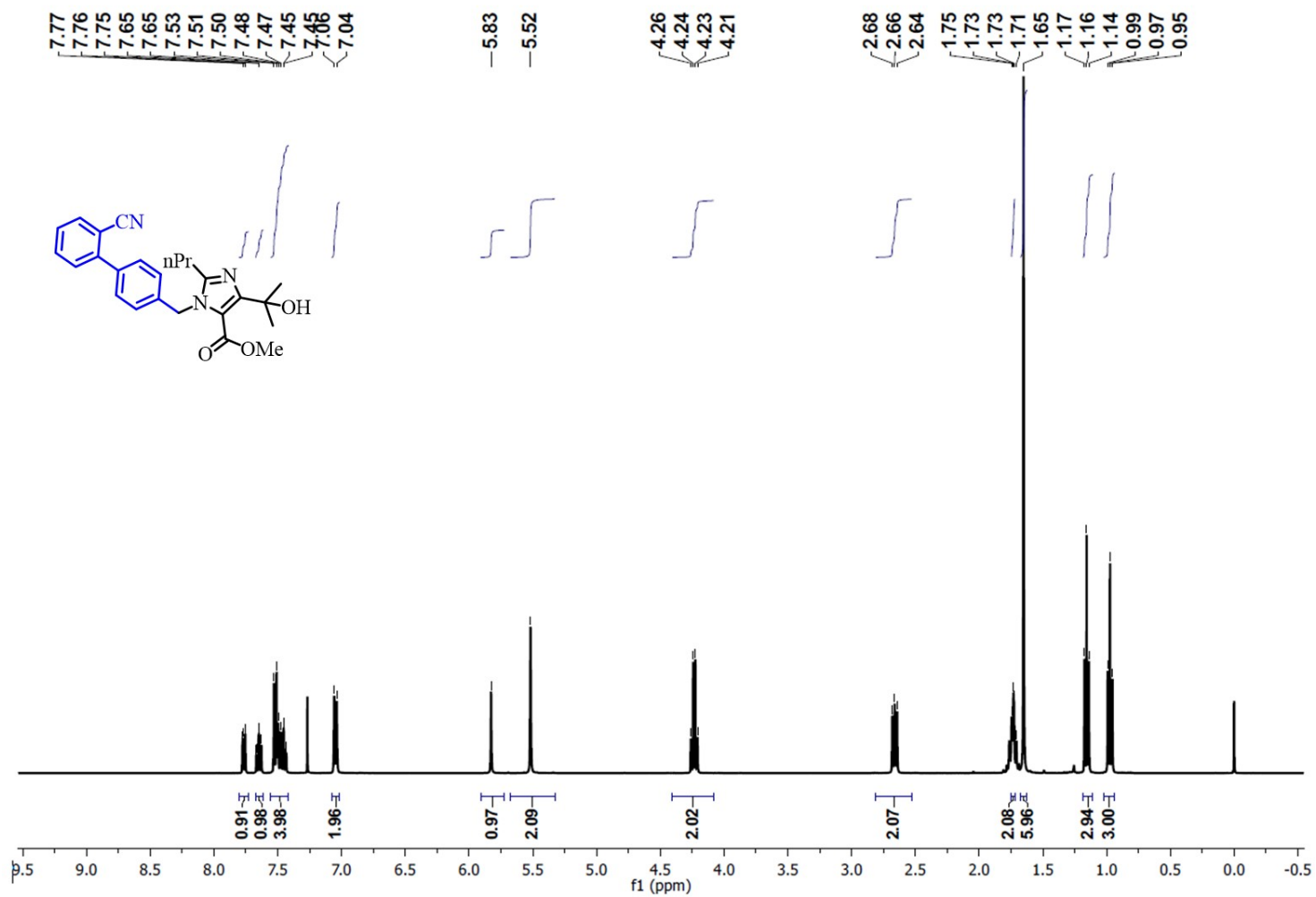
Fig. S47 ^{1}H NMR spectra of methyl 1-((2'-cyano-[1,1'-biphenyl]-4-yl) methyl)-4-(2-hydroxypropan-2-yl)-2-propyl-1*H*-imidazole-5-carboxylate (**4c**).
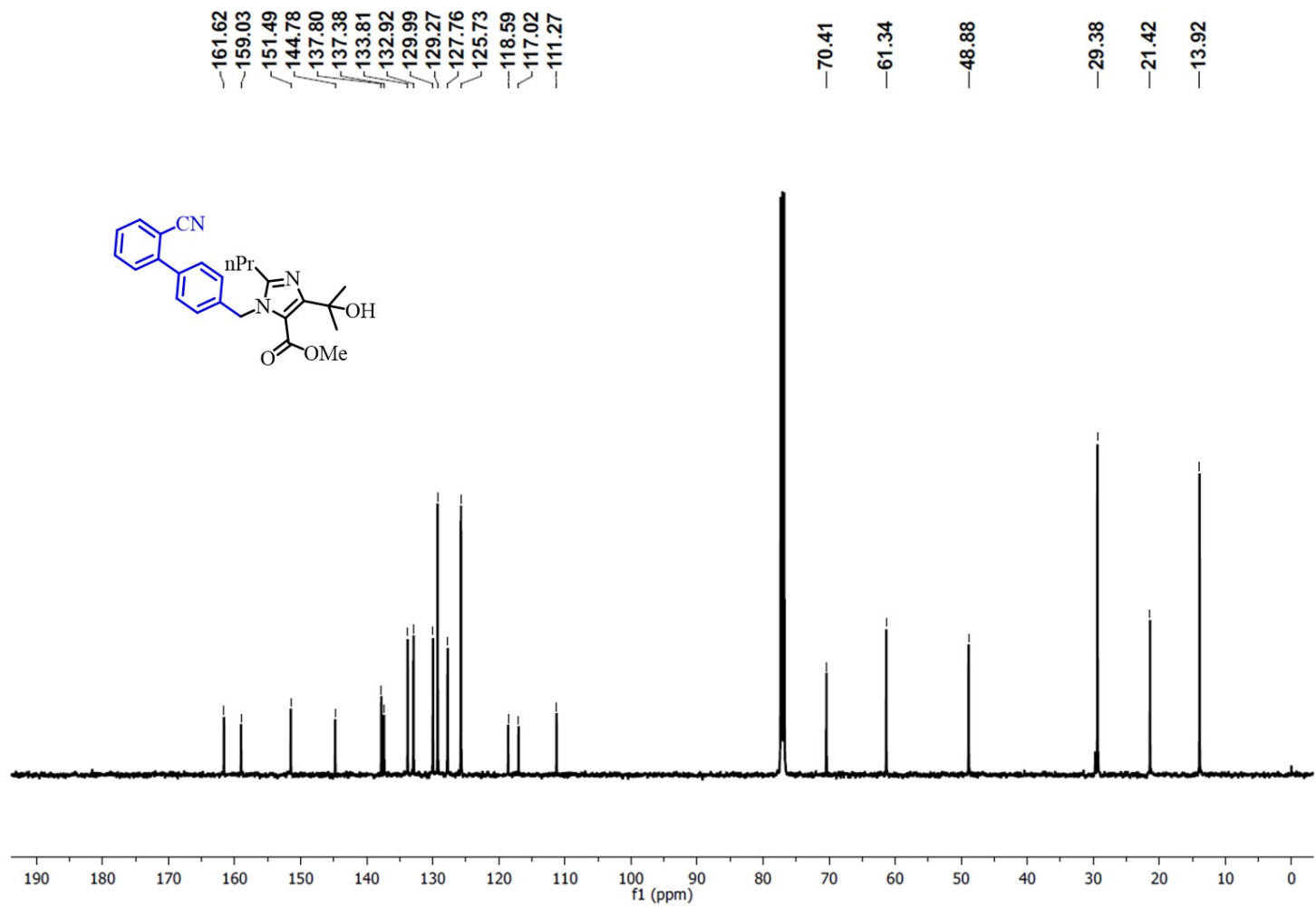
Fig. S48 ^{13}C NMR spectra of methyl 1-((2'-cyano-[1,1'-biphenyl]-4-yl) methyl)-4-(2-hydroxypropan-2-yl)-2-propyl-1H-imidazole-5-carboxylate **(4c)**.
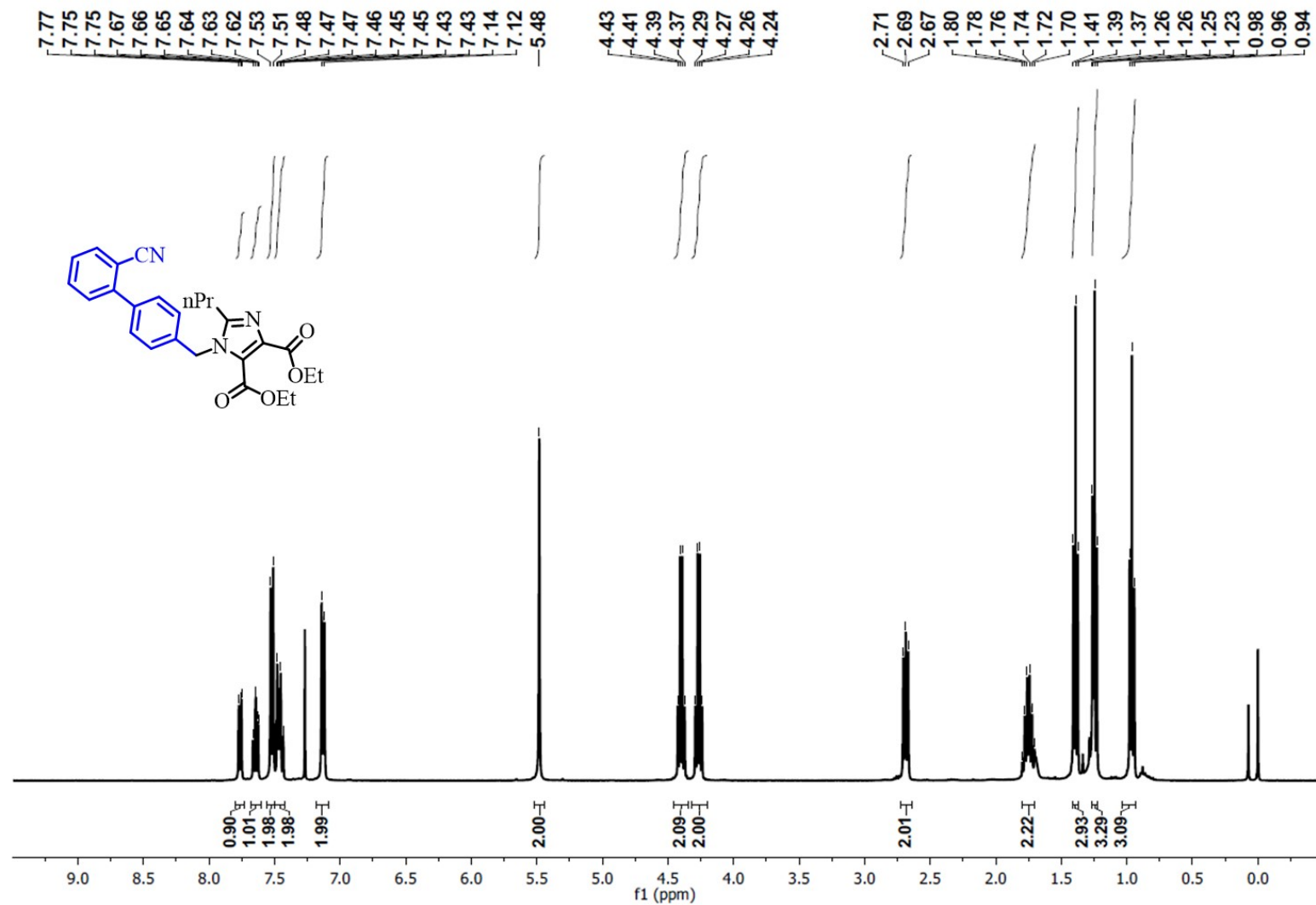
Fig. S49 ^{1}H NMR spectra of diethyl 1-((2'-cyano-[1,1'-biphenyl]-4-yl) methyl)-2-propyl-1H-imidazole-4,5-dicarboxylate **(4d)**.

163.11
160.49
151.96
144.63
137.84
136.48
133.83
132.92
130.00
129.34
127.82
126.54
118.53
117.27
61.65
61.34
48.02
29.16
21.39
14.33
13.92

f1 (ppm)
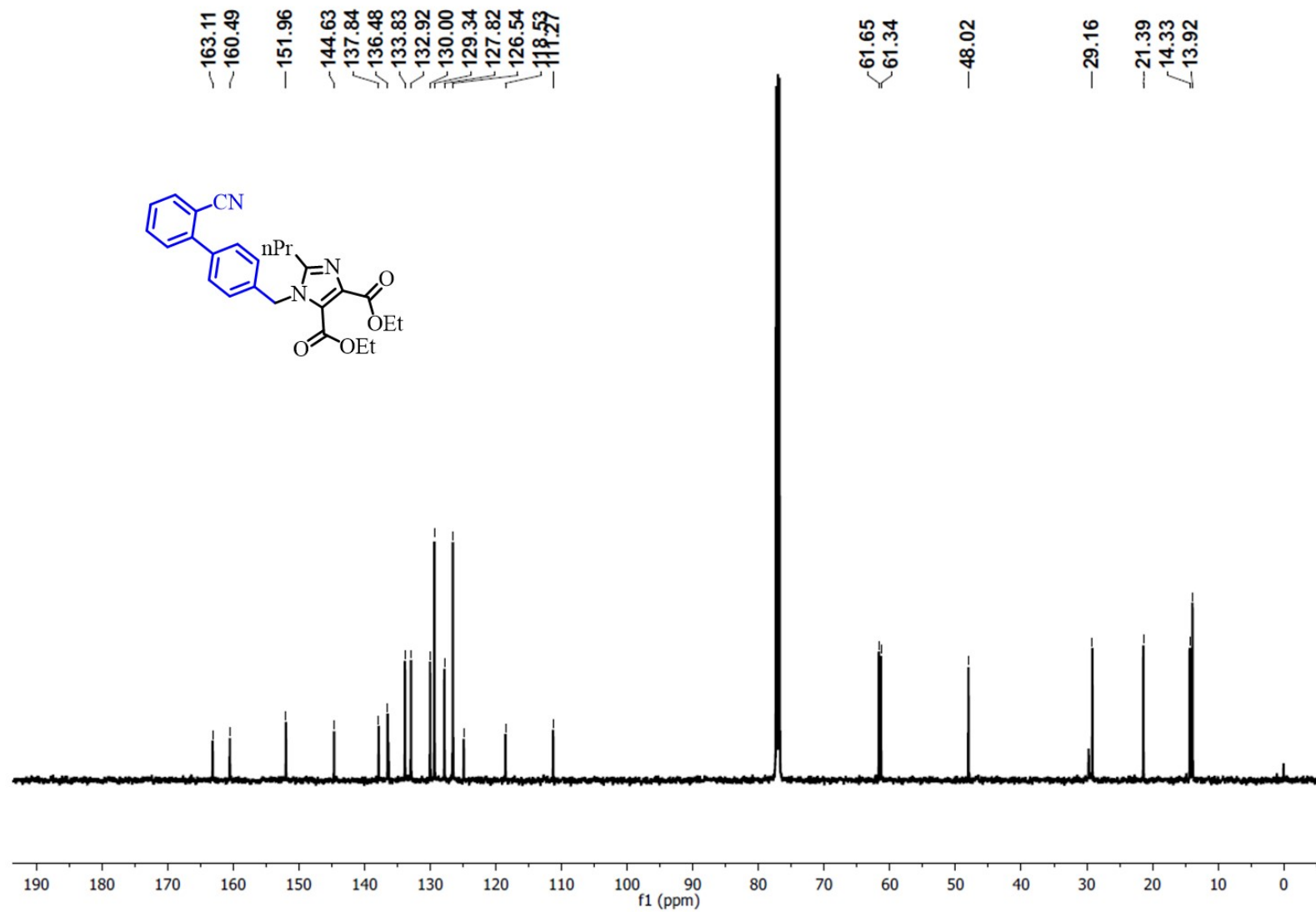
Fig. S50 ^{1}H NMR spectra of diethyl 1-((2'-cyano-[1,1'-biphenyl]-4-yl) methyl)-2-propyl-1H-imidazole-4,5-dicarboxylate **(4d)**.
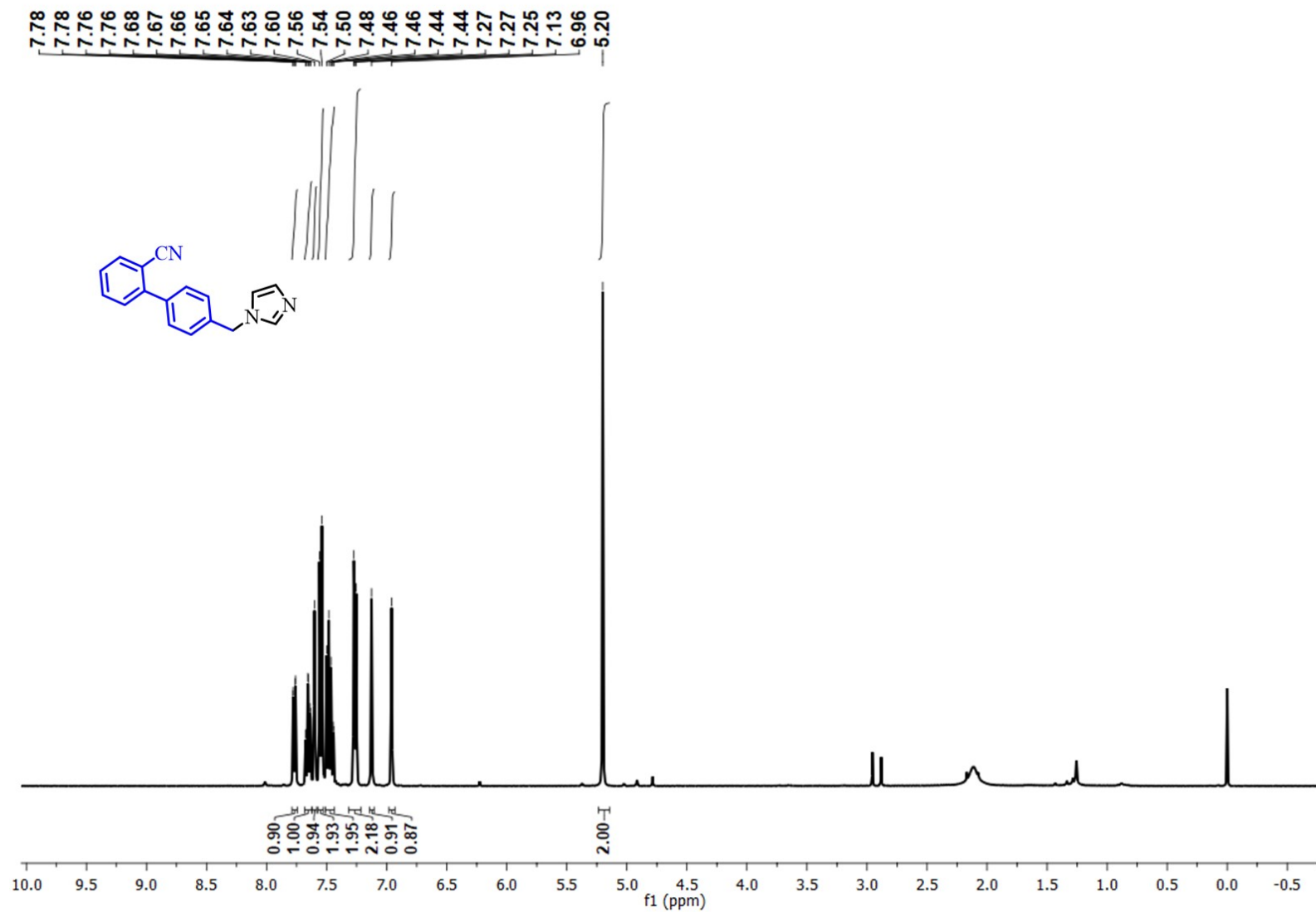
Fig. S51 ^{1}H NMR spectra of 4'-((1H-imidazol-1-yl) methyl)-[1,1'-biphenyl]-2-carbonitrile **(4e)**.
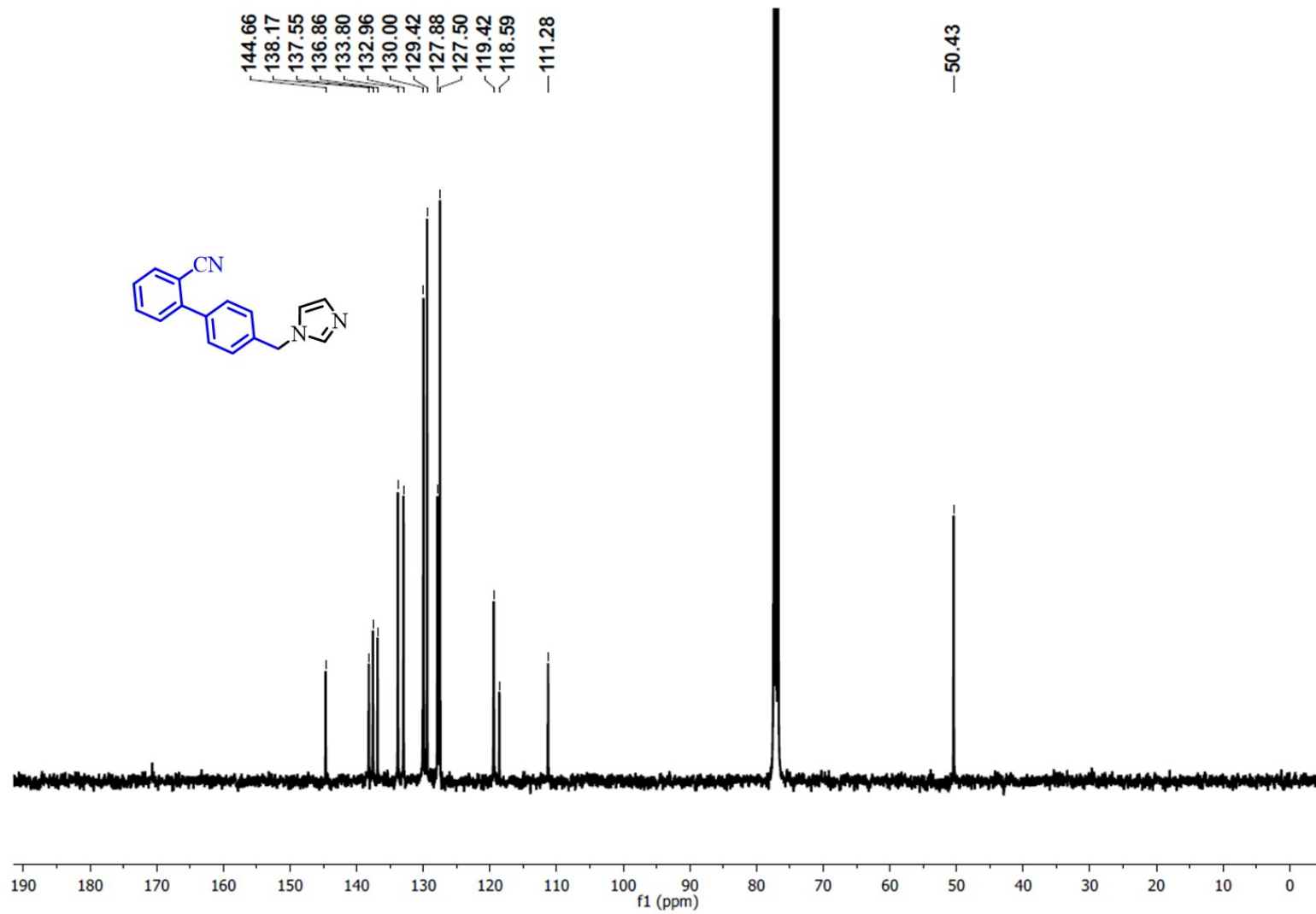
Fig. S52 ¹³C NMR spectra of 4'-((1H-imidazol-1-yl) methyl)-[1,1'-biphenyl]-2-carbonitrile **(4e)**.

144.66
138.17
137.55
136.86
133.80
132.96
130.00
129.42
127.88
127.50
119.42
118.59
111.28
50.43
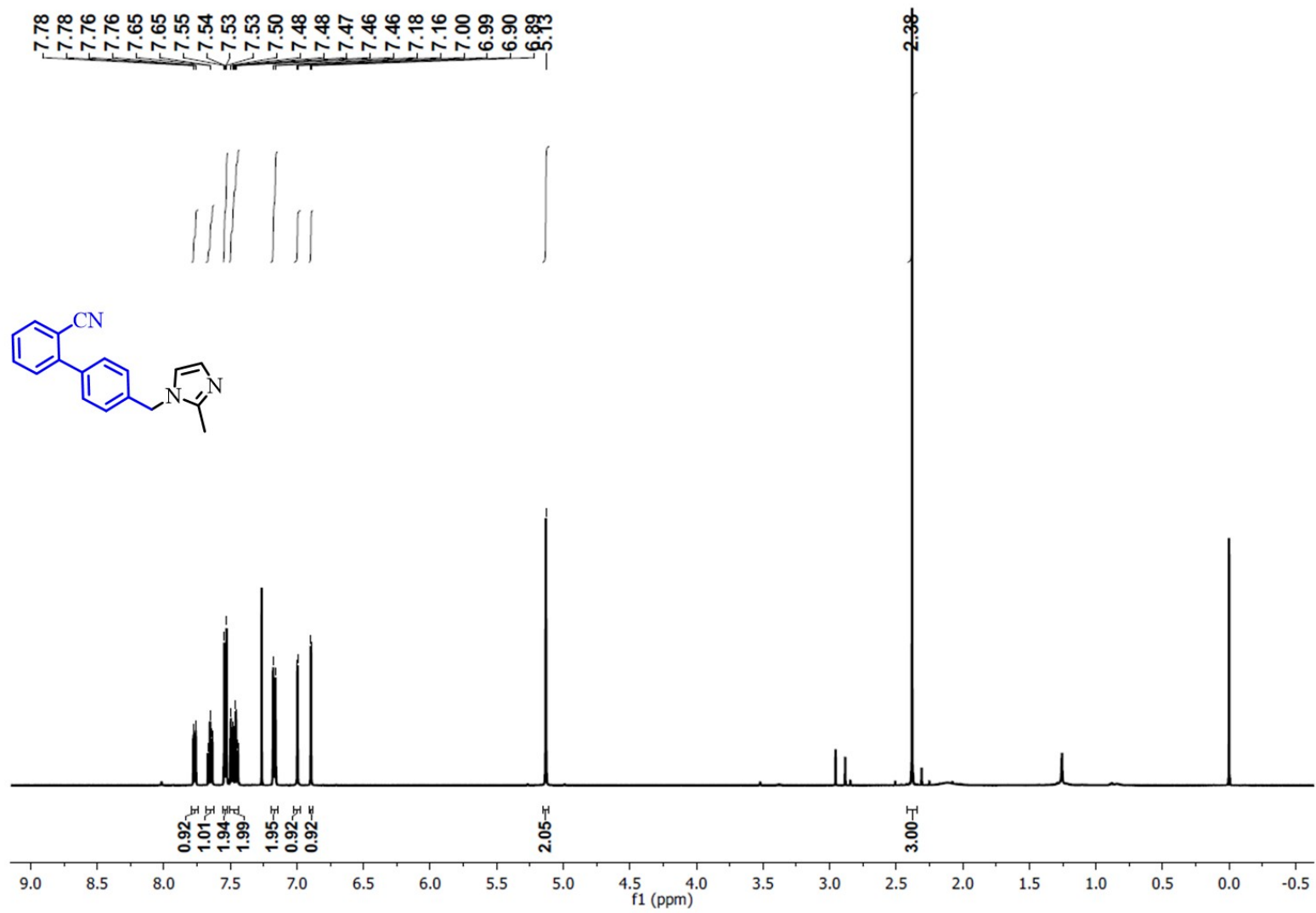
Fig. S53 ^{1}H NMR spectra of 4'-((2-methyl-1H-imidazol-1-yl) methyl)-[1,1'-biphenyl]-2-carbonitrile **(4f)**.
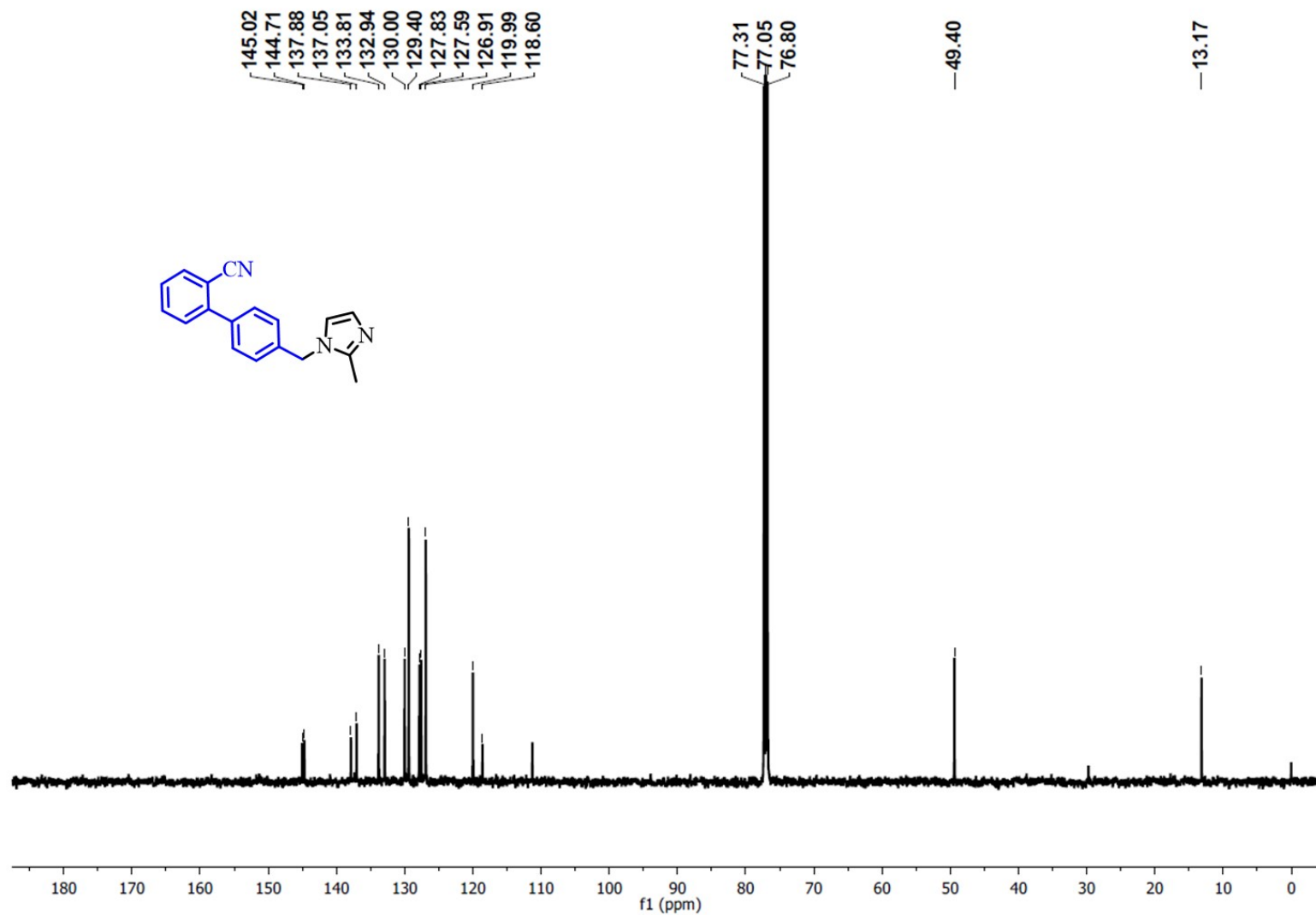
Fig. S54 ^{13}C NMR spectra of 4'-((2-methyl-1*H*-imidazol-1-yl) methyl)-[1,1'-biphenyl]-2-carbonitrile **(4f)**.
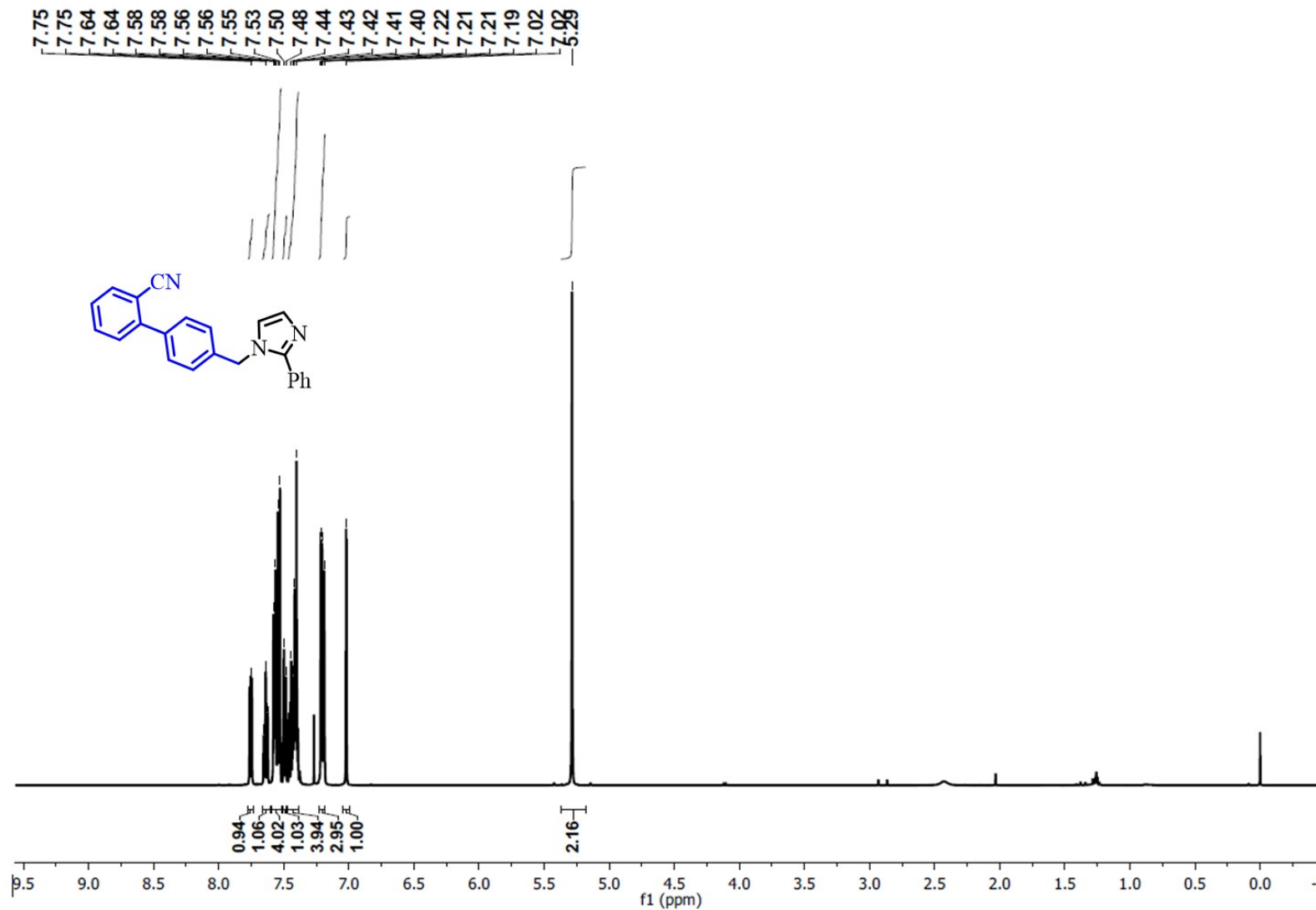
Fig. S55 ^{1}H NMR spectra of 4'-((2-phenyl-1H-imidazol-1-yl) methyl)-[1,1'-biphenyl]-2-carbonitrile **(4g)**.
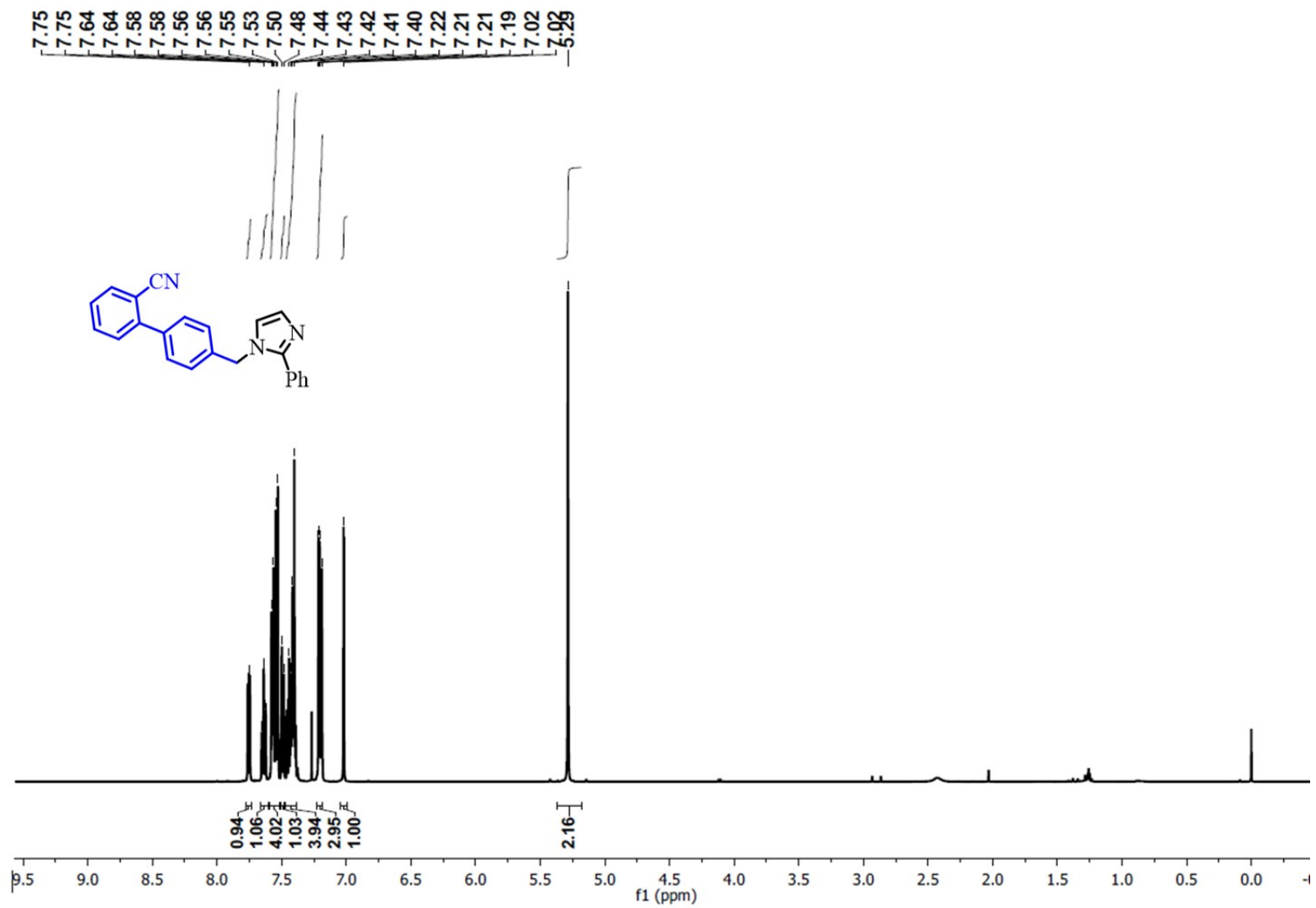
Fig. S56 ^{13}C NMR spectra of 4'-((2-phenyl-1*H*-imidazol-1-yl) methyl)-[1,1'-biphenyl]-2-carbonitrile **(4g)**.
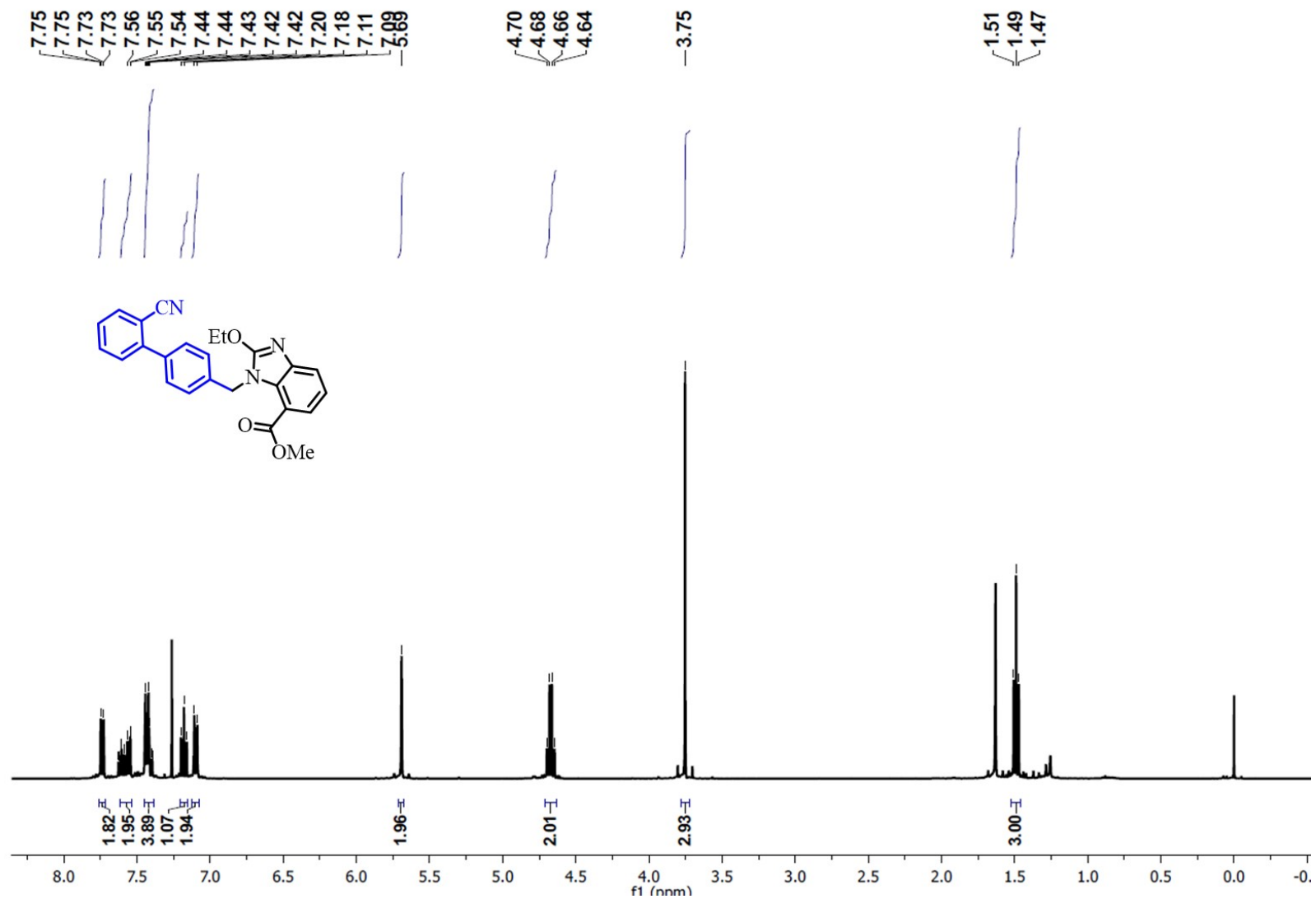
Fig. S57 ^{1}H NMR spectra of methyl 1-((2'-cyano-[1,1'-biphenyl]-4-yl) methyl)-2-ethoxy-1H-benzo[d]imidazole-7-carboxylate **(4h)**.
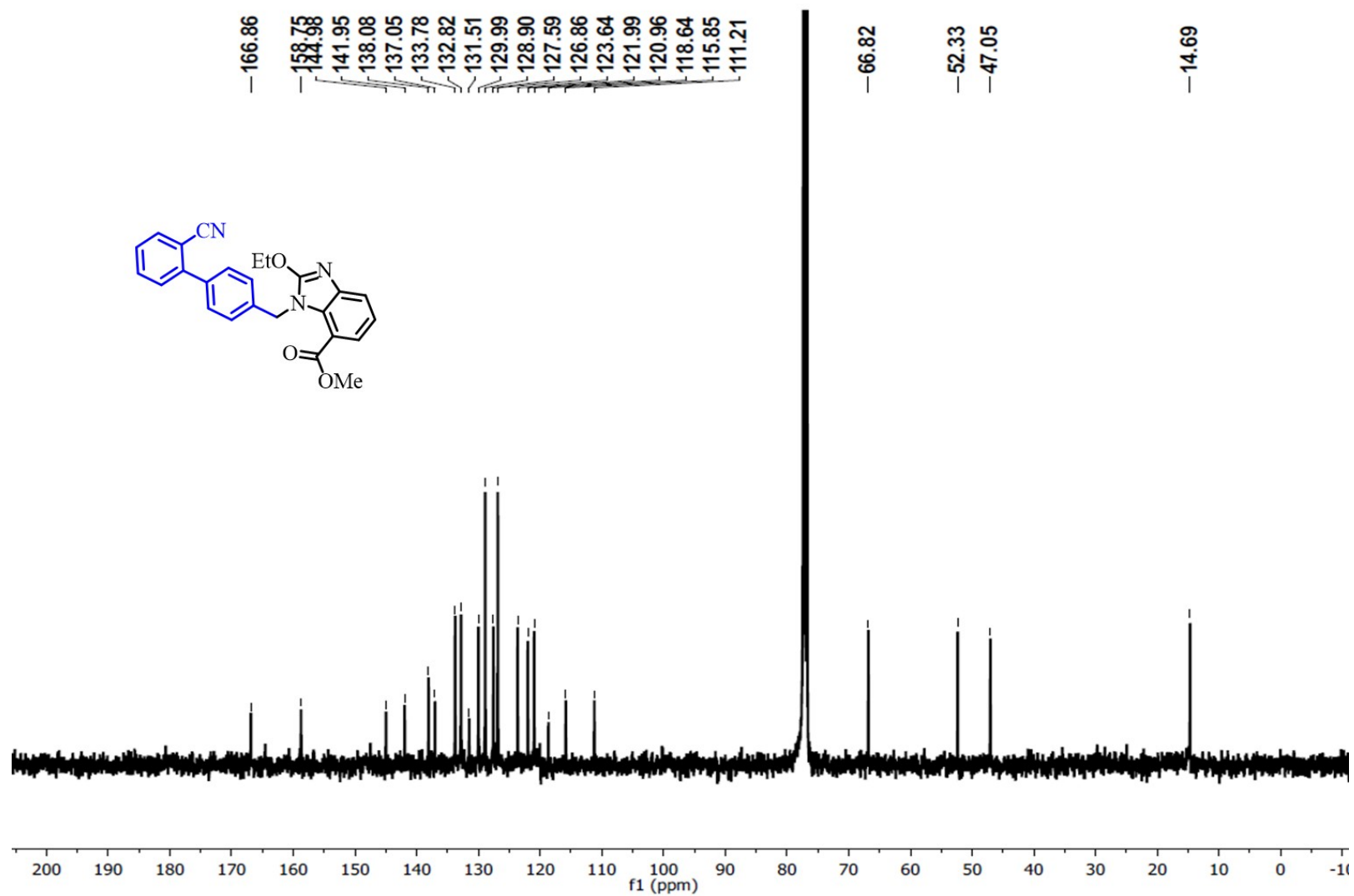
Fig. S58 ¹³C NMR spectra of methyl 1-((2'-cyano-[1,1'-biphenyl]-4-yl) methyl)-2-ethoxy-1*H*-benzo[d]imidazole-7-carboxylate **(4h)**.
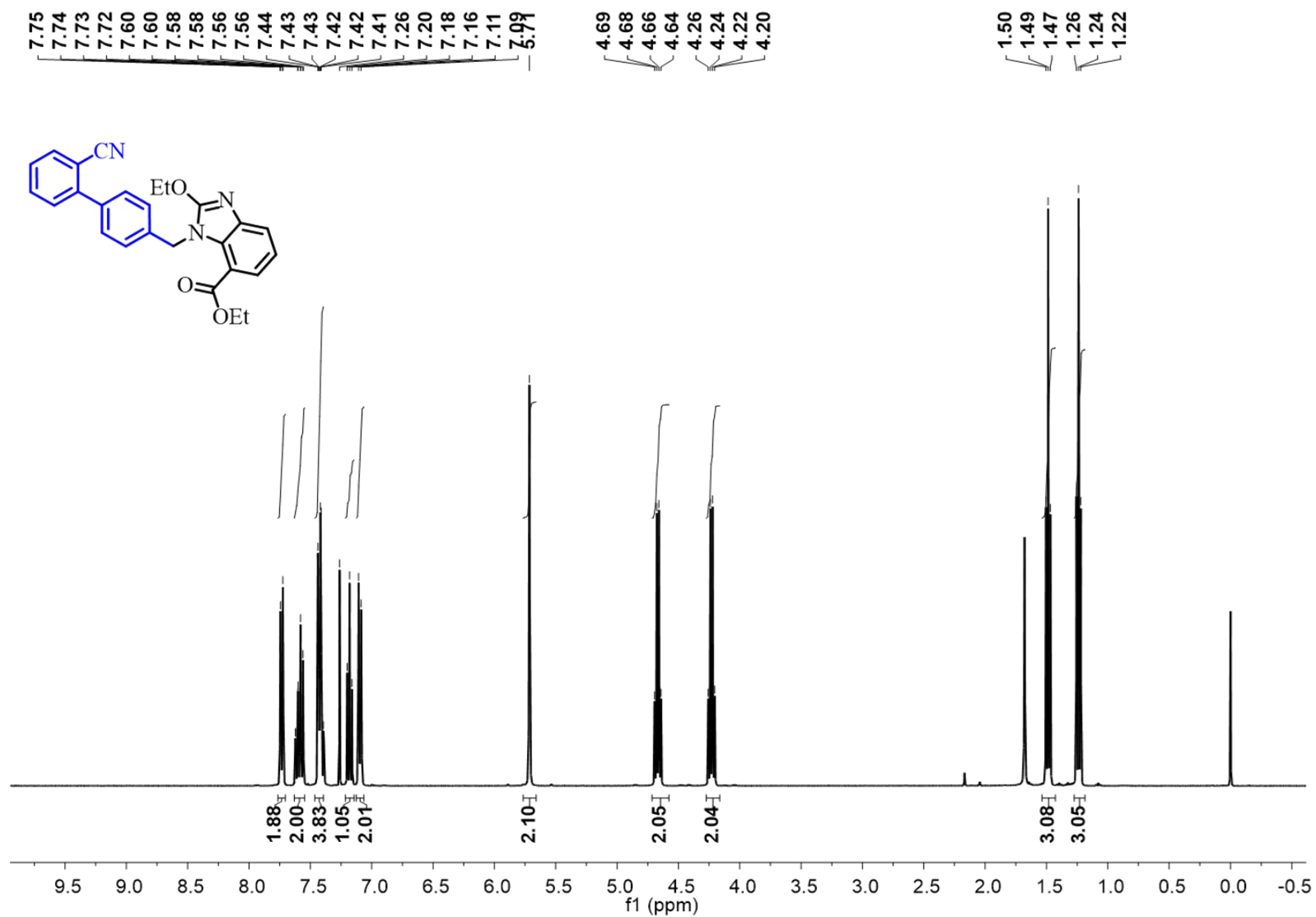
Fig. S59 ^{1}H NMR spectra of ethyl 1-((2'-cyano-[1,1'-biphenyl]-4-yl) methyl)-2-ethoxy-1H-benzo[d]imidazole-7-carboxylate **(4i)**.
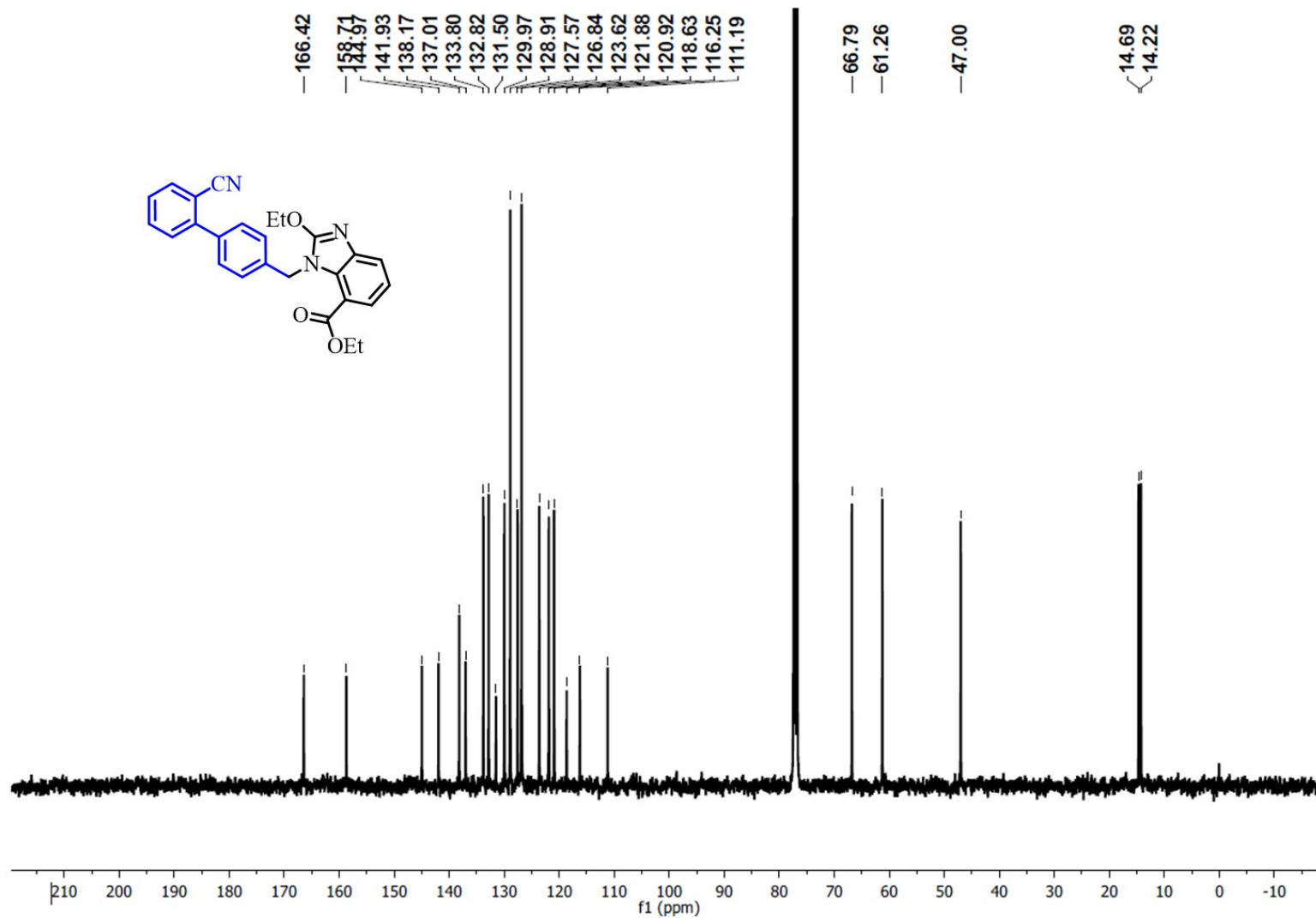
Fig. S60 ^{13}C NMR spectra of ethyl 1-((2'-cyano-[1,1'-biphenyl]-4-yl) methyl)-2-ethoxy-1*H*-benzo[d]imidazole-7-carboxylate **(4i)**.
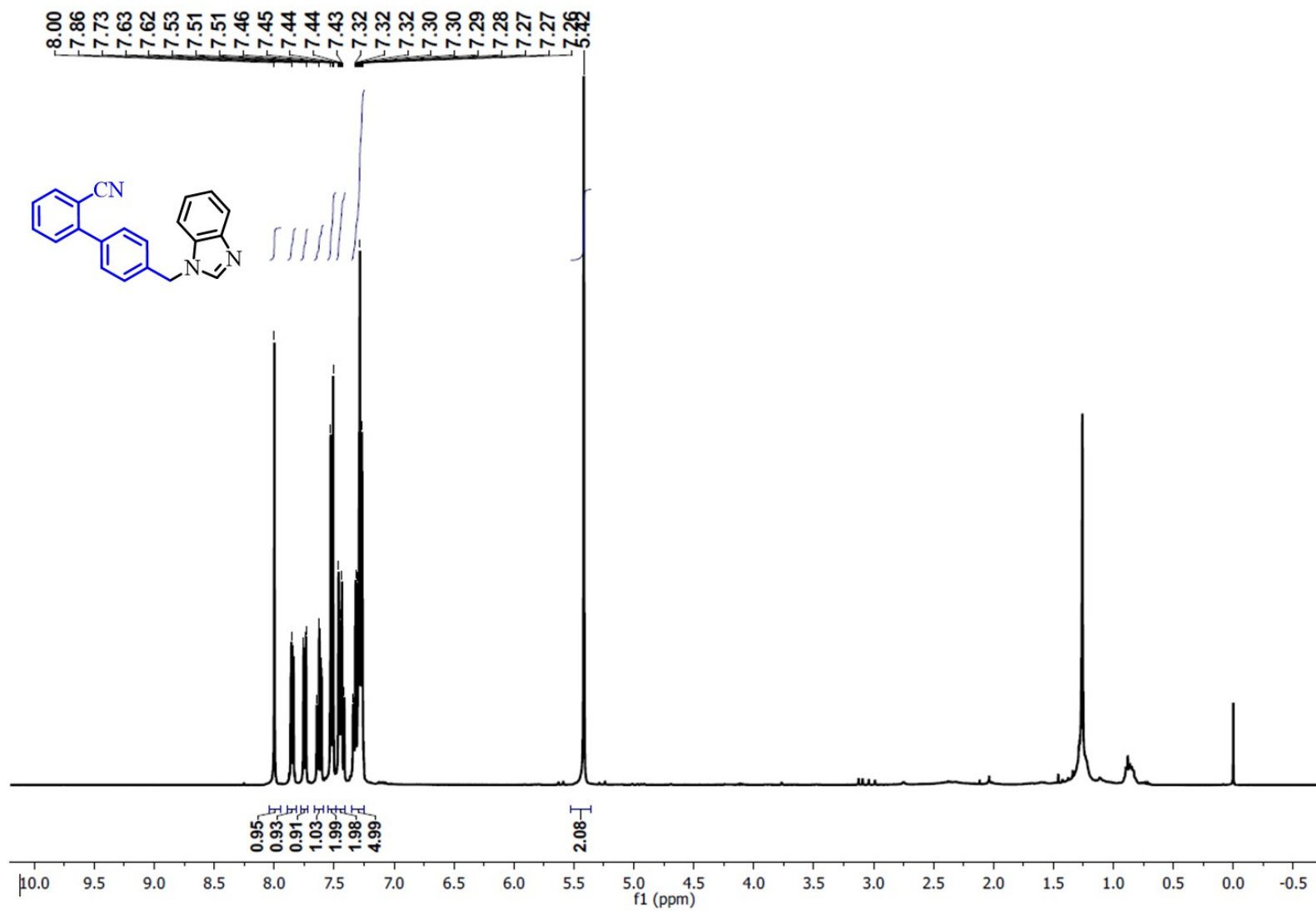
Fig. S61 ^{1}H NMR spectra of 4'-((1H-benzo[d]imidazol-1-yl) methyl)-[1,1'-biphenyl]-2-carbonitrile **(4j).**
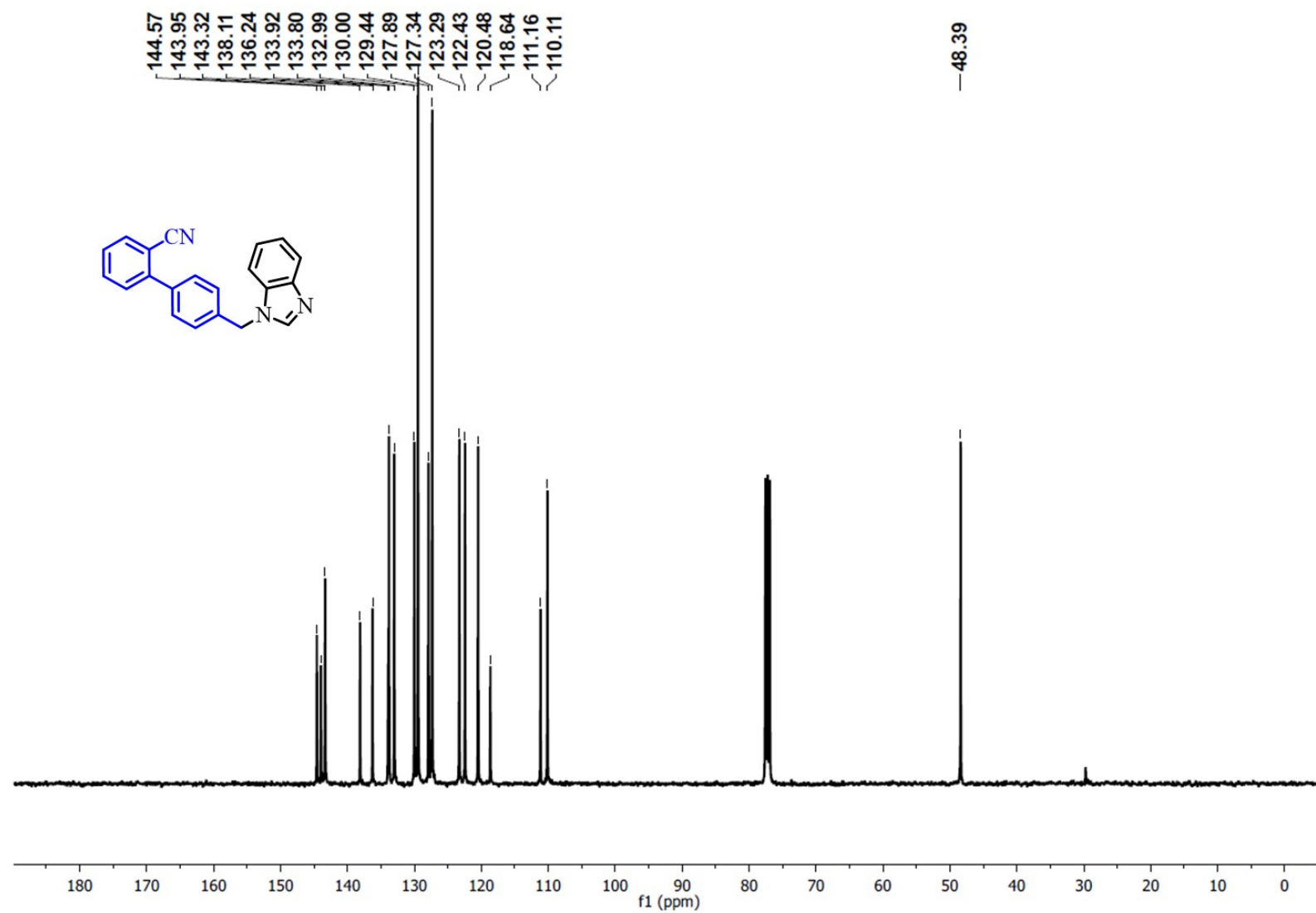
Fig. S62 ^{13}C NMR spectra of 4'-((1H-benzo[d]imidazol-1-yl) methyl)-[1,1'-biphenyl]-2-carbonitrile **(4j).**
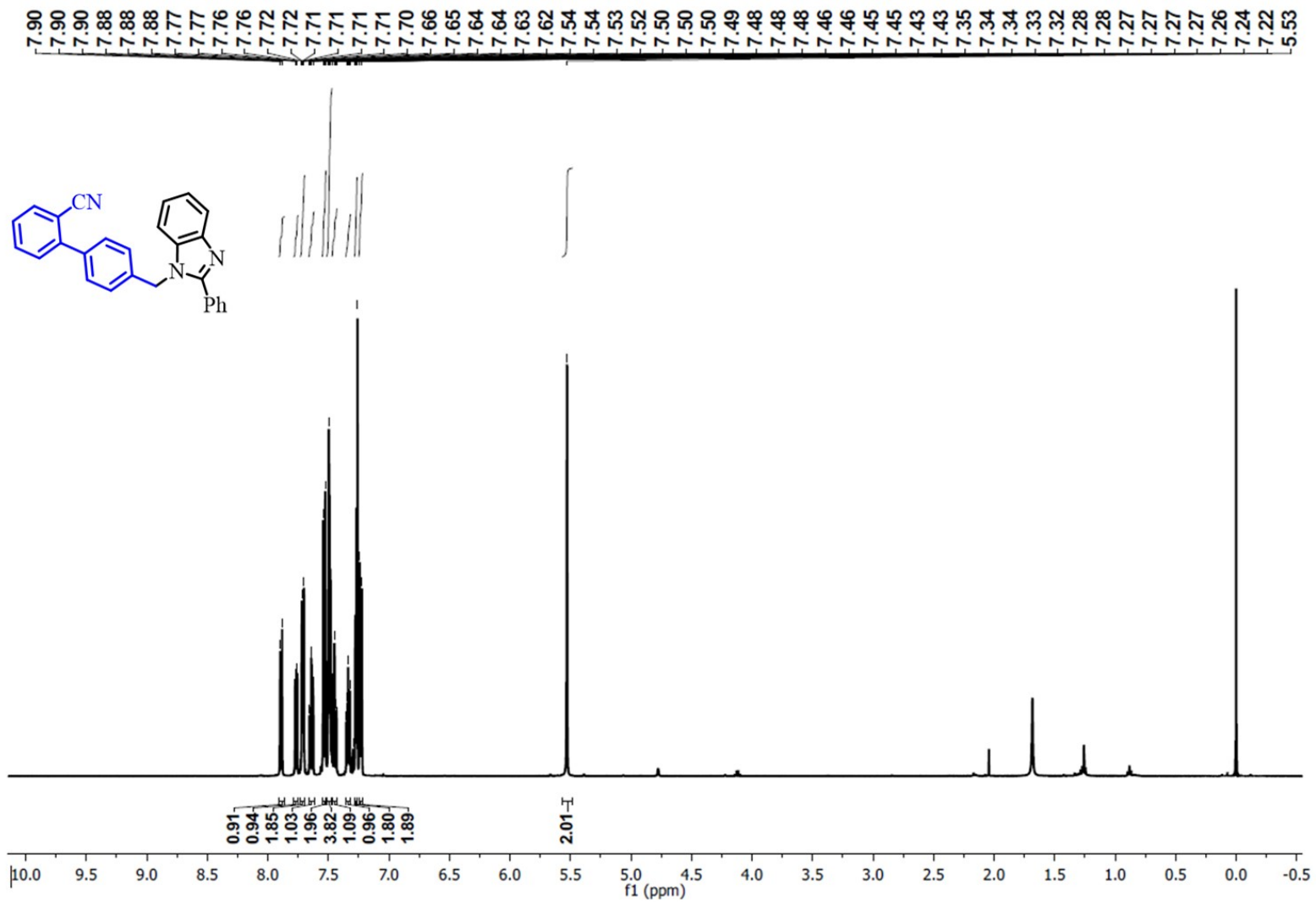
Fig. S63 ^{1}H NMR spectra of 4'-((2-phenyl-1H-benzo[d]imidazol-1-yl) methyl)-[1,1'-biphenyl]-2-carbonitrile **(4k)**.
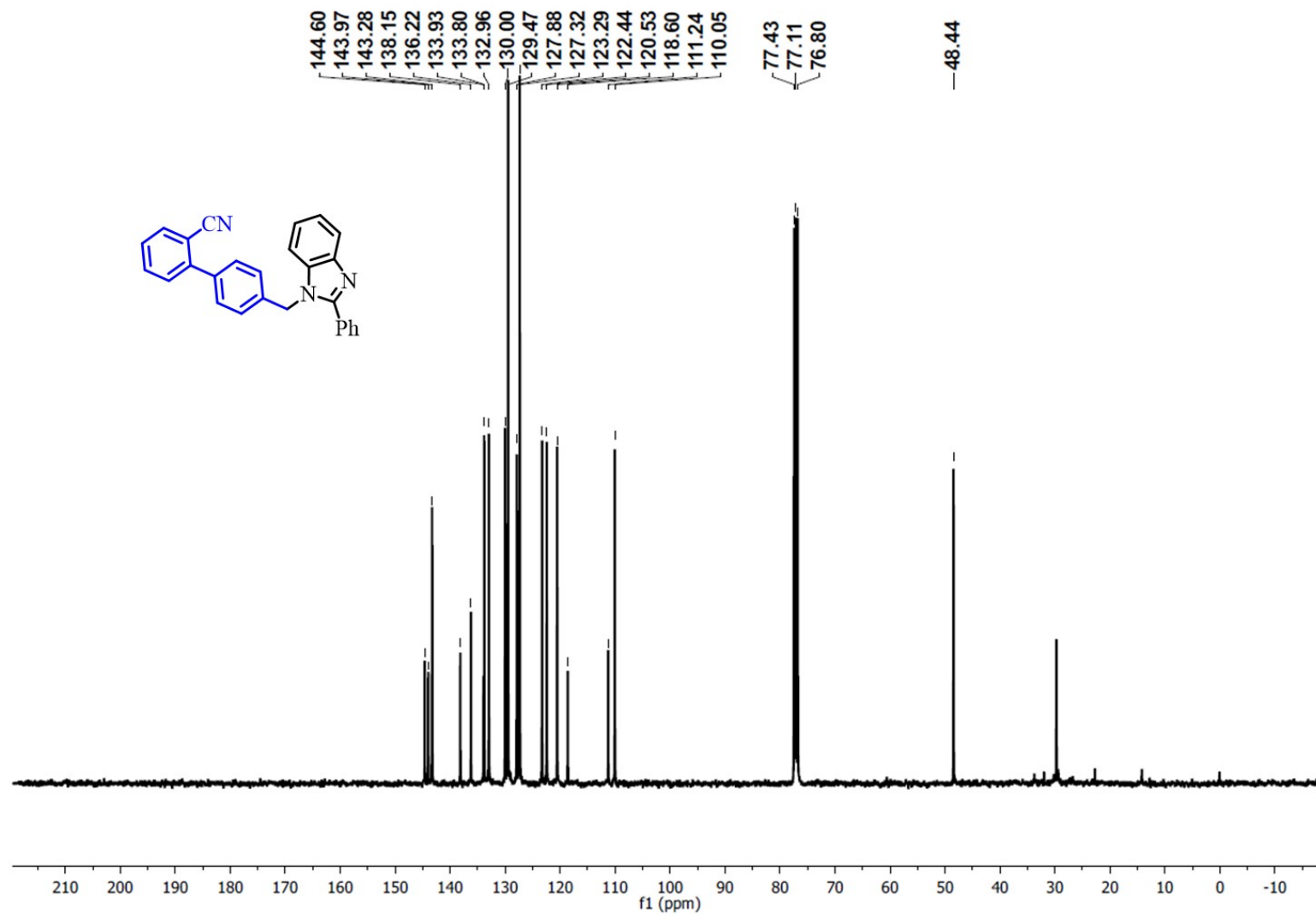
Fig. S64 ^{13}C NMR spectra of 4'-((2-phenyl-1*H*-benzo[d]imidazol-1-yl) methyl)-[1,1'-biphenyl]-2-carbonitrile **(4k)**.
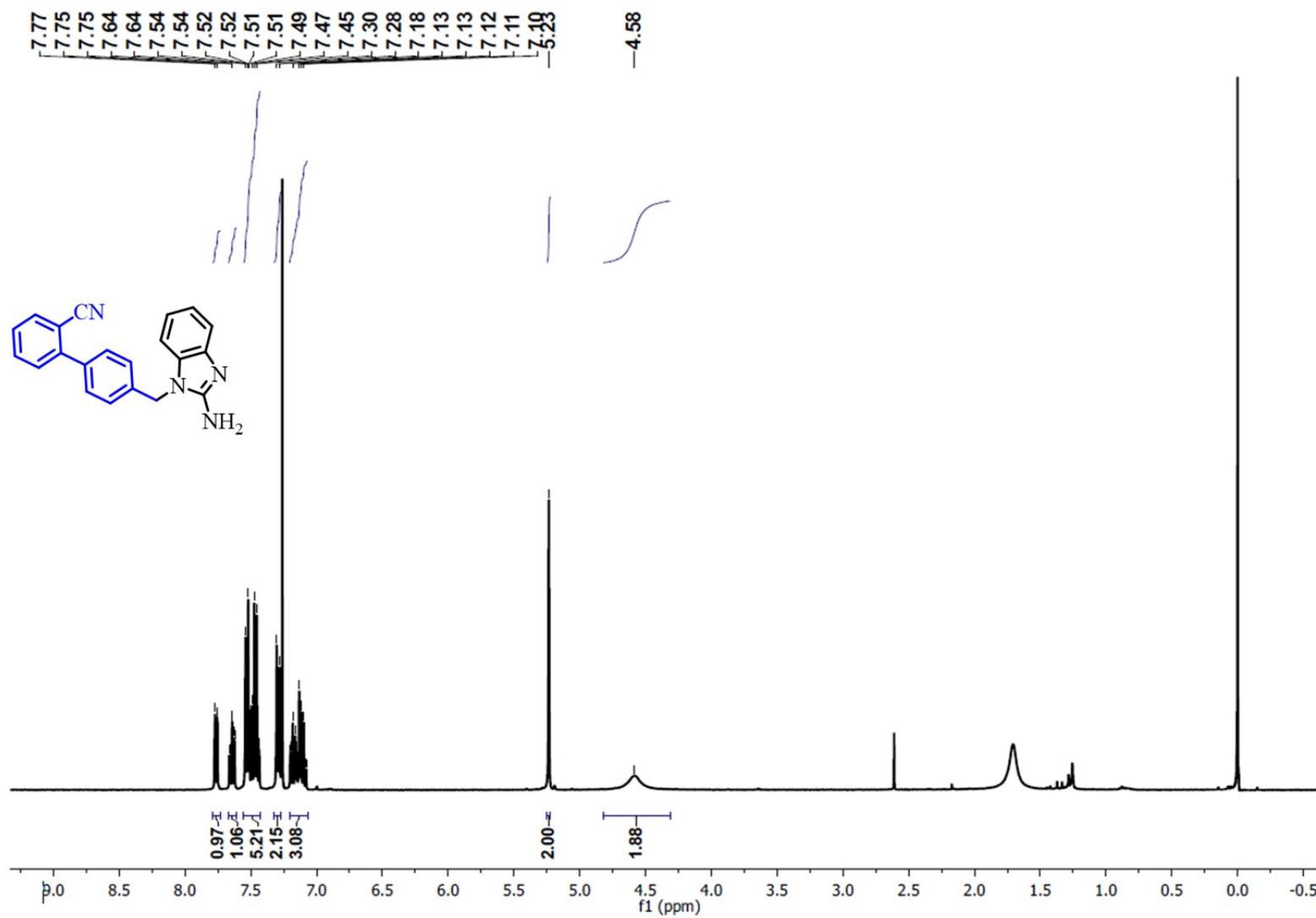
Fig. S65 ^{1}H NMR spectra of 4'-((2-amino-1*H*-benzo[d]imidazol-1-yl) methyl)-[1,1'-biphenyl]-2-carbonitrile **(4l).**
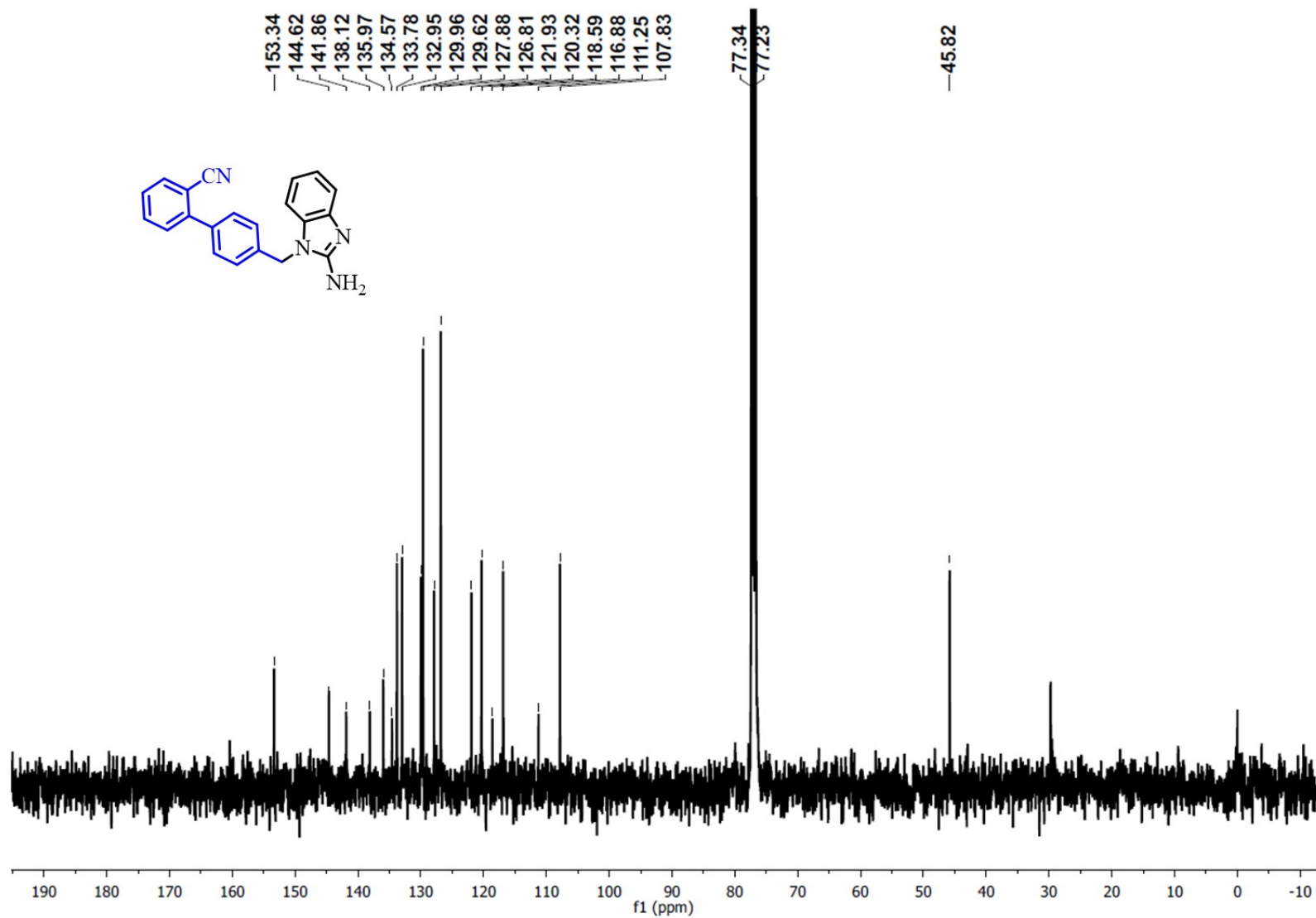
Fig. S66 ^{13}C NMR spectra of 4'-((2-amino-1H-benzo[d]imidazol-1-yl) methyl)-[1,1'-biphenyl]-2-carbonitrile **(4l).**
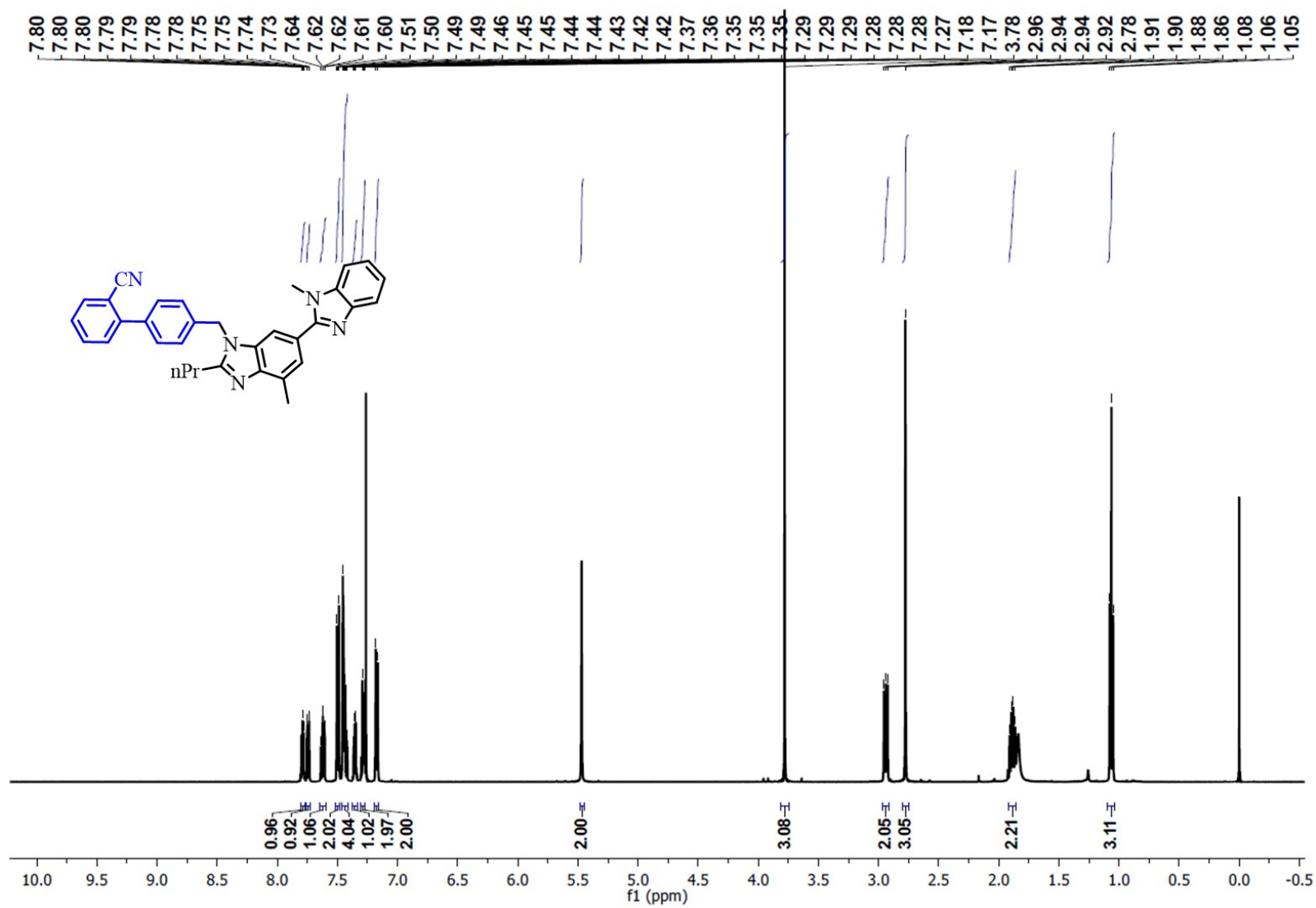
Fig. S67 ^{1}H NMR spectra of 4'-((1,7'-dimethyl-2'-propyl-1*H*,3'*H*-[2,5'-bibenzo[d]imidazol]-3'-yl) methyl)-[1,1'-biphenyl]-2-carbonitrile **(4m).**
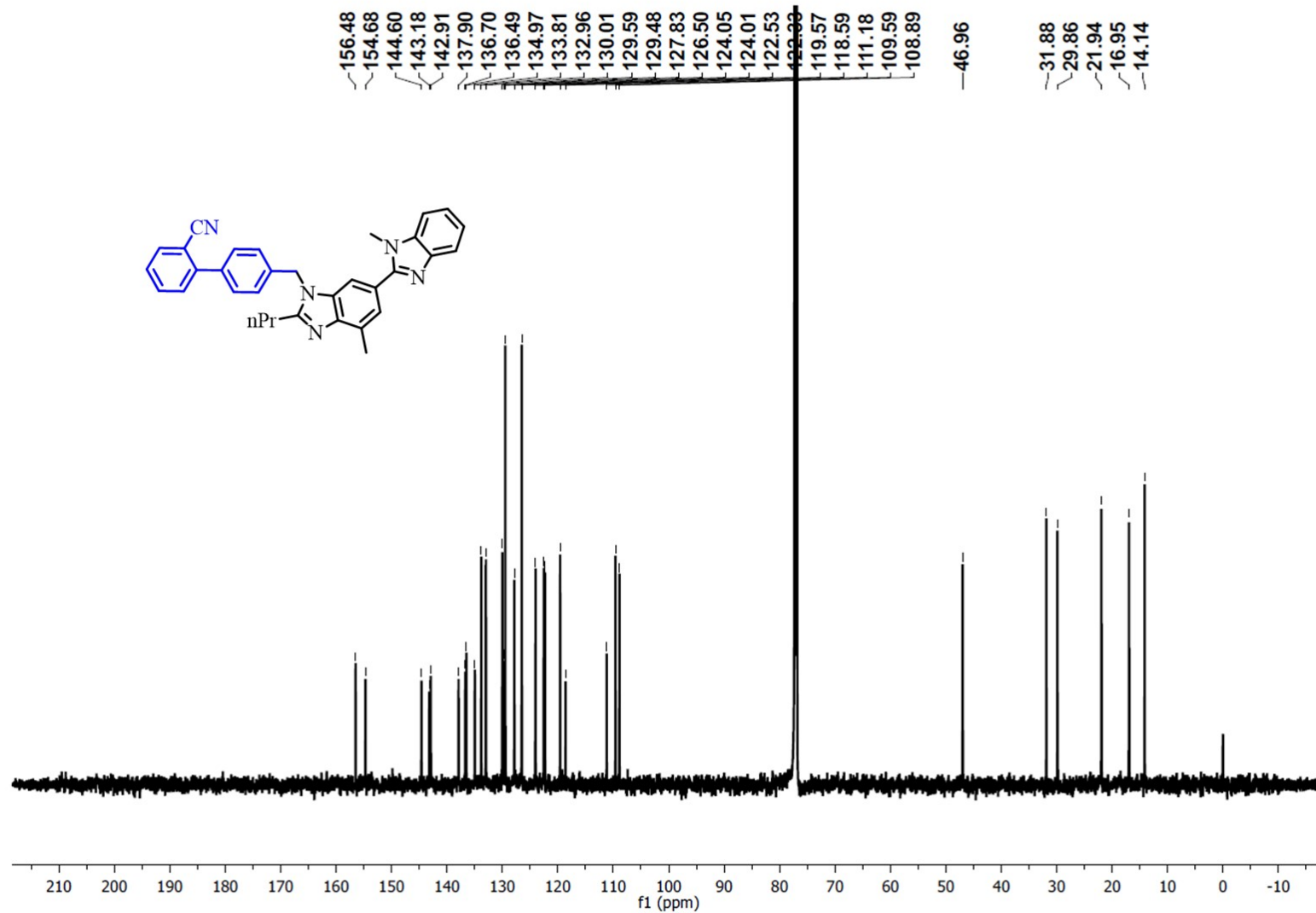
Fig. S68 ^{13}C NMR spectra of 4'-((1,7'-dimethyl-2'-propyl-1H,3'H-[2,5'-bibenzo[d]imidazol]-3'-yl) methyl)-[1,1'-biphenyl]-2-carbonitrile **(4m).**
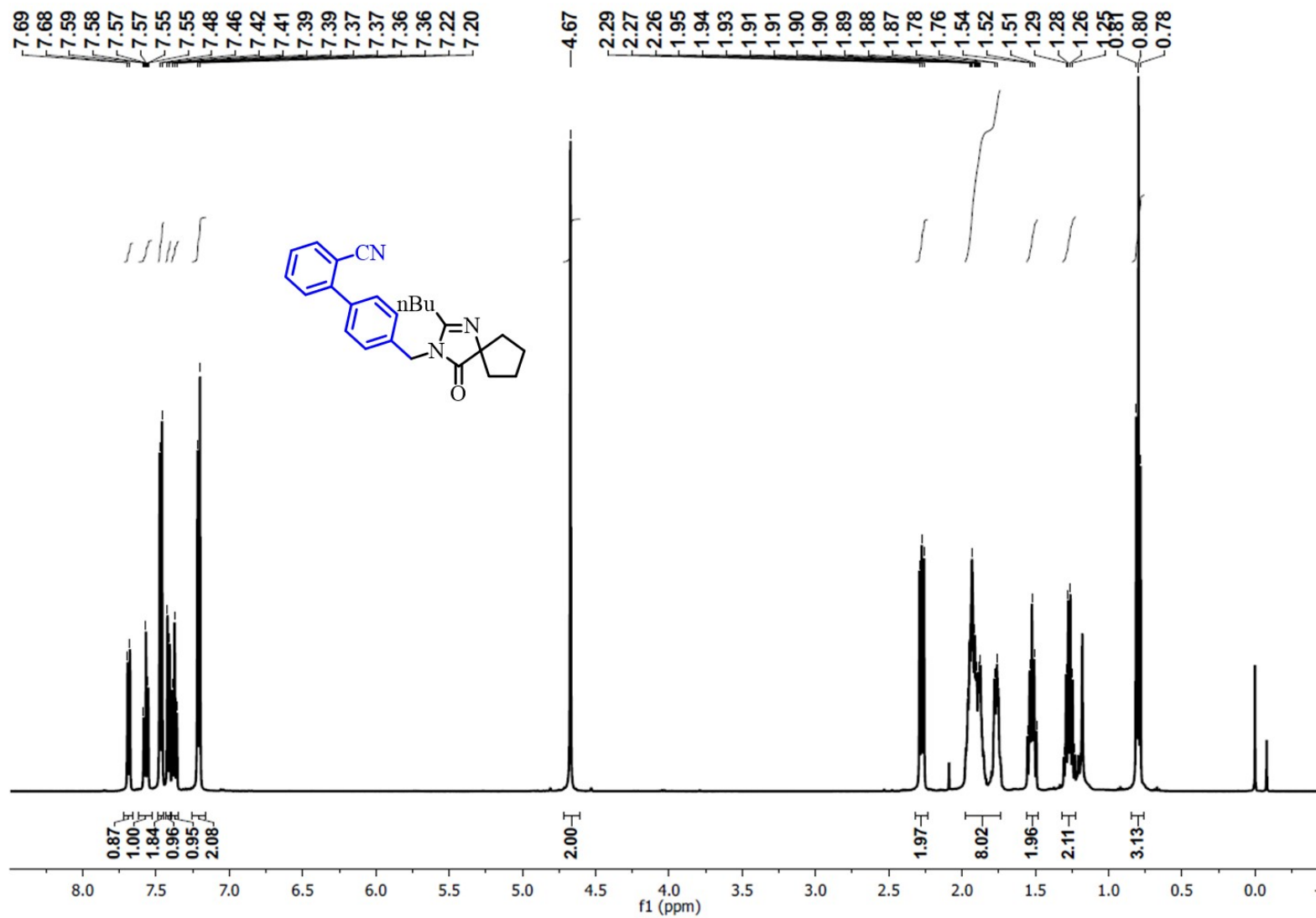
Fig. S69 ^{1}H NMR spectra of 4'-((2-butyl-4-oxo-1,3-diazaspiro [4.4] non-1-en-3-yl) methyl)-[1,1'-biphenyl]-2-carbonitrile **(4n)**.
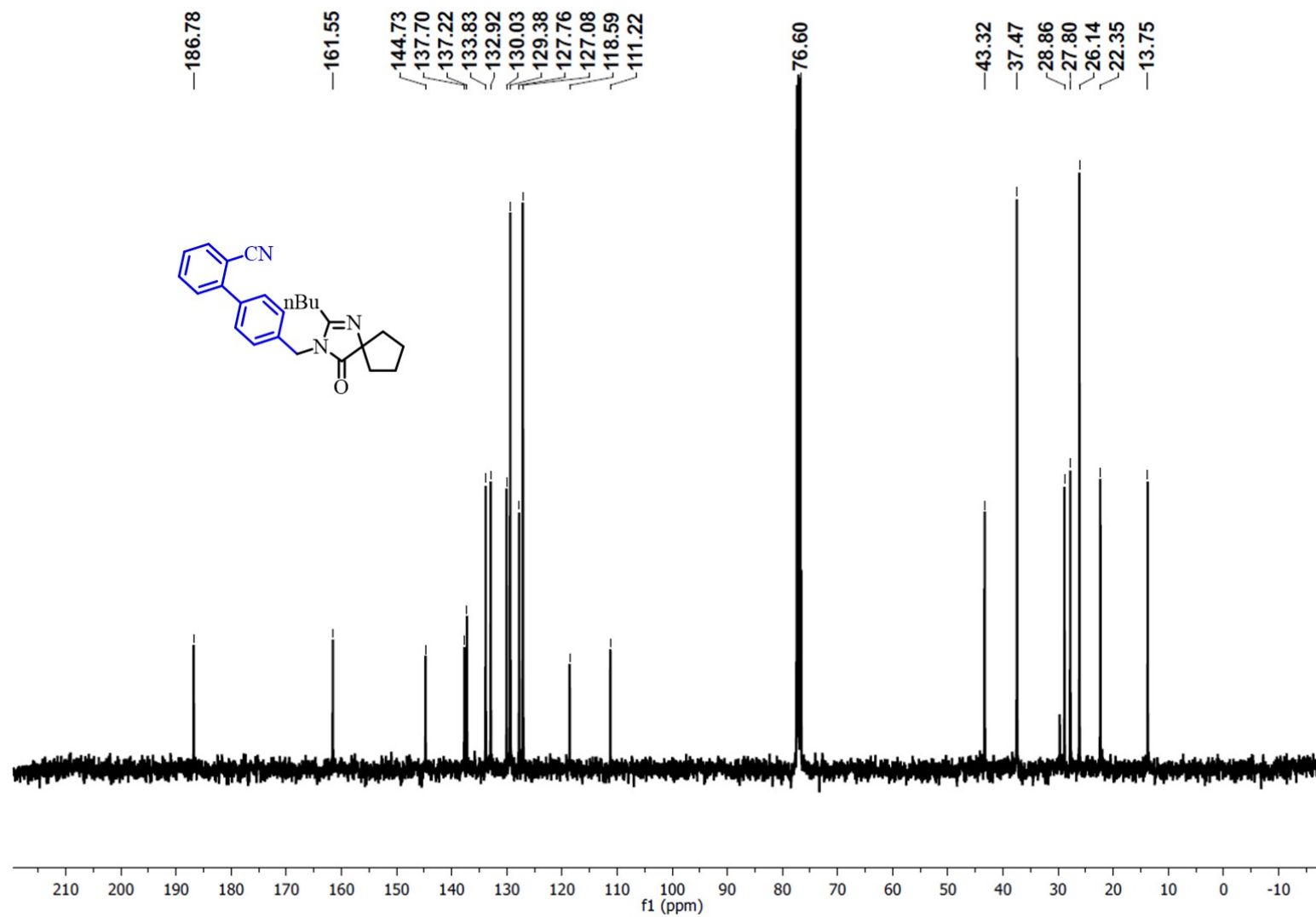
Fig. S70 ^{13}C NMR spectra of 4'-((2-butyl-4-oxo-1,3-diazaspiro [4.4] non-1-en-3-yl) methyl)-[1,1'-biphenyl]-2-carbonitrile **(4n).**
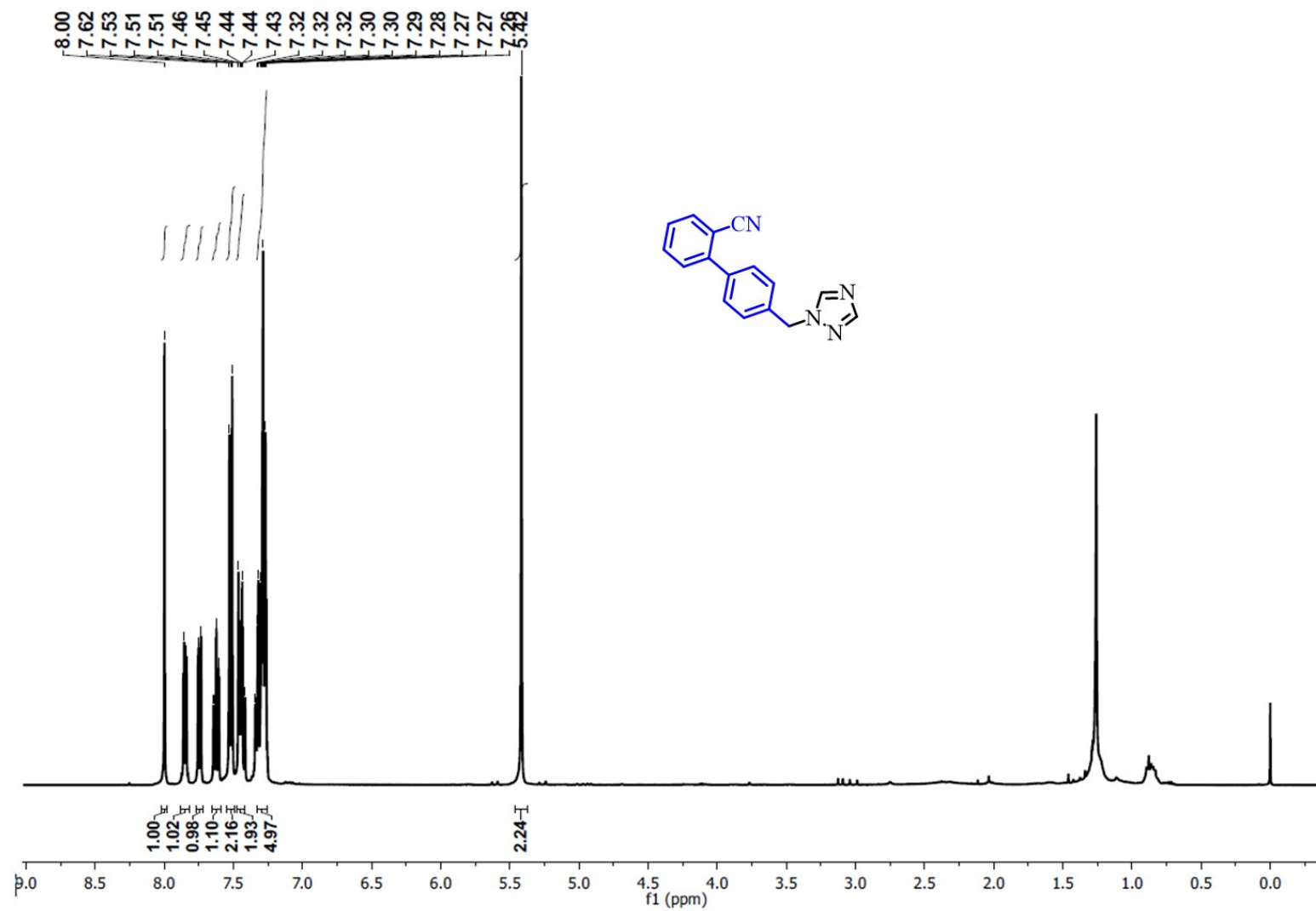
Fig. S71 ¹H NMR spectra of 4'-((1H-1,2,4-triazol-1-yl) methyl)-[1,1'-biphenyl]-2-carbonitrile **(4o)**.
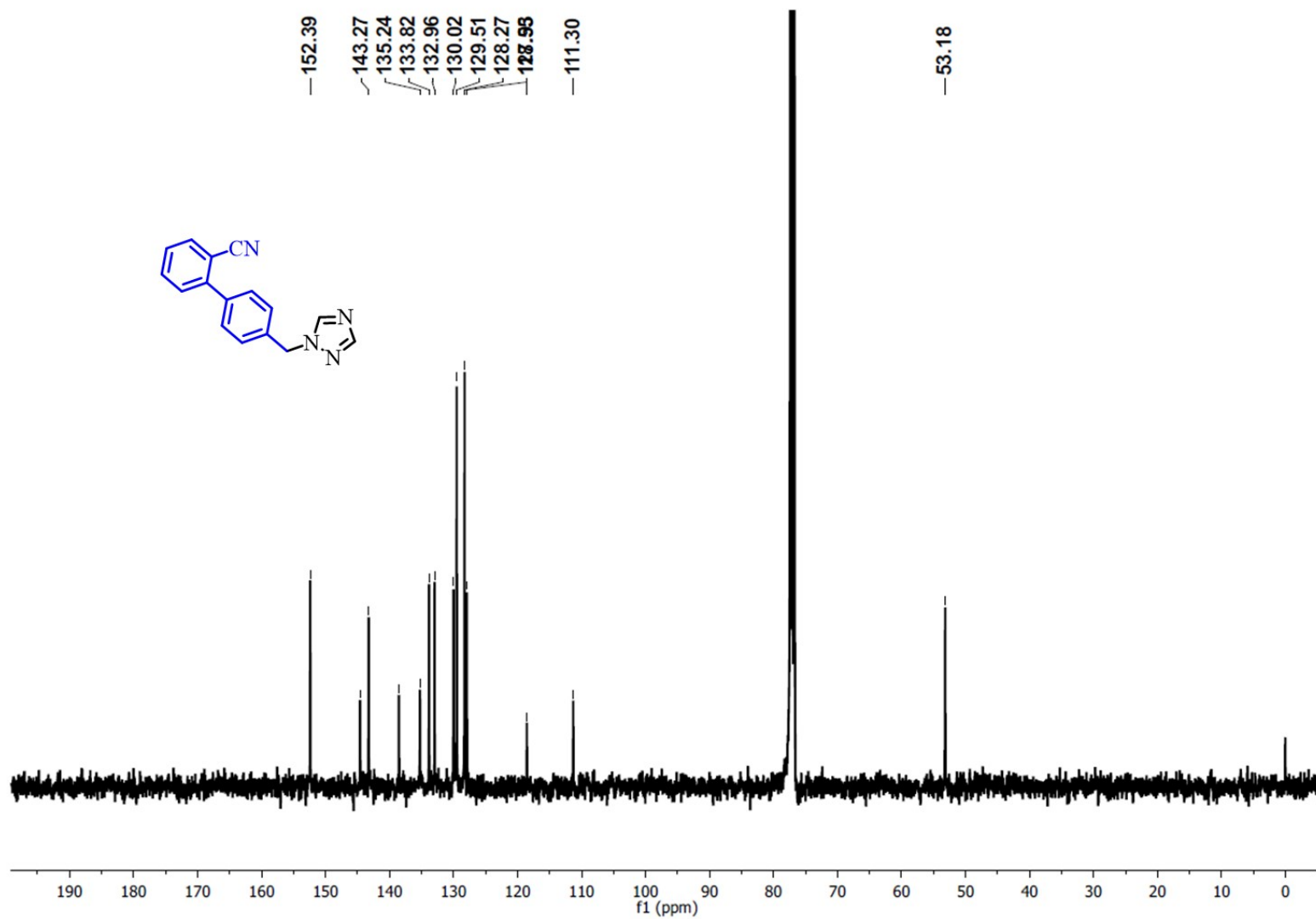
Fig. S72 ¹³C NMR spectra of 4'-((1*H*-1,2,4-triazol-1-yl) methyl)-[1,1'-biphenyl]-2-carbonitrile **(4o).**
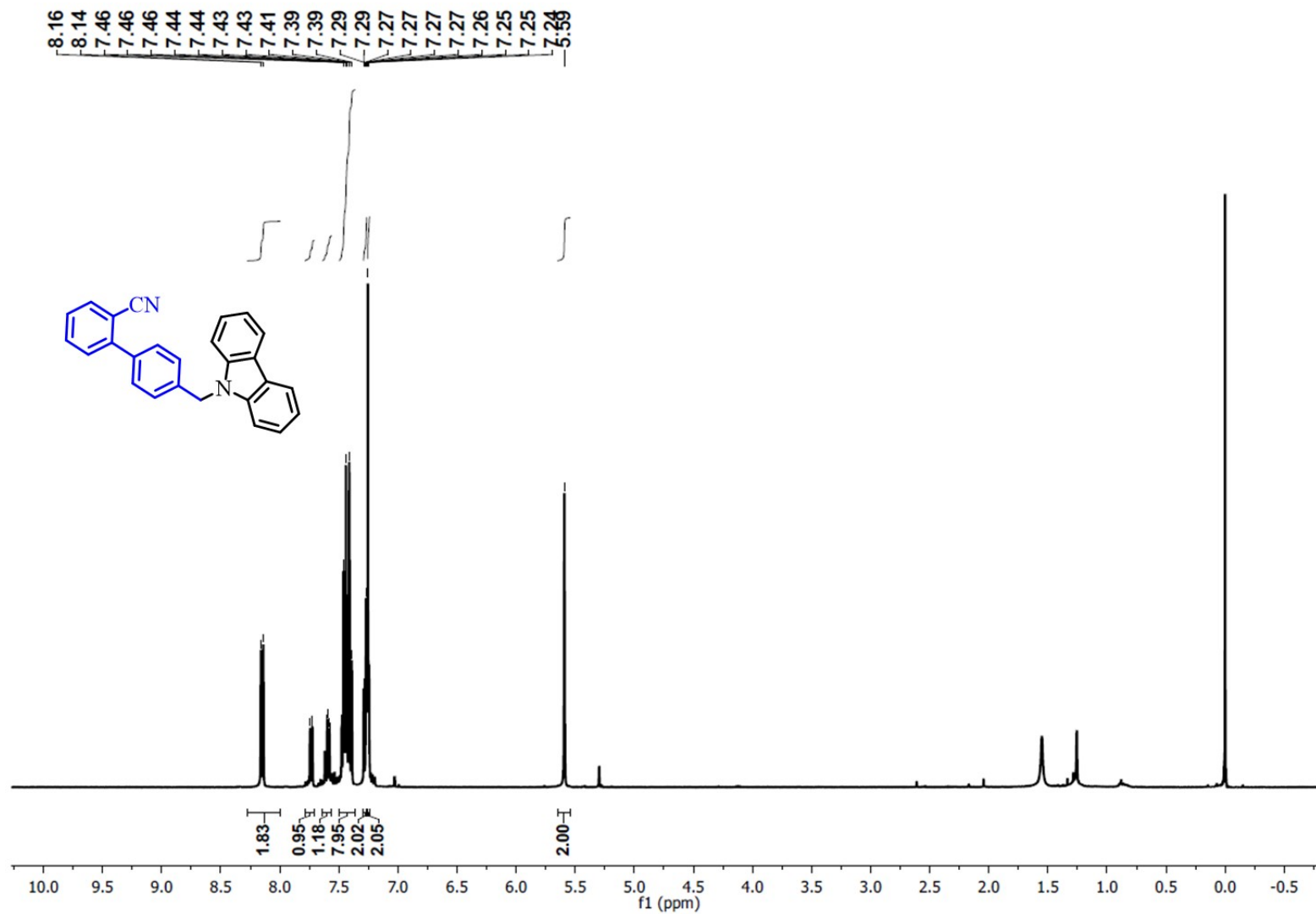
Fig. S73 ^{1}H NMR spectra of 4'-((9*H*-carbazol-9-yl) methyl)-[1,1'-biphenyl]-2-carbonitrile **(4p).**
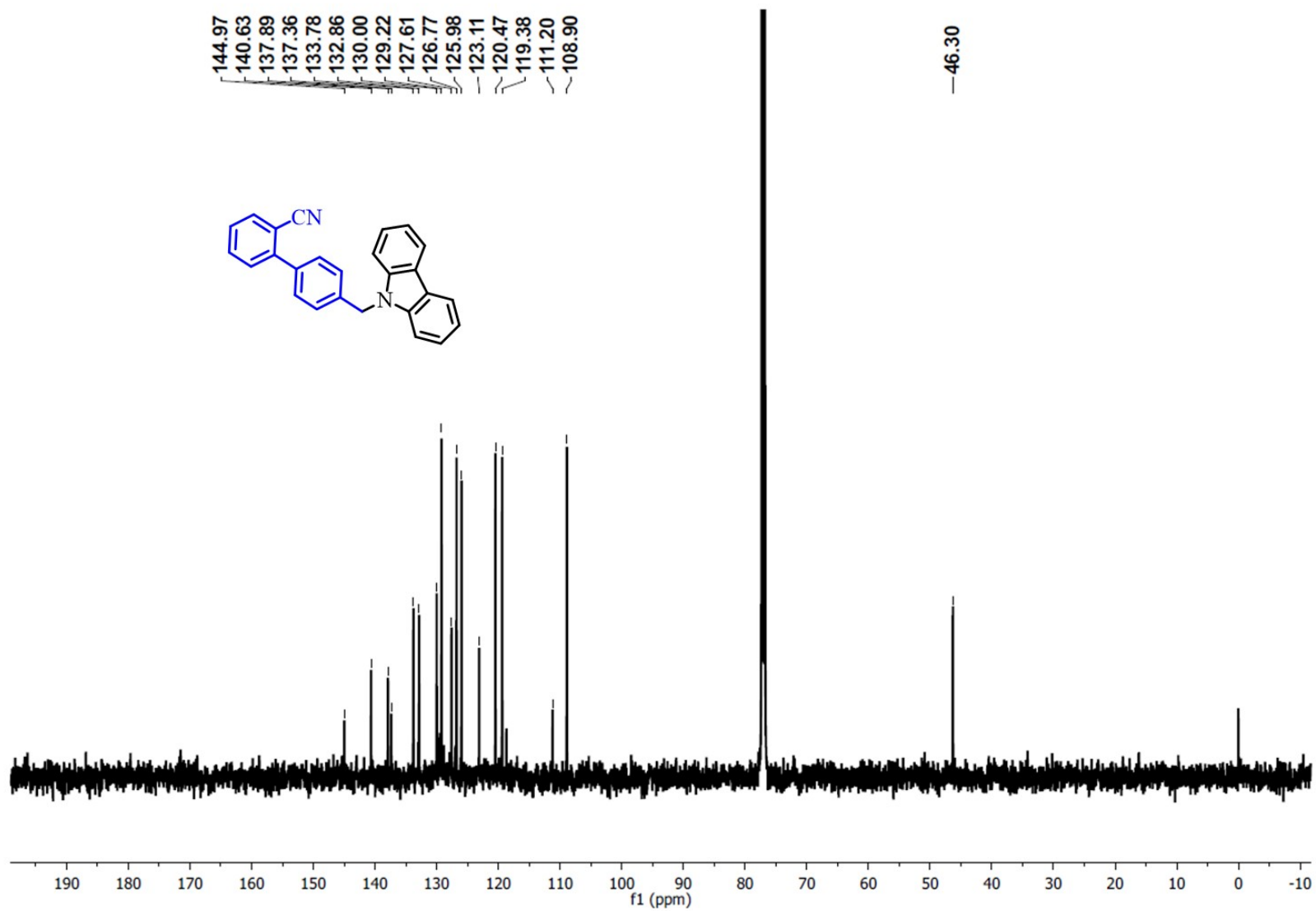
Fig. S74 ^{13}C NMR spectra of 4'-((9*H*-carbazol-9-yl) methyl)-[1,1'-biphenyl]-2-carbonitrile **(4p).**

S6.0 References:

1.   G.-N. Ahn, J.-H. Kang, H.-J. Lee, B. E. Park, M. Kwon, G.-S. Na, H. Kim, D.-H. Seo and D.-P. Kim, *Chem. Eng. J.*, 2023, **453**, 139707.

2.   A. Mottafegh, G.-N. Ahn and D.-P. Kim, *Lab on a Chip*, 2023, **23**, 1613-1621.

3.   D. Francis, A. J. Blacker, N. Kapur and S. P. Marsden, *Org. Process Res. Dev.*, 2022, **26**, 215-221.

4.   D. Cantillo, O. de Frutos, J. A. Rincon, C. Mateos and C. O. Kappe, *J. Org. Chem.*, 2014, **79**, 223-229.

5.   H. Thankappan, C. Burke and B. Glennon, *Org. Biomol. Chem.*, 2023, **21**, 508-513.

6.   S. Ni, M. A. E. A. A. A. El Remaily and J. Franzén, *Adv. Synth. Catal.,* 2018, **360**, 4197-4204.

7.   L. Pan, K.-M. Lee, Y.-Y. Chan, Z. Ke and Y.-Y. Yeung, *Org. Lett.*, 2023, **25**, 53-57.

8.   X. Tan, T. Song, Z. Wang, H. Chen, L. Cui and C. Li, *Org. Lett.*, 2017, **19**, 1634-1637.

9.   W. Ai, Y. Liu, Q. Wang, Z. Lu and Q. Liu, *Org. Lett.*, 2018, **20**, 409-412.

10.   M. Zhao, M. Li and W. Lu, *Synthesis*, 2018, **50**, 4933-4939.

11.   S. Stegbauer, C. Jandl and T. Bach, *Angew. Chem. Int. Ed.,* 2018, **57**, 14593-14596.

12.   C. C. Malakar, D. Schmidt, J. Conrad and U. Beifuss, *Org. Lett.*, 2011, **13**, 1972-1975.

13.   J. I. Kim and G. B. Schuster, *J. Am. Chem. Soc.*, 1992, **114**, 9309-9317.

14.   J. Wang, W. Wan, H. Jiang, Y. Gao, X. Jiang, H. Lin, W. Zhao and J. Hao, *Org. Lett.*, 2010, **12**, 3874-3877.

15.   A. Rana, B. K. Malviya, D. K. Jaiswal, P. Srihari and A. K. Singh, *Green Chem.*, 2022, **24**, 4794-4799.

16.   X. Bao, W. Zhu, R. Zhang, C. Wen, L. Wang, Y. Yan, H. Tang and Z. Chen, *Bioorg. & Med. Chem.*, 2016, **24**, 2023-2031.

17.   S. B. Madasu, N. A. Vekariya, C. Koteswaramma, A. Islam, P. D. Sanasi and R. B.

Korupolu, *Org. Process Res. Dev.*, 2012, **16**, 2025-2030.

18. 2009.

19. G. Y. Meti, R. R. Kamble, D. B. Biradar and S. B. Margankop, *Med. Chem. Res.*, 2013, **22**, 5868-5877.

20. K. Kubo, Y. Kohara, E. Imamiya, Y. Sugiura, Y. Inada, Y. Furukawa, K. Nishikawa and T. Naka, *J. Med. Chem.*, 1993, **36**, 2182-2195.

21. D. Sam Daniel Prabu, S. Lakshmanan, N. Ramalakshmi, K. Thirumurugan, D. Govindaraj and S. A. Antony, *Syn. Commun.*, 2019, **49**, 266-278.

22. V. Kandathil, B. Kulkarni, A. Siddiqa, M. Kempasiddaiah, B. S. Sasidhar, S. A. Patil and S. A. Patil, *Catal. Lett.*, 2020, **150**, 384-403.

23. T. Xu, W. Li, K. Zhang, Y. Han, L. Liu, T. Huang, C. Li, Z. Tang and T. Chen, . *J. Org. Chem.*, 2022, **87**, 11871-11879.

24. P. Ye, K. Sargent, E. Stewart, J.-F. Liu, D. Yohannes and L. Yu, *J. Org. Chem.*, 2006, **71**, 3137-3140.

25. F. Shuangxia, G. Zheng, T. Yelv, L. Hui and J. Guofang, *J. Chem. Res.*, 2015, **39**, 451-454.

26. P. Ambalavanan, K. Palani, M. N. Ponnuswamyand, R. A. Thirumuruhan, H. S. Yathirajan, B. Prabhuswamy, C. R. Raju, P. Nagaraja and K. N. Mohana, *Mol. Cryst. Liq.*, 2003, **393**, 75-82.